Impact of gas migration around nuclear wastes disposals: Modelling of the gas injection experiment PGZ3

Auteur : Meunier, Fanny
Promoteur(s) : Collin, Frederic
Faculté : Faculté des Sciences appliquées
Diplôme : Master en ingénieur civil des mines et géologue, à finalité spécialisée en ressources minérales et recyclage
Année académique : 2021-2022
URI/URL : http://hdl.handle.net/2268.2/14336

LIÈGE université
Sciences Appliquées

Academic year
2021 - 2022

Impact of gas migration around nuclear wastes disposals: Modelling of the gas injection experiment PGZ3

AUTHOR

FANNY MEUNIER

JURY MEMBERS

F. COLLIN, promoter
F. NGUYEN
G. CORMAN
R. DE LA VAISSIÈRE (ANDRA)

Master's thesis presented in partial fulfilment of the requirements for master's degree "Ingénieur civil des mines et géologue" at the University of Liège

ACKNOWLEDGMENTS

This section aims at thanking warmly every person who contributed directly and indirectly to the realisation of this master's thesis.

First, I would like to thank my promoter, Frédéric Collin, for all the precious time he could allocate to help me at every step. I would not have been able to go through all Lagamine's specific features without him.

Next, thank you to Gilles Corman and Rémi de la Vaissière for having provided me with all the needed material for the realisation of this work. And, more specifically to Gilles for his precious advices during the proofreading of this thesis draft.

Then, during the last months, when I was not at university working on this thesis, I was at home talking and thinking about it. Therefore, I would like to thank my family for their constant support and patience, even though the subject of my preoccupations might have seemed a little abstract to them. A special though to Yohan who had to deal with explanations he didn't understand a word but also with all the "I won't make it" in moments of doubt (during the writing of this thesis but also during the last five years…).

I also think about Sarah with who we mutually shared our joys and fears during these last few months. Thank you for having been so invested in listening to me talking about this thesis but also to having read it and giving me some useful advice. But more globally, I want to thank her and Camille for having made these last five years more bearable.

Moreover, during these writing months, I also had the chance to make my internship at the VTT (research centre of Finland). Even though I used no results from the work performed there, all theoretical knowledge as well as the way of working helped me a lot. Therefore, I would like to thank Sami Naumer and Veli-Matti Pulkkanen for that.

Finally, a thought also for Justin with whom I shared the room these last months. Thank you for the tricks and tips with Lagamine but also for being supportive all the way long, especially the last few weeks.

ABSTRACT

Since the day nuclear power plants were put into service, the best solution to deal with radioactive wastes that emanate from the process is sought. In this framework, national organisations (ONDRAF for Belgium, ANDRA for France, etc.) were implemented to do some research on the topic. The one solution they favour for the long-term management of nuclear wastes is the deep geological repository. However, these comprise a lot of technical issues. One of them is the generation of gas by corrosion of metal compounds (such as canisters containing the wastes) that could rise in pressure and lead to bedrock fracturing, resulting in a lack of tightness of the disposal. ANDRA tries to study this phenomenon by experimental in-situ campaigns (carried out in an underground lab) during which gas is injected into the bedrock. The aim of this master's thesis is to reproduce one of these campaigns (namely PGZ3) by developing various numerical models with an increasing complexity.

A first part of this work aims at giving an overview of theoretical notions required to understand the specifications of the development of the numerical models. These notions cover background information about the management of nuclear wastes, including deep geological disposals in more details, the hydromechanical behaviour of porous media and gas transport in porous environments. A brief presentation of the PGZ3 experiment is also made.

Then, the first model that is developed is a purely hydraulic one-dimensional one. The latter allowed to identify the sequence of simulation steps needed to set the right boundary and initial conditions to perform a gas injection into the model. It also helped to get a first idea of the hydraulic variables evolutions and to calibrate parameters.

The next step is the introduction of mechanics in addition to the gas and water flows. This step is highly important as it allowed to identify stresses induced by the gas pressure. It was then possible to highlight eventual fracturing when the gas injection rate is important.

Finally, a two-dimensional model was developed to identify the parameters affecting the distribution of pressures along the borehole from which gas is injected. Indeed, in-situ results showed evidence that the gas might percolate along the contact surface between the rock and the tube. Factors affecting that eventual percolation are then highlighted in the last part of the work.

To conclude, the results obtained by numerical simulations are compared to the in-situ experiment results. Both seem to follow the same trends and reach similar pressure values.

RÉSUMÉ

Depuis le jour où les centrales nucléaires ont été mises en service, des recherches sont réalisées afin de trouver la meilleure solution pour traiter les déchets radioactifs qui émanent du processus. Dans ce cadre, des organismes nationaux (ONDRAF pour la Belgique, ANDRA pour la France, etc.) ont été mis à contribution pour effectuer des recherches sur le sujet. La solution privilégiée pour la gestion à long terme des déchets radioactifs est le dépôt en couches géologiques profondes, mais celui-ci comporte de nombreux problèmes techniques. L'un d'entre eux est la génération de gaz par la corrosion des composés métalliques (tels que les fûts contenant les déchets) qui pourrait augmenter en pression et conduire à la fracturation de la roche-mère, entraînant un manque d'étanchéité du stockage. L'ANDRA tente d'étudier ce phénomène en réalisant des campagnes expérimentales in-situ (réalisées dans un laboratoire souterrain) au cours desquelles du gaz est injecté dans la roche-mère. L'objectif de ce travail de fin d'études est de reproduire l'une de ces campagnes (à savoir PGZ3) en développant différents modèles numériques de complexité croissante.

Une première partie de ce travail vise à donner un aperçu des notions théoriques nécessaires à la compréhension des spécifications du développement des modèles numériques. Ces notions couvrent le contexte de la gestion des déchets nucléaires, y compris les stockages géologiques profonds plus en détail, le comportement hydromécanique des milieux poreux et le transport de gaz dans les milieux poreux. Une brève présentation de l'expérience PGZ3 est également faite.

Ensuite, le premier modèle développé est un modèle unidimensionnel purement hydraulique. Celui-ci a permis d'identifier la séquence d'étapes de simulation nécessaire pour établir les bonnes conditions aux limites et initiales afin de réaliser une injection de gaz dans le modèle. Elle a également permis de se faire une première idée sur l'évolution des variables hydrauliques et de calibrer les différents paramètres du modèle.

L'étape suivante est l'introduction de la mécanique en plus des flux de gaz et d'eau. Cette étape est très importante car elle a permis d'identifier les contraintes induites par les pressions de gaz. Il a alors été possible de mettre en évidence une éventuelle fracturation lorsque le taux d'injection du gaz est important.

Enfin, un modèle bidimensionnel a été développé pour identifier les paramètres affectant la distribution des pressions le long du forage à partir duquel le gaz est injecté. En effet, les résultats in-situ ont montré que le gaz pourrait percoler le long de la surface de contact entre la roche et le tube. Les facteurs affectant cette éventuelle percolation sont alors mis en évidence dans la dernière partie du travail.

Pour conclure, les résultats obtenus par les simulations numériques sont comparés aux résultats des expériences in-situ. Les deux semblent suivre les mêmes tendances et atteindre des valeurs de pression similaires.

TABLE OF CONTENT

TABLE OF FIGURES

GENERAL INTRODUCTION

Since the day nuclear power plants were put into service, the best solution to deal with radioactive wastes that emanate from the process is sought. In this framework, national organisations (ONDRAF[1] for Belgium, ANDRA[2] for France, etc.) were implemented to do some research on the topic. The one solution they favour for the long-term management of nuclear wastes is the deep geological repository. However, these comprise a lot of technical issues. One of them is the generation of gas by corrosion of metal compounds (such as canisters containing the wastes) that could rise in pressure and lead to bedrock fracturing, resulting in a lack of tightness of the disposal. ANDRA tries to study this phenomenon by experimental in-situ campaigns (carried out in an underground lab) during which gas is injected into the bedrock. The aim of this master's thesis is to reproduce one of these campaigns (namely PGZ3[3]) by developing various numerical models.

A first part of this work is devoted to the presentation of background information about nuclear energy, the types of wastes that are generated from it and the possible measures concerning their management. A special attention has been given to deep geological disposals and their technical challenges. One of them, gas generation from corrosion, being the main topic of this thesis, is more deeply introduced.

To be able to develop a hydromechanical numerical model, physical laws and equations behind the software should beforehand be understood. Consequently, these are presented in the following chapters.

Once the general context and theoretical notions will be covered, the second and main part of the thesis focuses on the numerical models developed to reproduce the PGZ3 experiment. Multiple simulations with an increasing complexity were performed. Indeed, at first, simulations consist in a flow model in one dimension. Then, gradually, an Excavated Damage Zone (EDZ), the mechanics and a two-dimensional model are introduced. For each one of them, a description of the model (geometry, initial and boundary conditions, etc.) is proposed before the presentation of the results. These latter include the evolutions of water and gas pressures, water saturation and mechanisms of gas transport, but also, for models comprising mechanics, evolutions of stresses and deformations. The last two aim at identifying a potential fracturing of the bedrock and, consequently, preferential pathways for radioactive compounds leak. Finally, a last chapter is dedicated to the comparison of these numerical simulations results with the ones observed in situ.

The goal by the end of this work is then to characterise the gas migration through the bedrock and determine whether it could cause fracturing problems or not. This by reproducing the PGZ3 experimental procedures in the best way possible, with the help of numerical simulations.

[1] National Organisation for Radioactive Wastes and enriched Fissile materials
[2] National Agency for Radioactive Wastes management
[3] PGZ means perturbations induced by gas

In the current socio-political context, nuclear energy as a source of electricity, together with the choice for treatment of radioactive wastes are highly controversial topics for multiple reasons. This thesis aims at presenting the feasibility of one aspect (gas generation) of deep geological storage only from a scientific point of view and not at participating to whatever socio-political debate.

Part I THEORETICAL BACKGROUND

Chapter I.1 GLOBAL CONTEXT

Section 1.1 NUCLEAR ENERGY

1.1.1 GLOBAL AND NATIONAL OVERVIEWS

Due to the constant development of new technologies, growth of population and increase in standards of living, the need for electricity has steadily risen over the last decades. There are several ways of producing electricity. Among them, nuclear power plant is the one which we will focus on in this work.

As it can be seen in Figure 1, in 2019, it accounted for 10% of the world electricity[4] production, after coal, hydroelectricity, and natural gas. Moreover, it can be noticed that nuclear electricity generation remains steady since the 90s.

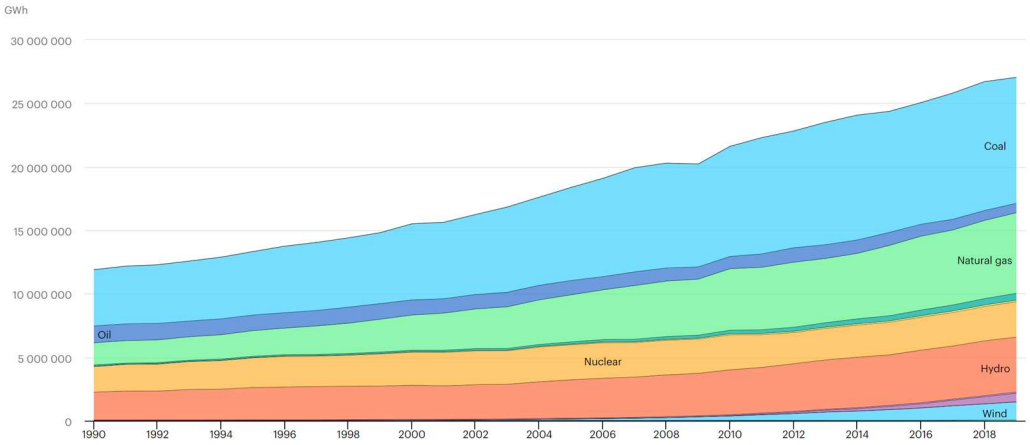

FIGURE 1 – WORLD ELECTRICITY GENERATION BY SOURCE IN 2019 (IEA, 2021)

Concerning the distribution of the world production (see **Erreur ! Source du renvoi introuvable.**), the 441 nuclear reactors are mostly concentrated in the most developed countries. However, according to the World nuclear association (2022), more than thirty new countries (called emerging nuclear energy countries) plan or have already started to introduce nuclear energy as part of their energy mixes. Among them, there are for examples Bangladesh or Turkey which already have plants under construction. The world distribution of nuclear energy production is then expected to change in the upcoming decade.

At national scales, Belgian and French nuclear electricity generations are more important and account for around 50%[5] and 65%[6] of the energy mixes respectively in 2019 (IEA, 2021).

[4] World total electricity production in 2019 was 27 TWh.
[5] Belgian total electricity production in 2019 was 88 GWh.
[6] French total electricity production in 2019 was 580 GWh.

In this context, the management of nuclear power plants from the building of the installations to their functioning and dismantling is an essential topic. Each country has its own management procedures. In Belgium, there are multiple organisms which take part to these management processes, including ENGIE (exploitation of power plants), Synatom (management of the radioactive substances), AFCN[7] (safety controls), ONDRAF (wastes management), etc. But over these organisms, the final decisions about the global management are taken by the Belgian Government.

Rank	Countries	Operable reactor net capacity [MW]	Rank	Countries	Reactors under construction net capacity [MW]
1	USA	94.7	1	China	19.4
2	France	61.3	2	India	6
3	China	52.1	3	South Korea	5.3
4	Japan	31.7	4	Turkey	3.3
5	Russia	27.8	5	United Kingdom	3.3
6	South Korea	23.1	6	UAE	2.7
7	Canada	13.7	7	Japan	2.7
8	Ukraine	13.1	8	Russia	2.6
9	Spain	7.1	9	USA	2.2
10	India	6.9	10	Bangladesh	2.1
/	Belgium	5.9	/	Belgium	N/A

TABLE 1 – TOP 10 COUNTRIES OWNING OR BUILDING NUCLEAR REACTORS (WORLD NUCLEAR ASSOCIATION, 2022)

1.1.2 NUCLEAR POWER PLANT FUNCTIONING

To understand where the nuclear wastes come from, it should first be understood how a nuclear power plant works.

The chemical process under the functioning of a nuclear power plant is nuclear fission. It consists of splitting, through the collision with a neutron, an unstable nuclear atom (such as Uranium 235) in two lighter atoms. This reaction releases a huge amount of energy, as well as radioactive rays and some neutrons. The latter collide in turn with other heavy nuclear atoms, provoking fission chain reactions.

In Figure 2, the whole process of electricity production through nuclear energy is presented. The fission process happens in the reactor and releases a huge amount of heat. This heat energy makes water temperature, included in an external circuit around the heart of the reactor (primary circuit), rise. The rise in primary circuit temperature makes water temperature in the secondary circuit increase as well. As temperature rises, water circulation is allowed (by evaporation). It leads then to the rotation of a turbine, connected to a generator which produces electricity. After its passage through the turbine, water of the secondary circuit is cooled down by a third water circuit connected to a cooling tower.

[7] Federal Agency for Nuclear Control

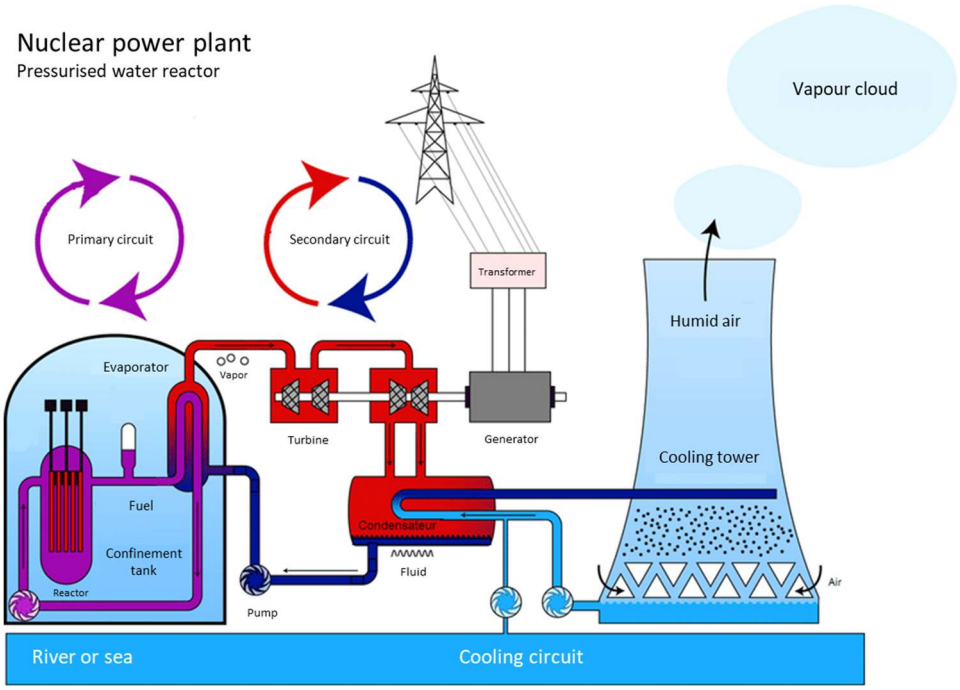

FIGURE 2 – NUCLEAR POWER PLANT FUNCTIONING (ADAPTED FROM COCHARD (2017))

More specifically, in the reactor, uranium is under the form of fuel pellets. Twenty-five of these are assembled to form fuel pencil of about four meters long. Fuel pencils are in turn put together to constitute fuel bundle. These latter are then put in state in the nuclear reactor to form a layer producing around 1000 MW (depending on the type of reactor). These different elements are represented in Figure 3. The fuel has a lifetime of about three to four years. This means that, every three years, it is estimated that 72 tonnes of spent uranium are taken out of the reactor and is most of the time considered as a waste (not useful anymore). The main issue with these wastes of spent fuel is radioactivity. Indeed, it is considered more than 10,000 times bigger than radioactivity of uranium ore (when it comes out of discharge from the reactor). (Collin, 2021; NWMO, 2022)

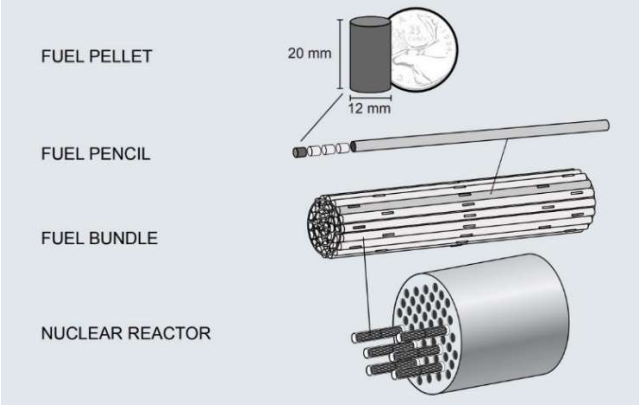

FIGURE 3 – URANIUM ASSEMBLIES IN NUCLEAR POWER PLANTS (NWMO, 2022)

In this framework, radioactive wastes are produced of course through the process of electricity generation but also through the dismantling of old plants as well as daily equipment also account. It can be added that radioactive wastes can also be generated in other fields such as medicine, agriculture, research, etc. These wastes present specific properties that require proper management. This is the subject of the following section.

1.1.3 URANIUM AS A RESOURCE (UPSTREAM MATERIAL)

This section aims at a better understanding of the uranium extraction, production, and enrichment steps, before its implementation in nuclear powerplants.

To begin with, the uranium is extracted from minerals (pitchblende/uraninite or brannerite) with concentrations ranging from 0.1 to 20%. In 2020, the world production was around 50 kt. The four major producing countries were Kazakhstan (40%), Australia (12%), Namibia (10%) and Canada (8%) (L'élémentarium, 2022). The reserves and resources reach namely 10 Mt and 22 Mt[8] (NEA & IAEA, 2020).

Different extractive technologies can be applied to recover uranium, depending on the nature of the deposit (type of rock, depth, size, etc.). The main technique (applied to 55% of 2020 production) was in situ leaching. It consists in injecting leaching agents (such as sulfuric acid) in the rock layer containing the uranium, which will be dissolved and transported in the solution. The enriched solution is then pumped back and treated in surface to recover uranium. Given the reduced costs needed to perform the process, this extraction process allows the recovery of uranium from deposits which have lower grades. However, it is only feasible in very specific geological contexts (permeable layer surrounded by non-permeable layers). Therefore, in other deposits, more conventional extraction techniques such as open-pit and underground mining are applied. However, due to the radioactive characteristic of uranium, very automated equipment is used to avoid contact between workers and radiations. It can be added that a small part of uranium (7%) is also produced as a by-product of other metals such as copper, zinc, etc. (L'élémentarium, 2022)

The enriched solution is then concentrated by hydrometallurgy to form a substance called yellow cake. The uranium contained in the yellow cake is only made up of less than 1% uranium 235, the rest being other isotopes (mostly uranium 238). However, because of its chemical nature, only uranium 235 is suitable for fission. Therefore, the concentrate still needs to go through multiple processes (purifications, conversions, etc.) to obtain its final form used in nuclear power plants.

It is important to mention that the energy extracted from one kilogram of uranium is equivalent to three million times what is extracted from one kilogram of coal or to one million times from one kilogram of oil.

1.1.4 RADIOACTIVE COMPONENTS (DOWNSTREAM MATERIAL)

After fission, multiple products, in addition to uranium, can be found in nuclear power plants. These are given, with their half-life time for radioactive components, in Table 2 below. The production quantities correspond to the products found after the irradiation (at 33,000 MW/day) of one tonne of uranium oxide (enriched at 3.5% for ^{235}U), after a three-year cooling. The need for a long-term management of these wastes is highlighted from these data as half-life times from fission products reach thousands of years.

[8] Reserves corresponding to "reasonably assured resources" and resources to "inferred resources" and "identified recoverable resources" in NEA & IAEA (2020).

Products	Mass [kg]	Half-life time [years]
Uranium 238	941	4.5 billion
Uranium 235	10	700,000,000
Uranium 236	4	23,420,000
Plutonium 238	0.17	86
Plutonium 239	5.72	24,400
Plutonium 240	2.21	6,600
Neptunium 237	0.42	2,140,000
Americium 241	0.22	432
Americium 243	0.10	7,380
Curium 245	0.02	8,532
Others	36	/

TABLE 2 – FISSION PRODUCTS FOR ONE TONNE URANIUM (L'ÉLÉMENTARIUM, 2022; RADIOACTIVITY.EU, 2022)

1.1.5 INTERNATIONAL AUTHORITIES

At the international level, there are reference organisations for regulating the different aspects of nuclear energy. A first one is the International Atomic Energy Agency (IAEA), it is an agency of the United Nations. Its role is to promote the safe use of nuclear energy (including limiting its use as a weapon). The agency owns numerous revues and journals which share about innovative technological aspects of nuclear energy, some of which were used to produce this work. Other organisations are the World Nuclear Association (WNA) and the Nuclear Energy Agency (NEA).

However, these organisations only provide norms and rules to ensure safe handling of radioactive substances. They do not impose treatment or management methods to deal with nuclear wastes. Therefore, as it will be explained in the next section of this work, it exists numerous ways to manage these, according to the decisions taken individually by each country.

1.1.6 MEASUREMENT UNITS FOR RADIOACTIVITY

It exists several units to characterize radioactivity. The first one is the Becquerel (Bq) which measures the activity of a radioactive source, i.e. the number of nuclei that emit radiation per unit of time. One becquerel is equivalent to one radioactive decay per second.

Then, the Gray (Gy) measures the absorbed quantity of radioactivity, i.e. the energy given to matter by ionising radiation passing through it. One gray is equivalent to one joule absorbed per kilogram of matter.

Finally, the Sievert (Sv) is the unit that allows the measurement of the impact on human beings. Indeed, it is not a quantity physically measurable, it is obtained by multiplying the absorbed energy (quantity in gray) by coefficients which depend on the type of radiation and on the impacted tissue.(AFCN, 2017)

Section 1.2 NUCLEAR WASTES

1.2.1 TYPES OF NUCLEAR WASTES

It exists different types of nuclear wastes. Upon the country, classifications can differ from each other. In Belgium, they are categorized according to their radioactive activity as well as their half-life time (see Table 3).

	Low activity wastes	Medium activity wastes	High activity wastes
Short lifetime wastes	Category A	Category A	Category C
Long lifetime wastes	Category B	Category B	Category C

TABLE 3 – CLASSIFICATION OF NUCLEAR WASTES

The activity is determined upon the sievert quantity. The ranges for the classifications are <5 mSv for low activity, between 5 mSv and 2 Sv for medium activity and > 2 Sv for high activity wastes. As for the lifetime, it is considered short if the half-life time remains below 30 years. (ONDRAF, 2022c)

According to the category a waste belongs to, its treatment will be adapted. Indeed, category A nuclear wastes are currently disposed in surface. However, for wastes of category B or C, as they will emit harmful radiations for thousands of years, surface disposal can't be a long-term solution. Disposal options, alternatives and pre-treatment will be further discussed in point 1.2.2. However, Belgian authorities, as well as other countries, consider deep geological disposal as the best option for now (IAEA, 2003; ONDRAF, 2022c).

The volume of radioactive wastes upon their categories for different countries are presented in Table 4 below.

	Category A	Category B	Category C
Belgium[9]	70 500 m^3	8900 m^3	3000 m^3
France[10]	971,000 m^3	136,700 m^3	4,190 m^3
Europe[11]	5,280,000 m^3	1,520,000 m^3	N/A

TABLE 4 – VOLUME OF RADIOACTIVE WASTES

It should be noted that, even though category A represents more than 85% of nuclear wastes volume, il only contains 1% of the radioactivity. On the other hand, more than 90% of the total radioactivity is contained in category C wastes. This means that most of radioactivity, and thus of harmful components, is contained in a limited volume of wastes. The management issue consists then in the radioactivity level of the wastes more than in their volume.

[9] Estimated cumulated volume in 2070 (Collin, 2021)
[10] Cumulated volume in 2020 (ANDRA, 2020)
[11] Estimated cumulated volume after final dismantling of power plants (Jungjohann et al., 2019)

1.2.2 TREATMENT SOLUTIONS

Before disposal, some treatment measures can/must be undertaken, among which: volume reducing, confinement or temporary disposal.

The reduction of volume is necessary to limit the space needed in disposals. It can be performed by several techniques, such as:

- **Compacting**

According to their physical characteristics, radioactive waste compaction can take different forms. Indeed, solid and flammable wastes are incinerated at 1000°C, then the ashes are placed in steel canisters[12] which are mechanically compacted in a "supercompactor". As for solid but non-flammable wastes, they are directly placed in barrels which also undergo the "supercompactor". Finally, liquid wastes can be treated by chemical or thermal ways. (ONDRAF, 2022b)

- **Recycling**

A difference should be made between open and closed fuel cycles. The usual ones are the open cycles and are performed in most countries. However, some countries such as France, India or Russia perform closed cycles which consist in using again a part of the spent fuel as a reactive in the nuclear power plants, this is called reprocessing or recycling. The process consists in reprocessing spent fuel to split it in several components, including uranium and plutonium. The part of spent fuel which can't be recycled (minor actinides, fission and activation products) is considered as a waste (category C). (IAEA, 2022)

- **Transmutation**

It consists in transforming radioactive nuclei with a long lifetime to elements with a shorter one. It happens thanks to the absorption of an additional neutron by the nuclei which conducts to the modification of its properties (such as radioactivity or lifetime) or to fission. However, this reaction can't be applied to all components of high activity wastes and is, therefore, not an alternative to deep geological disposal. (IRSN, n.d.)

- **Plasma technology**

This process aims to reduce the volume of wastes by 80 by melting them with a plasma torch heated at 5000°C. The technology was lately optimized by Belgoprocess (a subsidiary of ONDRAF) but is not yet used. (Forum Nucléaire, 2022)

After volume reduction, the next step is to immobilize and confine the nuclear wastes. To do that, wastes are placed in steel barrels which are then filled with cement. Finally, the canisters are disposed in temporary or final disposals, according to their category.

1.2.3 LONG-TERM MANAGEMENT POSSIBILITIES

Concerning the final disposal, as already said previously, it can be done in surface or in the subsurface at low or high depth. It should be noted that other solutions were considered but were abandoned for obvious reasons. One example would be the storage in seas or oceans. This was actually performed by some countries (including Belgium) in the 1950s but was obviously forbidden for environmental reasons. Another example would be the possibility of sending wastes to space. However, for logistical, economic, ethical and environmental reasons, this possibility is not conceivable.

[12] Canisters are round or cylindrical containers used for storing such things as food, chemicals or rolls of film (Oxford Languages, 2022) but these are also used to store radioactive wastes.

As represented in Figure 4, it is possible to store wastes at various depths in the subsurface. However, the greater the depth, the better the isolation with human activities at the surface. As a consequence, wastes of category A would be more suitable for surface disposals while those of categories B and C should be stored as deep as possible to be the most isolated from the living environment. However, a compromise should be found with the costs (the deepest, the most expensive).

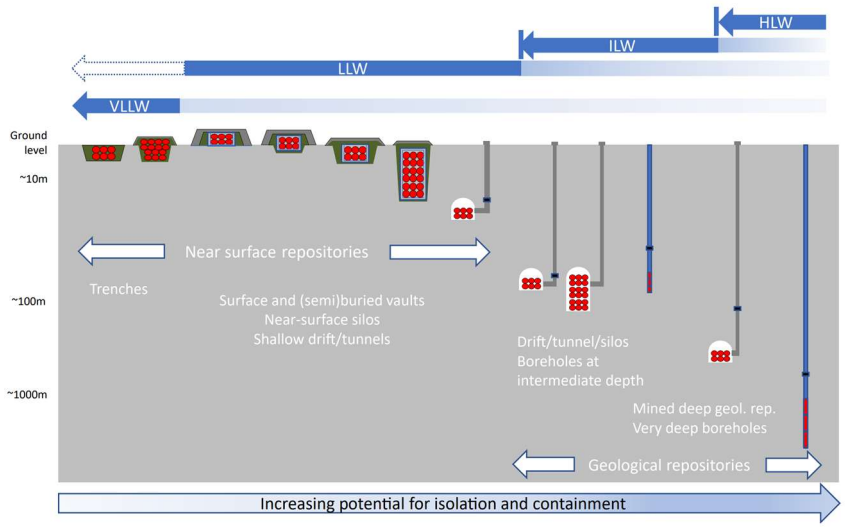

FIGURE 4 – DISPOSALS POSSIBILITIES IN THE SUBSURFACE WITH INCREASING DEPTH (IAEA, 2020)

Another aspect that is discussed when broaching deep-geological storage is the possibility of **retrievability** of wastes. In other words, it is the non-permanent characteristic of the disposals. There are multiple reasons why the retrievability of wastes is considered, from which:

- The development of new technological strategies to treat nuclear wastes in safer ways, as well as new social or environmental considerations that could give future generations elements to take more appropriate decisions on the management.
- The occurrence of an unexpected technical limit compromising the effectiveness of disposal.
- Providing (or improving) public confidence.
- Enabling the exploitation of the radioactive wastes as mineral resources (which is not economically viable and technically feasible for now but could be in the near future).

However, it exists also some reasons why the retrievability should not be implemented or not for too long. Some of them are:

- The future generations, which didn't take advantage of nuclear energy, should not be responsible, economically and socially, for the monitoring and the permanent closure of the storage.
- The retrievability would go against the "Treaty on the Non-Proliferation of Nuclear Weapons"[13].

[13] This treaty was signed in 1972 by the IAEA (International Atomic Energy Agency) and various States and it states that nuclear safeguards can only be abandoned if the nuclear material is practicably irretrievable. (IAEA, 2009)

- Higher costs required (longer monitoring, adapted system components…).
- The site might be abandoned opened if the socio-political context is no longer favourable.
- The long-term safety could be reduced due to the faster degradation of engineered barriers.

Once again, each country will adopt its own strategy for the retrievability including the application of the measure or not, the time during which the disposal should stay open, the buffer material, as well as technological adaptations. Indeed, these considerations also depend on the storage characteristics such as the rock type, the layout of the disposal, etc. (IAEA, 2009)

1.2.4 NATIONAL MANAGEMENT DECISIONS

From all the possibilities that were presented in the previous section, each country has its own management procedure concerning radioactive wastes.

First, in Belgium, there are multiple organisms/companies taking part to the nuclear waste pathway. Indeed, as shown in Figure 5, ENGIE deals with the electricity production and management of centrals, ONDRAF (and its subsidiary, Belgoprocess) is in charge of the disposal, while Synatom deals with all the other aspects (providing the uranium, treatment of wastes before disposal, etc.). Above these actors, the Belgian federal government and, more specifically, the ministers of energy and economic affairs take the main decisions. (Synatom, 2022)

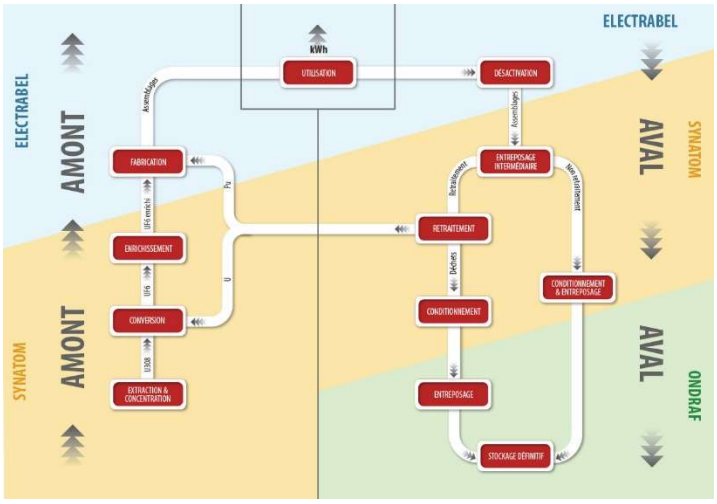

FIGURE 5 – ACTORS IN NUCLEAR WASTES MANAGEMENT IN BELGIUM (SYNATOM, 2022)

For now, the Belgian government has taken decisions over the management of radioactive wastes of category A, but not yet for categories B and C. Wastes of category A will be disposed in surface in a big hall, currently under construction, in Dessel. As for wastes of categories B and C, they are currently in temporary surface storages (in pools or halls nearby the electricity production plants). However, the project for the final disposal currently considered by ONDRAF would be the deep geological storage.

Then, in France, the approval of the government for the deep geological disposal for high activity wastes has already been given. ANDRA studies then a potential location for the building of the infrastructure (project CIGEO). (ANDRA, 2022)

Finally, Finland or Sweden are examples where the deep geological storage for categories B and C radioactive wastes has been approved by governments and are expected to be in working conditions in the coming decade. (ANDRA, 2022)

Section 1.3 DEEP GEOLOGICAL STORAGE

1.3.1 PRINCIPLE

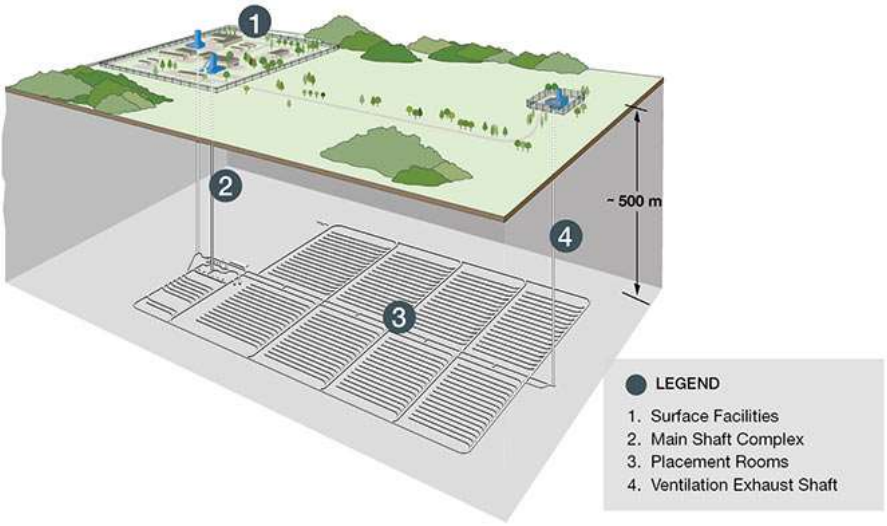

FIGURE 6 – DEEP GEOLOGICAL DISPOSAL GENERAL VIEW (SOS GREAT LAKES, 2022)

As represented in Figure 6, deep geological disposals consist in a large network of galleries from which start storage rooms of radioactive wastes. This infrastructure is to be found at high depth in the underground. One reason for that is that the major principle of deep geological storage is the combination of the retaining effects of multiple layers around the radioactive wastes to avoid the spreading of radionuclides. As shown in Figure 7, the frequent layers are the matrix mix in which the wastes are placed, the steel canisters and bentonite additionally to the appropriate geological layer. The latter however corresponds to the main protecting layer because the human-built facilities are destined to disappear at relatively short term (compared to the radioactive wastes lifetime). As the disposal is located in the deep underground, some supplementary facilities (such as access and ventilation shafts and a surface accommodation) are necessary.

Bentonite is a material mostly made of clay minerals used to protect and isolate the canisters from the environment, ensure a good contact between the canisters and the rock and retain and retard radionuclides migration (Jenni et al., 2019). It should be noted that, in some disposals, due to the constraint of letting the possibility of reversibility for disposals, the quantity of bentonite should not be too important.

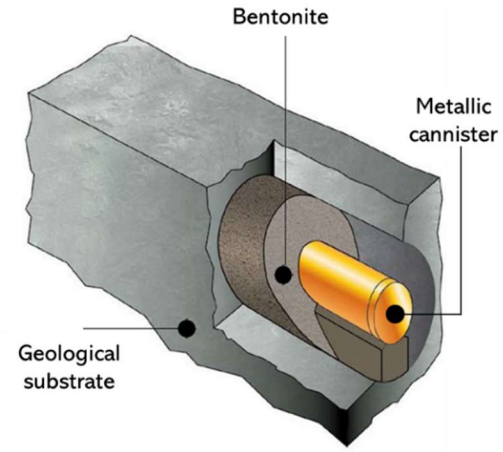

FIGURE 7 – MULTI-LAYER DISPOSAL REPRESENTATION (NORRIS, 2017)

The disposals can take different forms, the galleries can be either horizontal or vertical (see Figure 8). For example, in Finland and Sweden, the vertical configuration has been chosen while, in the French project CIGEO, horizontal galleries were preferred. One reason for that is again the possibility of recovery of the wastes in the long-term in horizontal ones.

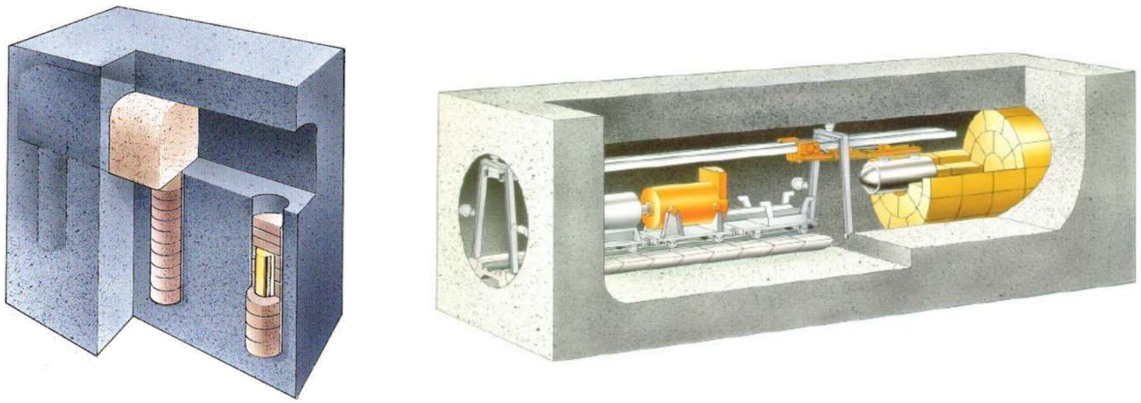

FIGURE 8 – VERTICAL (LEFT) AND HORIZONTAL (RIGHT) PLACEMENT OF GALLERIES (COLLIN, 2021)

Another configuration that was studied is the possibility of using old mines galleries for the storage instead of building new underground networks. However, these are only considered for radioactive wastes of categories A or B (Popov et al., 2019). Advantages of this technique are the fact that galleries and drifts are already built (costs are highly reduced) and the possibility of retrievability. However, retaining equipment in mines are most often designed to hold on only for a short period of time. Depending on the desired retrievability period, stability issues could occur, precautions should then be taken.

1.3.2 GEOLOGICAL LAYERS TO HOST WASTES

Deep geological repository includes the host rock as the main part of the insulation barrier between the environment and radioactive components. Therefore, the geological layer should include some criteria to ensure good conditions for the disposal, including long-term stability for the wastes. The present point aims at identifying these criteria and potential types of rock fitting these. The ones that could be identified are given below (ANDRA, 2005a; Collin, 2021; IAEA, 2009):

- **Low permeability**

The low permeability of the geological layer ensures a limited flow of the underground water through it. The flow should indeed be limited as it could favour the transport of potential radioactive components that would have leaked out of the disposal.

- **Homogeneity**

The presence of heterogeneous properties would complexify the study of the site of interest as well as drilling techniques.

- **No tectonic movements**

Tectonic events could induce fractures that would create preferential paths with high permeability for groundwater flow. It could also compromise the tightness of the multi-barrier and induce leaking of nuclear wastes with still a high radioactivity level.

- **Low economical interest**

As wastes should stay confined during tens of thousands of years before reaching an acceptable level of radioactivity, it must be ensured that the geological layer in which they are stored has no economic interest. This criterion can be hard to determine as it is impossible to know what kind of rocks/minerals could be valuable in thousands of years.

- **Few fissures**

Fissures could induce mechanical instability as well as preferential paths for groundwater, both having consequences mentioned hereabove. However, it should be noted that in some cases fractures (when they are filled with material with a low permeability) have retardation effects in the migration of radionuclides.

- **Stability**

Mechanical stability has already been broached through tectonic movements. However, the geological layer should also have mechanical properties that allow the drilling of stable galleries with the less retaining equipment possible (to reduce costs).
Chemical stability should also be ensured. A rock inducing water with a neutral or slightly alkaline pH is preferred to ensure long-term stability of building materials.

- **Thickness**

The layer of interest should be as thick as possible to welcome the whole underground infrastructure, including enough galleries to be able to store the entirety of wastes.

- **High thermal conductivity**

As nuclear substances will dissipate heat during the first decades of the disposal, a high thermal conductivity is an advantage. Indeed, the rock would be able to evacuate heat and not accumulate it too much in the disposal cells which could harm the equipment. Another problem with high temperatures in the repository is that it induces larger water pressures which would then lead to rock fracturing.

The types of rocks which could respect these conditions are granite/basalt (crystalline rocks), salt (evaporites) and clay. Advantages and drawbacks of each of these three geological layers for deep geological disposals are presented in Table 5 below.

Type of rock	Advantages	Drawbacks
Crystalline	- High mechanical strength, self-support, not much engineering support required - Low permeability - Low economic interest - High thermal conductivity	- Fragile material (fracture networks) - Difficult characterisation of fractures - No fracture cicatrisation

Argillaceous	- High mechanical strength - Low permeability - Low economical interest	- Plastic behaviour which could induce EDZs around excavations (engineering support required = liners) - Sealing significant (plastic clay) or speculative (clay rock)
Salt	- Liner usually not required - Low permeability - Significant creep - Sealing of fractures - Low economical interest	- Not suitable for retrievability - Sensitive to water inflow

TABLE 5 – ADVANTAGES AND DRAWBACKS FOR EACH TYPE OF ROCK (COLLIN, 2021; IAEA, 2009)

1.3.3 UNDERGROUND RESEARCH LABS (URL)

In order to study the feasibility of such storage infrastructures in a given layer of interest, some countries invested in underground labs in which a whole set of tests are performed. Such laboratories are built in Belgium, France, Switzerland, Finland, Sweden, China, Canada, etc.

Their aim is to characterise the geological layer in various aspects such as the mechanical properties, the response to heat or to gas generation, the insulation properties to radioactivity, etc. Therefore, based on the observations, simulations of the long-term behaviour of the rock can be performed and the feasibility of the project can be assessed.

The Belgian URL is located in Mol in Boom Clay. It was opened in the 1980s to demonstrate the feasibility of building an operational disposal. The main challenge was building a stable infrastructure in the geological layer which is composed of poorly indurated clays. This challenge was met and furthermore, the actual experimental results confirm the workability of the site to welcome such an infrastructure. (ONDRAF, 2022a)

The one we will focus on in this work is the French lab located in Bure (Meuse department). The geological formation in which it can be found is the Callovo-Oxfordian argillite. A deeper characterisation of this one is made in the next chapter. Its purpose is the same as other URL, i.e. highlighting the feasibility of a disposal in the geological layer of interest.

1.3.4 TECHNICAL ISSUES

Due to the complexity of such an infrastructure that a deep-geological storage of radioactive wastes represents, a lot of technical constraints can be identified. The main issue broached in this thesis is the gas generation arising from the corrosion of the canisters. However, this section aims at giving an overview of the multiple challenges met during the disposal lifetime.

One of them is the effect of temperature. Indeed, the radioactive wastes (exothermic material) emit a large amount of heat even though decreasing with time. According to (ANDRA, 2005b), the temperature inside the storage should not rise above 90°C but is negligeable between 100 to 250 meters away from it. Temperature increase could have impacts on hydraulic circulation as well as on chemical and mechanical processes.

As for the hydraulic aspect, the repository will be impacted by hydraulic circulations as much as it will disrupt the global circulation equilibrium. Indeed, during the building stage as well as the period before the closing, water is pumped or the ventilated air flow in the galleries. Both will impact the initial water flow in the geological layer. However, as rocks with a low permeability are mostly chosen, this perturbation should not reach other geological layers. As for the impact of hydraulic circulations on the repository longevity, it will mostly happen after the closing. These should induce the corrosion of the metal canisters and therefore produce hydrogen (this topic is more deeply approached in the following sections). Hydraulic circulations could as well initiate chemical processes or contribute to the transport of radioactive substances at longer term.

Chemical processes could also be broached. These mostly consist in corrosion of metallic elements, degradation of concrete and alteration of wastes, these having an impact on the leaking of radioactive compounds.

Lastly, mechanical effects also play a major role on the long-term efficacity of the disposals. Like for the hydraulic circulations, the building of the infrastructure will disturb the local initial equilibrium state of mechanical stresses. However, these perturbations should only impact the very near environment of galleries. Indeed, galleries are located far enough from each other not to couple their mechanical effects. As for the longevity of the disposal, it will also be directly impacted by the mechanical properties of the materials in which the disposals are built. Naturally, if mechanical failures appear, they could favour hydraulic flows and all interactions, including the faster propagation of radionuclides.

Naturally, as already said, all these mechanisms are coupled and have impacts on each other. For example, the temperature and water saturation speed chemical processes up. These coupling are sump up in Figure 9. Nonetheless, these won't be further described in the framework of the present thesis. (ANDRA, 2005b)

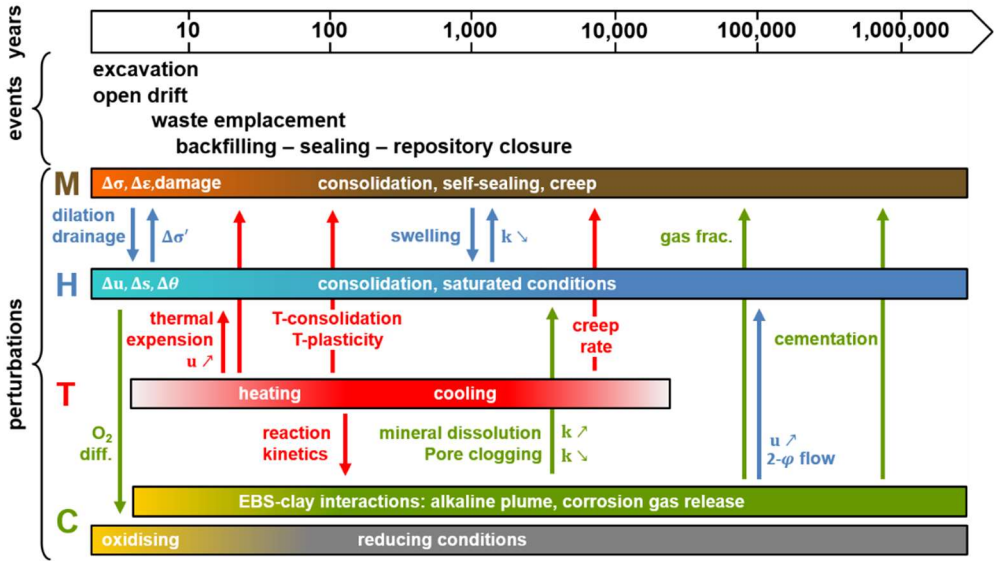

FIGURE 9 – THERMO-HYDRO-MECHANICAL (THM) EFFECT IN DEEP GEOLOGICAL REPOSITORIES (SILLEN, 2012)

Chapter I.2 FLUIDS BEHAVIOUR IN POROUS MEDIA

In order to understand how the gas generation can have an impact on the rock medium, some mechanical and hydraulic principles in porous media should be first presented. This is the purpose of the present section.

It should be noted that all equations and principles are described hereunder for biphasic flows, namely air and water. However, these can be adapted for other fluids such as hydrogen in place of air. By the way, during numerical simulations performed in Part II and Part III, it is imposed that only two fluids can coexist. Therefore, these couples will be air and water before the injection of hydrogen gas, and hydrogen and water after.

Section 2.1 DEFINITION OF POROUS MEDIA

In the medium we are looking at, three phases co-exist. First, the solid phase which is composed of solid grains, and which is therefore discontinuous. In the pores between the grains, gas and liquid phases are present. Mainly, the gas phase is composed of air and, the liquid one, of water. However, water can be found as liquid water but also in form of water vapour, then in a gaseous form. In the same way, air is mainly present as dry air in the gas phase but can also take the form of dissolved air the liquid phase. This is sum up in Figure 10 below.

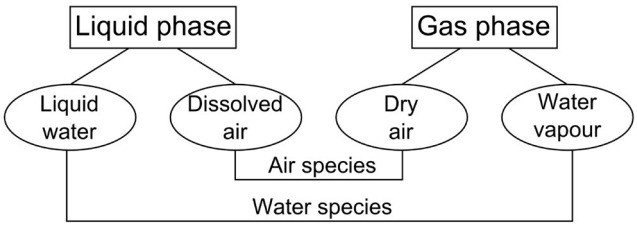

FIGURE 10 - COMPOSITION OF LIQUID AND GAS PHASES (COLLIN, 2003)

The proportion of air which will be dissolved in water is controlled by the Henry's law (Eq. 1 below). It states that the ratio of the volume of dissolved air in water and of the water volume amounts to a constant, the air solubility coefficient, this one being dependent on temperature and water density.

$$\frac{V_{da}}{V_w} = H^s(\rho_w, T) \qquad \text{(EQUATION 1)}$$

With V_{da} the volume of dissolved air in water, V_w the water volume and H^s the air solubility coefficient.

These three phases interact with each other following different principles (such as capillarity) which are defined hereunder.

Section 2.2 CAPILLARITY

As said previously, two fluids are in presence in the environment that is considered. When two immiscible fluids are in contact, an interface, on which superficial tensions are applied, is created between them. These superficial tensions result from the intermolecular forces difference inside a fluid or at its border with the other one. This is what is represented in Figure 11. (Gerard, 2011)

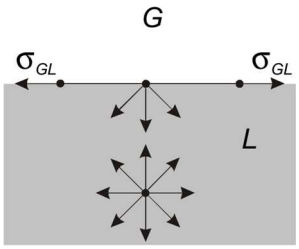

FIGURE 11 – INTRAMOLECULAR FORCES ON A WATER PARTICLE (GERARD, 2011)

A consequence of these tensions is capillarity. One way to understand the phenomenon is to have a look at the following example. In Figure 12, a capillary tube placed in larger vessel is represented. It can be noticed that water in the thinner tube rises above the level of water in the vessel. This is due to superficial tensions at the interface between both phases. The magnitude with which the liquid phase goes up in the tube depends on the tube radius, following Laplace's law (Collin, 2021; Gerard, 2011). This law states:

$$p_c = p_g - p_w = p_w g h = \frac{2\sigma_{GL}\cos\theta}{r} \qquad \text{(EQUATION 2)}$$

With p_c the capillary pressure, g gravity, h the height of water in the capillary tube, σ_{GL} the surface tensions between gas and liquid phases, θ the contact angle and r the radius of the capillary tube.

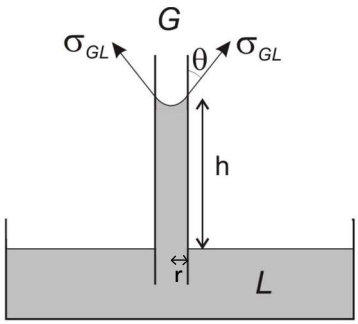

FIGURE 12 – CAPILLARY TUBE (GERARD, 2011)

This can be linked to a porous medium by the fact that pores between solid grains can be considered as small tubes in which capillarity effects are also observed (see Figure 13A). It is known that the smaller the solid grains, the smaller the pores between them. As a result, from Laplace's law, it can be stated that the smaller the solid grains, the more important capillary effects. It can also be added that surface tensions induce traction between grains, which are therefore attracted to each other and form a cohesive material. (Collin, 2021; Gerard, 2011)

However, the rocks considered in this master's thesis are clays. Due to the layered form of the clay minerals, the behaviour of the solid microstructure with water is slightly different (see Figure 13B). Indeed, water molecules are subjected to physico-chemical interactions of the clay minerals. However, evenif the behaviour is different, suction is defined as the difference between gas and water pressures (similarly to capillary pressure) and will be highly used further in this work to describe the hydromechanical behaviour of clay rocks. (Gerard, 2011)

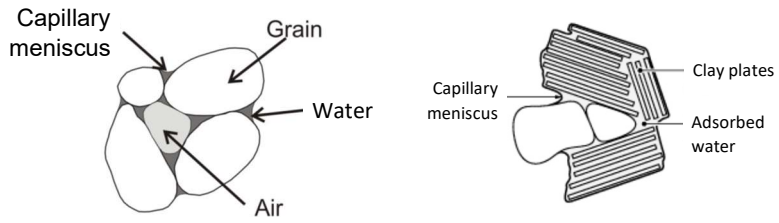

FIGURE 13 – REPRESENTATION OF CAPILLARY EFFECTS IN POROUS MEDIA (A – GRANULAR; B – CLAY) (ADAPTED FROM GERARD, 2011)

Section 2.3 RETENTION CURVE

Within the scope of saturation, it should first be introduced the notions of residual and effective saturations. Indeed, when a medium is dried or emptied, there is always residual water in smaller pores, whatever the capillary pressure which is imposed, this quantity is called residual saturation. In this situation the only way for water to be taken of the pores is evaporation. This phenomenon is the reason why an effective saturation is introduced. Its expression is defined in Equation 3. (Gerard, 2011)

$$S_{r,we} = \begin{cases} \dfrac{S_{r,w} - S_{res,w}}{1 - S_{res,w}} & \text{si } S_{r,w} > S_{res,w} \\ 0 & \text{si } S_{r,w} > S_{res,w} \end{cases} \qquad \text{(EQUATION 3)}$$

With $S_{r,we}$ [/] the effective water saturation, $S_{r,w}$ [/] the real water saturation and $S_{res,w}$ [/] the residual water saturation.

It should be noted that a residual gas saturation can be defined in a similar way as an immobilized fraction included in the liquid phase. The form under which gas can be found is small droplets and it can only be taken from there by dissolution and then diffusion in the liquid phase. (Gerard, 2011)

As introduced in the previous point, capillary effects play an important role when it comes to the characterisation of an unsaturated medium. Indeed, the degree of saturation of the porous medium (and therefore the relative quantity in each fluid) will be impacted by the capillary pressure. This influence can be modelled by a retention curve. It exists several mathematical models to represent the retention curve. However, in Gerard (2011), multiple models were applied to COX argillite and compared. The conclusion stated that both Vachaud-Vauclin and van Genuchten models (adapted in ANDRA (2005b)) were the most adapted to describe the rock we are interested in. The one that was chosen to build the numerical model in Parts 2 & 3 is the most used of both, van Genuchten. It is expressed upon Equation 4.

$$S_{r,w} = S_{res,w} + \left(1 - S_{res,w}\right)\left(1 + \left(\frac{p_c}{P_r}\right)^n\right)^{\frac{1}{n}-1} \quad \text{(EQUATION 4)}$$

Where p_c [Pa] is the air entry pressure, P_r [Pa] the van Genuchten capillary pressure and n [/] a model parameter.

A representation of this curve is made in Figure 14. The properties that were used correspond to different zones of the numerical model developed further in this work, i.e. P_r = 0.05 MPa (interval), 3 MPa (EDZ[14]), 15 MPa (COX), n = 1.49 (for all), $S_{r,res}$ = 0 (interval), 0.01 (EDZ & COX).

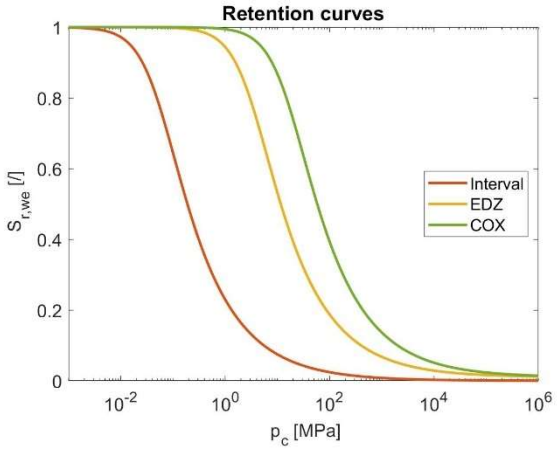

FIGURE 14 – RETENTION CURVES

Section 2.4 MULTIPHASE FLOW IN POROUS MEDIA

In order to solve the hydraulic part of the numerical model, the constitutive equations behind the model that will be used should be fully understood. These equations consist in flows of fluids, mass balances and state equations.

First, because fluids are compressible, the water and gas densities and viscosities that will be implemented in the different expressions depend on their pressures and temperature. State equations describe this phenomenon.

Then, displacement of fluids in porous media can be done under various forms, each of them being described by a mathematical expression. The different flows phenomena that will be considered in this work are the following:

- Advection of the liquid phase
- Advection of the gas phase
- Diffusion in the liquid phase
- Diffusion in the gas phase

Finally, mass balances should be made.

All equations mentioned in this point come from Collin (2021) and Lagamine (2020).

[14] See Section 2.8

Section 2.5 STATE EQUATIONS

There are four state equations for liquid phase and as many for gas phase. They first consist in density and viscosity expressions, then retention curve and relative permeability relations. These last two are described in other points of this work, only the first two are then given in the present point (Eq. 5 and 6).

$$\mu_w(T) = \mu_{w,0} - \alpha_w^T \mu_{w,0}(T - T_0) \quad \text{(EQUATION 5)}$$

Where μ_w [Pa.s] is the water dynamic viscosity, α [K^{-1}] the dynamic viscosity thermal coefficient for water and T [K] the temperature.

$$\rho_w(T, p_w) = \rho_{w,0}\left[1 + \frac{p_w - p_{w,0}}{\chi} - \beta_w^T(T - T_0)\right] \quad \text{(EQUATION 6)}$$

Where ρ_w [kg/m³] is water density, p_w [Pa] water pressure, $1/\chi$ [Pa^{-1}] water compressibility and β [K^{-1}] thermal expansion coefficient.

As for the air state equations, the first one describing the dynamic viscosity is similar to the one for the liquid phase. It is expressed as:

$$\mu_a(T) = \mu_{a,0} - \alpha_a^T . \mu_{a,0}(T - T_0) \quad \text{(EQUATION 7)}$$

Where μ_a [Pa.s] is the air dynamic viscosity, α [K^{-1}] the dynamic viscosity thermal coefficient for air.

The second equation which expresses the air density is however different to the one for water. Indeed, the gaseous phase is considered as an ideal gas, this is shown in Eq. 8.

$$\rho_a(T, p_a) = \rho_{a,0} . \frac{p_a}{p_{a,0}} . \frac{T_0}{T} \quad \text{(EQUATION 8)}$$

Where ρ_a [kg/m³] is the air density, and p_a [Pa] the air pressure.

It should be noted that the numerical model developed further will be computed at constant temperature. Therefore, the terms depending on temperature difference will cancel each other out.

2.5.1 ADVECTION OF LIQUID PHASE

The advection flux for the liquid phase is ruled by Darcy's law which can be expressed as:

$$q_l = -\frac{k k_r^w(S_{r,w})}{\mu_w}(\nabla p_w + \rho_w g \nabla z) \quad \text{(EQUATION 9)}$$

With k the intrinsic permeability, μ_w the water viscosity, ρ_w the water density, z the vertical coordinate, $S_{r,w}$ the water saturation and k_r^w the water relative permeability (this last one will be described in point 2.6.1).

2.5.2 ADVECTION OF GAS PHASE

Here also, the advection flux is defined by Darcy's law, which is expressed as:

$$q_g = -\frac{k k_r^g(S_{r,g})}{\mu_g}(\nabla p_g + \rho_g g \nabla z) \quad \text{(EQUATION 10)}$$

2.5.3 DIFFUSION IN LIQUID PHASE

The diffusion is represented by a Fick's law. In the liquid phase, it is expressed:

$$i_{(air)_d} = -\rho_w S_{r,w} n.\tau.D_{air}^w \nabla\left(\frac{\rho_{da}^w}{\rho_w}\right) \quad \text{(EQUATION 11)}$$

With $i_{(air)_d}$the diffused air, n the porosity, τ the tortuosity, D_{air}^w diffusion coefficient of air in liquid phase.

2.5.4 DIFFUSION IN GAS PHASE

For diffusion in the gas phase, Fick's law is expressed:

$$i_{(air)_g} = -\rho_g(1 - S_{r,w}) n.\tau.D_{air}^{vapour} \nabla\left(\frac{\rho_{air}^g}{\rho_g}\right) = -i_{(H_2O)_g} \quad \text{(EQUATION 12)}$$

With $i_{(H_2O)_g}$ the diffusive water vapour and the diffusion coefficient of dry air in the water vapour which is expressed:

$$D_{air}^{vapour} = D_0\left(\frac{P_0}{P_g}\right)\left(\frac{T}{T_0}\right)^{1.75} \quad \text{(EQUATION 13)}$$

2.5.5 MASS BALANCE

The mass balance can be done in different ways, according to chemical species (water and air) or to phases (liquid and gas). It was chosen in this work to be performed with chemical species. Moreover, the hypothesis of an equilibrium between the two phases was made.

First, the mass balance of water, as said previously, takes into account liquid water and water vapour:

$$\frac{\partial}{\partial t}(\rho_w \varphi S_{r,w} + \rho_{H_2O}^g \varphi S_{r,w}) + div(\rho_w q_l) + div\left(i_{(H_2O)_g} + \rho_{H_2O}^g q_g\right) - Q_{H_2O} = 0$$

With Q_{H_2O} the production – consumption of water (EQUATION 14)

Then, the mass balance of gas is the sum of contributions of dissolved air in water and of gaseous air:

$$\frac{\partial}{\partial t}(\rho_{air}^g \varphi S_{r,g} + \rho_{air}^g H_{air} \varphi S_{r,w}) + div\left(\rho_{air}^g q_g + i_{ai\ g}\right) + div(\rho_{air}^g H_{air} q_l + i_{ai\ d}) - Q_{air} = 0$$

(EQUATION 15)

Section 2.6 PERMEABILITY

A last aspect of fluid flow in porous media is permeability. Indeed, in Darcy's law appear variables called gas and water permeabilities which have major roles in the characterisation of fluids transport.

First, to understand what these represent, the notion of permeability should be introduced. The permeability of a rock is its capacity to be penetrated by a fluid. The higher the permeability, the easier a fluid flows though the porous medium. What is called intrinsic permeability allows to describe permeability independently of the fluid nature.

However, the degree of saturation of the medium has an impact on the value of its permeability. This is characterized by relative permeabilities.

$$k^{\text{unsaturated}} = k^{\text{saturated}}.k_r \qquad \text{(EQUATION 16)}$$

Relative permeability k_r as expressed in Equation16 is a coefficient which depends on the fluid nature. The ones that are interesting in the framework of this thesis are water and gas permeabilities. These have opposite behaviours with saturation. When a biphasic medium is saturated with water, water relative permeability is maximal while the gas one is minimal. This trend is inversed when a medium is saturated with air.

The relations between relative permeabilities and water saturation are computed thanks to mathematical models. Various models were developed; however, the focus here will be given to the ones that will be used in following numerical simulations.

2.6.1 WATER RELATIVE PERMEABILITY

The model that was chosen is the Van Genuchten one which is expressed:

$$k_{rw} = \sqrt{S_{rw}}\left(1-\left(1-S_{rw}^{\frac{1}{\text{CKW1}}}\right)^{\text{CKW1}}\right)^2 \qquad \text{(EQUATION 17)}$$

With CKW1 being an experimental constant (valued to 0.55 for COX, the interval and EDZ). The curve of water relative permeability in function saturation was plotted in Figure 15.

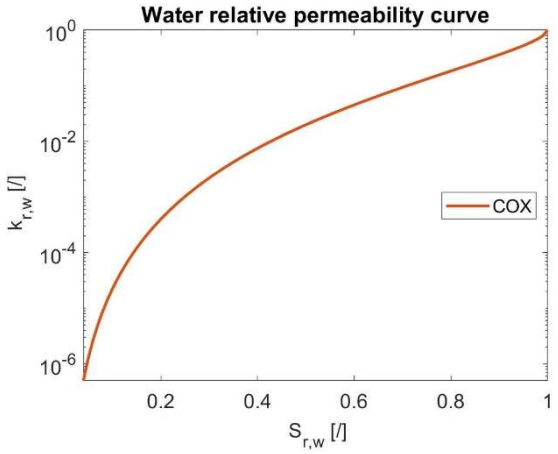

FIGURE 15 – WATER RELATIVE PERMEABILITY CURVE UPON VAN GENUCHTEN MODEL

In Darcy's law, this water relative permeability is multiplied with the permeability in saturated conditions (see Equation 9) whose value for the Callovo-Oxfordian formation is set to 5.10^{-20} m² (see Table 10).

2.6.2 GAS RELATIVE PERMEABILITY

The model chosen to express the gas relative permeability is the cubic relation which is expressed:

$$k_{ra} = \mathrm{CKA2}(1 - S_{we})^{\mathrm{CKA1}} \quad \text{(EQUATION 18)}$$

With CKA1 = 3 (for all environments) and CKA2 = 250 in the COX formation and 100 in the interval and EDZ.

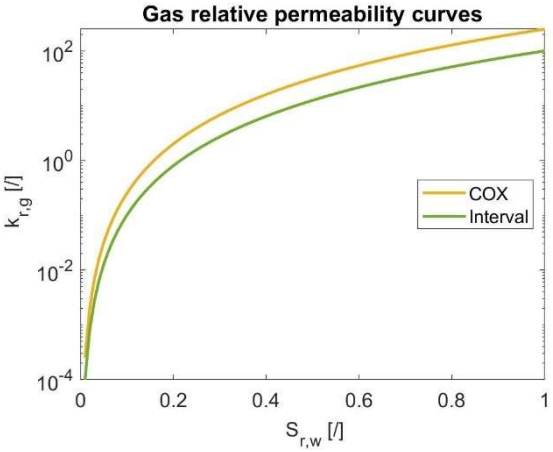

FIGURE 16 – WATER RELATIVE PERMEABILITY CURVE UPON CUBIC MODEL

As for water relative permeability, the gas one is multiplied by the permeability in saturated conditions whose value for each porous environment can be found in Table 10.

Section 2.7 HYDROMECHANICAL BEHAVIOUR

2.7.1 TOTAL AND EFFECTIVE STRESSES

Terzaghi principle states that the total stress a porous medium has two origins: pressure induced by water and stress at the contact surface of solid grains (called the effective stress). It is expressed like:

$$\sigma = p_w + \sigma' \quad \text{(EQUATION 19)}$$

Where σ [Pa] is the total stress and σ' [Pa] the effective stress.

However, Terzaghi made two hypotheses that cannot be respected in this master's thesis application. These hypotheses are the grain compressibility as well as the saturation of the media. For environments partially saturated and subjected to large stresses, the notion of effective stress of Bishop is introduced. In this case the total stress is expressed as:

$$\sigma = \sigma' + b\left(S_{r,w}p_w + \left(1 - S_{r,w}\right)p_g\right) \quad \text{(EQUATION 20)}$$

With b the Biot coefficient. The latter expresses the compressibility of solid grains through the following formulation:

$$b = 1 - \frac{K_d}{K_s} \quad \text{(EQUATION 21)}$$

With K_d being the compressibility modulus of the drained porous media and K_s the compressibility modulus of the solid grains.

Section 2.8 EXCAVATED DAMAGE ZONE

A last mechanical aspect that should be introduced is the presence of an excavated damage zone around a borehole when it is dig in clay or indurated rocks. Indeed, when a borehole is drilled at great depth, a mechanically altered area is developed around the borehole. The latter is due to the redistribution of stresses in the bedrock after the tunnel excavation.

The study of this area is highly important as the difference of mechanical properties will probably impact the way gas flows through the porous media. It should be noted that this aspect is easier to be studied in situ than on small samples. (Gerard, 2011)

Chapter I.3 GAS ISSUE

The purpose of this thesis is to determine the impact of gas generation in the deep geological nuclear waste deposits on the surrounding rock environment. More precisely, it should be determined if the impact of gas flow could damage the tightness of the repository. To do that, it should first be understood where the gas comes from and the different forms it can take to flow through a porous medium.

Section 3.1 GAS GENERATION

Gas in the context of deep geological deposits may have different origins and forms (Gonzalez-Blanco, 2017):

- Hydrogen production due to the anaerobic corrosion of metallic materials.
- Water vapour production due to the high temperature of the radioactive wastes.
- Methane and carbon dioxide production due to the degradation of organic materials.
- Various gas (hydrogen, oxygen, carbon dioxide, methane…) production due to gamma radiolysis.
- Helium production due to alpha decay.
- Radioactive gases production as product of fission or activation or daughter product of uranium and thorium decay.

In this thesis, it will be considered that all other sources than hydrogen production are negligeable. It is then more deeply investigated hereunder.

The metallic canisters in which the wastes are placed are the main source of corrosion. But, in some cases, other metallic elements such as stability elements or leftovers from the building phase of the repository can be found and play a role in the gas generation.

The chemical reaction that occurs and induces the production of hydrogen gas from metals is illustrated with iron as an example hereunder (Equation 22).

$$Fe_{(s)} + 2\ H_2O \rightarrow Fe(OH)_2 + H_{2(g)} \qquad \text{(EQUATION 22)}$$

Now that the origin and nature of gas is determined, it should be found the quantity of hydrogen that will actually be generated. As a first estimation, it is said that the production of hydrogen is proportional to the rate of corrosion of metal, the latter being the product of corrosion rate constant and the metal surface area (Gonzalez-Blanco, 2017). In Figure 17, an evolution of the quantity of gas generated (in a storage cell) based on the mean corrosion rate of radioactive wastes of type C is proposed (Gerard, 2011). It can be seen from it that the flux is the highest between 0 and 3,500 years and then decrease to reach a zero-flux generated after 50,000 years. Therefore, the gas migration is an issue which should be taken into consideration in the very first years of the deposits but also in long-term.

It should be noted here that for the numerical simulations that will be performed in Parts 2 and 3, the gas flux injected was not determined with the theoretical flux to be found in the present section but it was taken from PGZ3 experiment (the one which is modelled in the second part of this work) values.

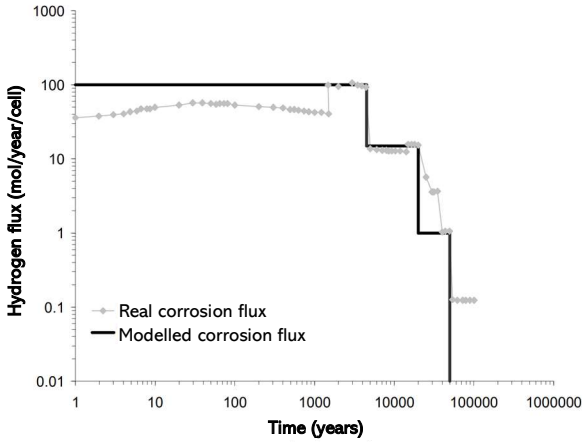

FIGURE 17 – HYDROGEN FLUX GENERATED BY CORROSION (GERARD (2011) ADAPTED FROM TALANDIER (2005))

Another issue with gas in the deep-geological deposits is due to the ventilation of galleries in the first years of the infrastructure. Indeed, there can be exchanges between the air in the deposits and pores of the rock. This can lead to the modification of the water saturation which can have various impacts such as the faster transport of radionuclides and a modification of the mechanical behaviour (Gerard, 2011). However, this part of the gas problematic won't be covered in this master's thesis.

Section 3.2 GAS MIGRATION

Once the gas is generated in the galleries, it can flow through the surrounding rocks following various transport mechanisms depending on the gas pressure. These mechanisms are illustrated in Figure 18 and described hereunder according to (Marschall et al., 2005).

- Low gas pressure – diffusive transport of gas dissolved in the pore-water:
  As mentioned in section 2.1, gas can be present in the liquid phase in a dissolved form. The proportion of gas in this form is controlled by Henry's law.
- Gas pressure reaches the air entry pressure – visco-capillarity two-phase flow:
  When gas pressure increases, it is not anymore only dissolved in water, but it forms its own gaseous phase. This new gas phase displaces the liquid phase according to the various multiphase principles approached in Chapter I-2, i.e. retention curve (including capillary forces), relative permeability, intrinsic permeability of the medium, etc.
- Gas pressure reaches the fracturing pressure – dilatancy-controlled gas flow, preferential paths:
  A further increase in gas pressure can modify the properties of the porous medium, such as the intrinsic permeability and the porosity, by the opening of preferential paths. The two-phase flow in the pores is still ruled by the laws cited hereabove, however their properties vary with the deformation state of the rock.
- Fast and high increase of gas pressure – gas transport along macroscopic tensile fractures:
  An even higher pressure can lead to the creation of macroscopic fractures in which gas can flow freely.

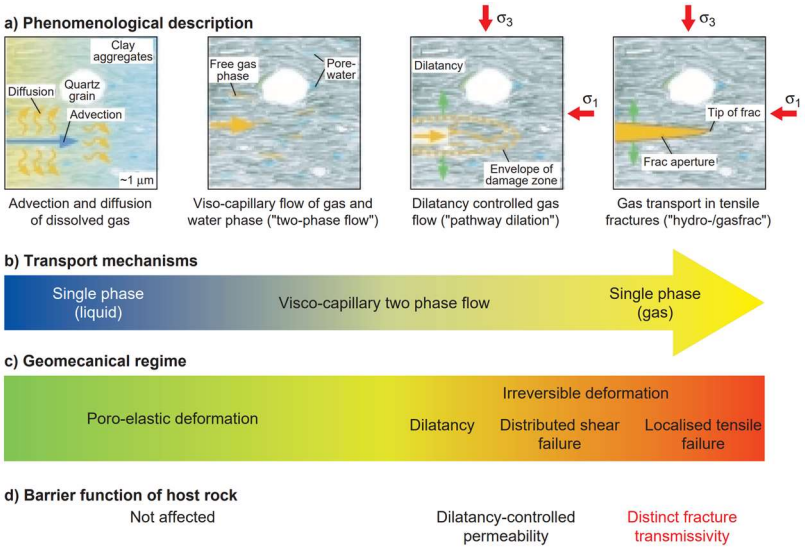

FIGURE 18 – GAS TRANSPORT MECHANISMS (MARSCHALL ET AL., 2005)

Section 3.3 STUDIES OVER THE GAS MIGRATION ISSUE

In order to understand the behaviour of gas in such environment, different means can be used. First, laboratory tests can be carried out to identify transport mechanisms at small scale and determine hydraulic and mechanical parameters of rock.

Then, in-situ campaigns of injection tests are conducted in underground laboratories. These allow to collect information about the overall behaviour at a bigger scale. Indeed, in-situ tests deal with higher volume of gas injected as well as fracture networks which have a large importance on mechanical and hydraulic behaviours of the porous media.

Finally, modelling can be complementary to in-situ tests. These latter have limits in terms of space, logistics and, of course, time. Indeed, as previously mentioned, radioactive wastes will stay active for thousands of years and, obviously, in-situ tests can't last more than a couple years. Therefore, modelling comes at a point where laboratory and in-situ tests reach their limits.

Section 3.4 PGZ3 EXPERIMENT

3.4.1 INTRODUCTION

The PGZ experiments are campaigns of gas injection tests whose aim is to understand the influence of hydrogen gas percolation, due to the corrosion of steel barrels containing nuclear wastes, on the mechanical behaviour of the rock formation in which the final deposit is planned to be built, being the Callovo-Oxfordian formation.

These campaigns started in 2009 and are currently still proceeding. There are, for now, 3 campaigns that were launched. The first one, PGZ1, focused on the gas transfers through argillite. More specifically, it allowed to get information on the generation of fractures caused by gas pressure increase. The second one, PGZ2 focussed more on the gas transfers in the bentonite-based materials. Finally, the objective of PGZ3 campaign is to precise results found during PGZ1, this is this last campaign we will focus on for the rest of this work (de la Vaissière, 2021).

As already mentioned, the first phase of the simulation consists in going through a one-dimensional axisymmetric model and then implementing a more complex two-dimensional axisymmetric model.

However, this first phase is also implemented step by step by running a purely hydraulic model in a homogenous environment to begin. After that, an excavated damage zone will be introduced. And finally, hydraulics will be coupled to mechanics in Chapter II-7. This gradual approach allows to adjust the material characteristics and the parameters of mechanical and hydraulic laws. But also, to identify how each phenomenon influences the results and to be able to reproduce in the best way possible what happened during PGZ3.

3.4.2 GEOLOGY AND ROCK PROPERTIES

As previously mentioned, the PGZ3 experiment is conducted at the underground laboratory of Bure in France, and, therefore, in the argillite of the Callovo-Oxfordian formation. This section aims at a better understanding of this geological layer properties and, therefore, why it was chosen to host the lab.

To begin with, a short description of the overall geological context is made. As mentioned in point 1.3.2, it is highly important to choose the right type of rock to build the repository. But it is also crucial to describe the layers surrounding the one of interest for various reasons. Some of these are adapting the drilling techniques to the type of surincumbent rocks, identifying the potential presence of an aquifer or highlighting a potential connectivity between layers.

The geological layout in the area is illustrated in Figure 19. It should be noted that the sequence is made only of sedimentary rocks and the general dip of these layers is 1°W. From bottom to top, here is a short description of each layer:

- Dogger formation: carbonates, mostly formed of calcite. It is referred to as the First Jurassic Aquifer. Its transmissivity ranges from 7.10^{-8} and 7.10^{-5} m²/s (Rebeix et al., 2011)
- Callovo-Oxfordian formation: mostly argillite (deeper described below).
- Oxfordian formation: this formation is highly similar to Dogger formation. Indeed, it is formed of carbonates, mostly composed of calcite with a few dolomites and clay. It is also an aquifer whose name is the Second Jurassic Aquifer. However, its transmissivity ranges from $1.3.10^{-7}$ and 2.10^{-3} m²/s.
- Kimmeridgian formation: marls and argillaceous limestones.
- Tithonian formation: carbonates referred to as "Barrois limestone".

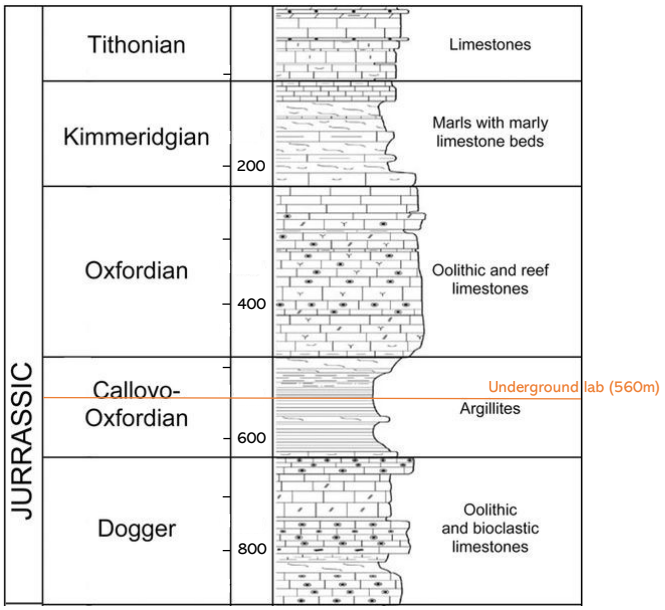

FIGURE 19 – GEOLOGICAL LOG OF BURE AREA (ADAPTED FROM JEAN-BAPTISTE ET AL. (2017))

Different studies such as Rebeix et al. (2011) were made to characterise the water flows in both Jurassic aquifers. This aspect is quite important as formations directly at the top and at the bottom of the COX formation are aquifers. Therefore, if a connection between both is detected, this would induce a water flow through the layer containing the radioactive wastes and, thus a risk of contamination. The results indicate that no flow could be observed between Oxfordian and Dogger aquifers, meaning that concerns about risks of dispersion of contaminated water can be avoided.

Next, a deeper description of the geological history of the formation of interest is given. The Callovian and Oxfordian are geological stages of, respectively, the middle and upper Jurassic. This means that the formation studied here was deposited roughly between 163 and 157 million years ago. The global environmental context at this time in the Paris Basin (geological area to which Bure belongs) was at first a deep ocean which tended then to the development of a carbonate platform. The nature of the bedrock is then a consequence of the conditions of this environment.

In addition, it is obvious but important to notify that the type of rock is sedimentary. Then, according to the change of environment, three lithostratigraphic units can be identified in the formation, listed here from the base: (Armand et al., 2017)

- Clay unit: from the environmental context, which is deep-sea, fine deposits could be expected. Indeed, the mineral composition is, on average, 45% clay, 15% carbonates and 20% silicates.
- Transition unit: transition between the two other units.
- Silty carbonate-rich unit: due to the lowering of sea level and development of carbonate platform, sediments in this unit are coarser and tend more to carbonates and silty minerals, with less clay ones.

From the conditions that were mentioned in point 1.3.2 and the information hereabove, it can be deduced that the unit targeted for the building of the underground disposal is the clay one since clay is more adapted to deep geological disposals than carbonates and silicates.

3.4.3 EQUIPMENT DESCRIPTION

As already mentioned, the PGZ3 experiment has been carried out in the continuity of PGZ1. Its objective is to study the effect of the stress orientation but also the effect of gas injection kinetic on the gas fracturing process. (de la Vaissière, 2021)

In this framework, 5 boreholes were drilled from highly dense network of drifts located in the underground lab in Bure. Their characteristics can be found in Table 6. It can be noted that the last borehole has a larger diameter. This is due to results of PGZ1 suggesting that the size and the shape of the borehole damage zone (which is of course larger for more important boreholes) influence the gas fracturing process.

Name	Direction	Drift[15]	Length [m]	Diameter [mm]
PGZ1002	Parallel to minor horizontal stress	GEX	35.01	76
PGZ1003	Parallel to major horizontal stress	GEX	35.06	76
PGZ3001	Parallel to major horizontal stress	GRM	35.04	76
PGZ3002	Parallel to minor horizontal stress	GRM	35.00	76
PGZ5301	Parallel to major horizontal stress	GVA3	35.10	146

TABLE 6 – PGZ3 BOREHOLES CHARACTERISTICS (DE LA VAISSIÈRE, 2021)

Each borehole is equipped in a similar way which consists of an alternance of one-meter-long intervals, 1.5-meter-long packers, and resin. The way these three layers are embedded and repeated is represented in Figure 20 and Figure 21. Intervals are the elements from which water or gas is injected and in which pressure measures are performed. Packers are inflated with water to keep intervals steady whatever the conditions they are subjected to. Moreover, resin is used to insure stability and low compressibility of the overall system (de La Vaissière & Talandier, 2022).

In Figure 20, it can also be seen the different components of intervals, namely from inside to outside: a borehole annular, a porous sinter (with 30% porosity), a small void for technological reasons and finally an inner tube made of stainless steel. Not represented in the sketch, there are also hydraulic lines passing through the interval as well as through the packers. These allow to monitor water and gas pressures but also to inject both fluids.

Depending on the borehole and the interval, the volume of this equipment is more or less important. Moreover, the latter could also be impacted by the convergence of the borehole wall. However, to perform gas injection, it is highly important to precisely know the available volume for fluids in the interval. This is why the subject will be broad again further when performing the numerical simulations.

[15] Drifts correspond to the different wings of the URL

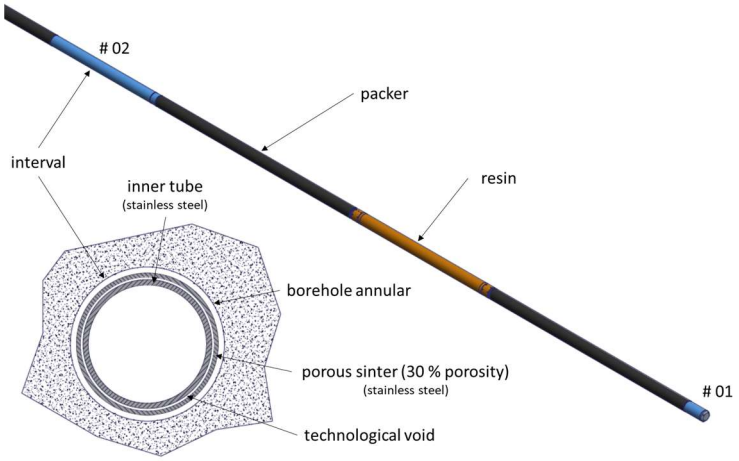

FIGURE 20 – BOREHOLE REPRESENTATION (DE LA VAISSIÈRE & TALANDIER, 2022)

3.4.4 PROCEDURE DESCRIPTION

To observe gas impacts in the porous medium, the main part of the experiment thus consists in gas injections (through the intervals). Moreover, in order to highlight a possible link between the injection rate and the fracturing pressure, it will be injected through two different protocols that are fast and slow injection tests.

The protocol for the fast injection tests consists in alternances of injection and recovery phases. During the injection phases, the gas will be inserted at a constant flow rate of 500 mLn/min[16]. This stage is performed until a fracture is created, then the system undergoes a recovery stage. After that, the injection starts again with the aim of re-opening the fracture to identify its closure pressure and its orientation. These are performed in intervals n°4 of boreholes PGZ1002 and PGZ1003.

Concerning the slow gas injections tests, they consist of multiple cycles of injection and shut-in phases, which should last respectively 14 and 21 days. However, unlike fast protocols, during the injection phases, the gas is injected at a constant flow rate of 1 mLn/min. The procedure should proceed until a fracture is created. Then, the system is left at recovery phase for a long time before starting again with the same procedure. The boreholes in which the slow protocol is applied are intervals n°2 of PGZ3001 and PGZ3002 and interval n°4 of PGZ5301.

Section 3.5 MASTER'S THESIS QUESTION

This thesis aims at describing in multiple ways the gas flow in the rock medium around the storage cells. Indeed, to ensure the best possible isolation of radiation contained in the wastes, the medium should remain intact. However, as seen in Section 3.2, a too large gas pressure could induce fractures and therefore create preferential paths for the propagation of radioactive components from the storage cells. The goal by the end of this work is then to characterise the gas migration through the bedrock and determine whether it could cause fracturing problems or not. In order to do that, numerical simulations representing an in-situ experiment (PGZ3) will be carried out.

[16] mLn/min means millilitre per minute in normal conditions of temperature and pressure.

Part II NUMERICAL SIMULATIONS (1D)

Chapter II.4 INTRODUCTION

This chapter is devoted to the first practical part of the work. It consists in establishing a model with similar characteristics as the experiment PGZ3 and comparing the results with the ones obtained experimentally. More precisely, several models with increasing complexity will be implemented, starting with a simplistic one-dimensional axisymmetric and purely hydraulic configuration, and moving to a two-dimensional hydromechanical model.

The different numerical simulations are be performed with the finite element code LAGAMINE developed by the Department of Geotechnics of Applied Sciences Faculty from the University of Liège.

To perform the in-situ experiment, different steps before the gas injection were required. These will also be implemented in the models. In a chronological order, these steps are the excavation of the gallery and positioning of the equipment (intervals, packers and resin), then there are steps that will be called maintenance and draining. Lastly, the gas is injected through the intervals.

To replicate each of these stages in the model, specific water and gas pressures as well as hydraulic and mechanical boundary conditions will be imposed in the interval. These are all described hereunder.

Chapter II.5 MODEL 1D (NO EDZ)

In a first case, it will be considered an interval with a diameter of 76mm and a slow gas injection test (see point 3.3.4). Then, additional cases with varying parameters, a larger borehole diameter and fast injection test will be presented.

Section 5.1 MODEL GEOMETRY

As already said, the first model that is studied is a one-dimensional axisymmetric one, shown in Figure 22. It represents one of the intervals (the one in which gas is injected) and the rock in its extension, as it is represented in Figure 21 and Annex 1. The symmetry axis coincides with the left border of the interval.

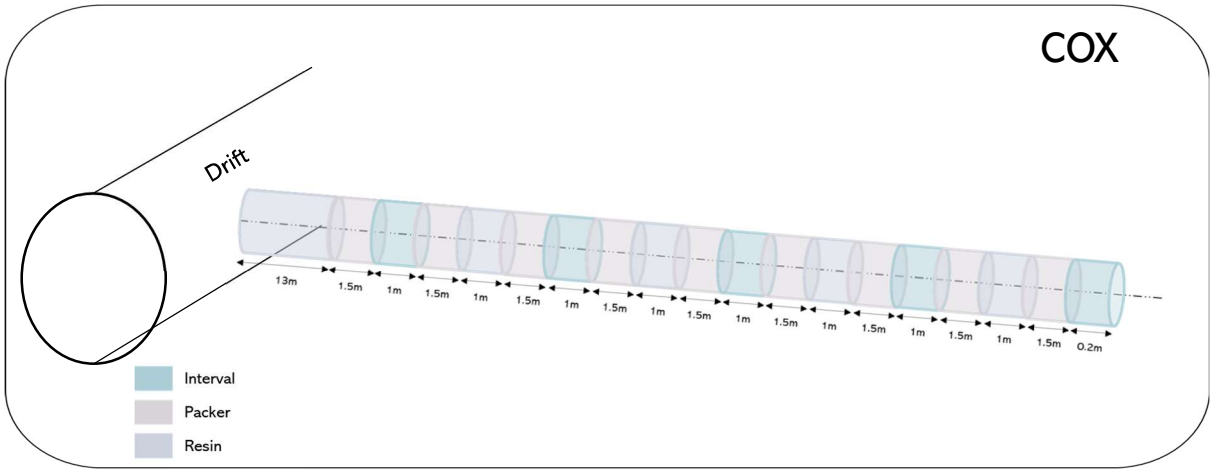

FIGURE 21 – PGZ GEOMETRY

The dimensions are the following. The height of the interval (then, of the whole model) is 0.5m, while the length is 5m. The height does not correspond to the real one (one meter) because of numerical needs. Indeed, it was chosen to include only one mesh element on the model height in the first simple axisymmetric model that is developed. Therefore, the real height would have led to too thin mesh elements. As for the length, it needed to be as large as possible for the boundary conditions not to impact the results but not too much, so that the model does not include too many mesh elements. The value of five meters was set according to Charlier et al. (2012).

The next step was to impose the number of mesh elements. Obviously, as gas will be injected in the domain through the interval, the mesh should be more refined around it. This is what can be observed in Figure 22. It should also be noted that the zone at the right of the interval will be designated as the excavated damage zone (see Section 2.8) in further simulations, it requires therefore more precision, this is why one hundred elements are set in this small area.

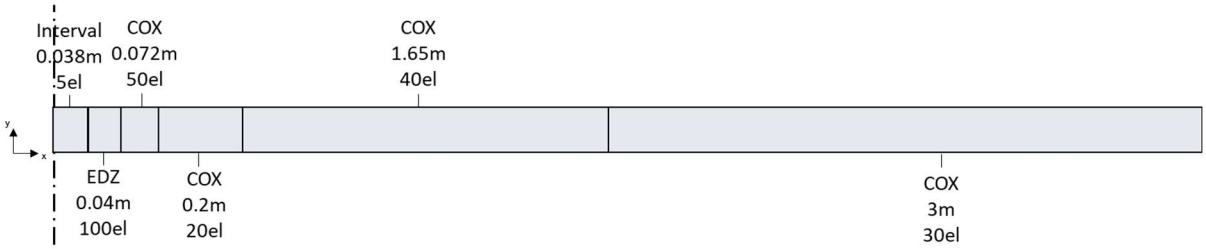

FIGURE 22 – 1D AXISYMMETRIC MODEL GEOMETRY

Section 5.2 MODEL LAWS

The modelling aspect that this section focusses on is the mathematical models chosen to run the simulations. As already mentioned, an hydromechanical model is developed. For the mechanical part, the model was imposed to follow an elastic behaviour. As for the hydraulic equations, these were described in Chapter I.2.

It should also be added that, even though the thermal character of radioactive wastes, all simulations will be performed at constant temperature (303 K).

Section 5.3 MODEL PARAMETERS

For each area delimited in Figure 22, mechanical and hydraulic properties are imposed. These are presented in the Table 7 to 10 below. The two first tables correspond to mechanical and hydraulic properties of the interval, while the two followings present the properties for the COX argillites. At first, in the zone representing the EDZ, the properties of Callovo-Oxfordian rocks are applied. The properties that are applied in this area will then be presented further (see Chapter II.6), when they will be applied.

Mechanical parameters	Value
Young's modulus E	100 MPa
Poisson's coefficient ν	0.3
Density	2300 kg/m³

TABLE 7 – MECHANICAL PROPERTIES OF THE INTERVAL

Hydraulic parameters	Value
Intrinsic permeability k	10^{-12} m²
Porosity n[17]	50%
Van Genuchten's coefficient n	1.49
Van Genuchten's parameter P_r	0.05 MPa
Maximal saturation S_{max}	1
Residual saturation S_{res}	0
Tortuosity τ	1

TABLE 8 – HYDRAULIC PROPERTIES OF THE INTERVAL

[17] The porosity of the injection chambre is an artificial one. Indeed, it is applied to fit the volume of the interval in the model with reality. The large difference between both (50%) comes from the fact that some equipment (such as pipes, annular) are not represented in the model and the cavity walls which converged in part (not a perfect cylinder as in the model).

Mechanical parameter	Value
Young's modulus E	4000 MPa
Poisson's coefficient ν	0.3
Biot's coefficient b	0.6
Initial total stress σ_0	2.46*9.81*560= 13.6MPa
Density ρ	2300 kg/m³
Tensile strength R_t	0.9-5.4 MPa

TABLE 9 – CALLOVO-OXFORDIAN FORMATION MECHANICAL PROPERTIES

Hydraulic parameters	Value
Horizontal intrinsic permeability $k_{xx} = k_{yy}$	5.10^{-20} m²
Vertical intrinsic permeability k_{zz}	$1.33.10^{-20}$ m²
Tortuosity τ	0.3
Porosity n	15%
Van Genuchten's coefficient m	0.55
Van Genuchten's coefficient n	1.49
Van Genuchten's parameter P_r	15 MPa
Maximal saturation S_{max}	1
Residual saturation S_{res}	0.01
Multiplication coefficient of $k_{r,g}$	250
Minimal value of relative permeability $k_{r,min}$	1.10^{-7} [18]

TABLE 10 – CALLOVO-OXFORDIAN FORMATION HYDRAULIC PROPERTIES

It should also be presented fluids (water and hydrogen gas) properties. These are to be found in Table 11.

Fluids parameters	Value
Water density	1000 kg/m³
Water dynamic viscosity	0.001 Pa.s
Water liquid compressibility	5.10^{-8} 1/Pa
Hydrogen gas density	0.079 kg/m³
Hydrogen gas dynamic viscosity	$0.88.10^{-5}$ Pa.s
Henry's coefficient	0.019

TABLE 11 – FLUIDS PROPERTIES

All information in the previous tables were found in multiple sources that are Plúa et al. (2021), Pham (2006), Charlier et al. (2012) and Gerard (2011).

[18] This value was found through a parametric study which is to be found in Section 5.6

Section 5.4 INITIAL & BOUNDARY CONDITIONS

As already mentioned, the simulation will be performed in four different stages. The initial and boundary conditions that are described in this section present the model in its initial state (before all stages). The additional conditions applied at each step will be described in the following sections. Moreover, it is important to mention that the results at final time of each step correspond to the initial state of the following.

At t = 0 sec, water and gas pressures are constant all over the domain. They are valued respectively at 4.7 MPa and 0.1 MPa (corresponds to the atmospheric pressure) (Gerard, 2011).

As for boundary conditions, it is only imposed that water and gas pressures are equivalent to their initial value at the right border of the model (representing the distance at which phenomena that will be imposed in the interval are supposed not to impact the environment properties anymore). Both initial and boundary conditions are represented inFigure 23. Additionally to these conditions, it should be remembered that no water or gas flux is allowed through the model boundaries.

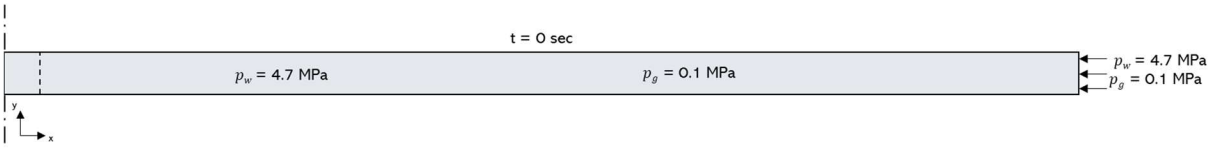

FIGURE 23 – INITIAL AND BOUNDARY CONDITIONS FOR 1D MODEL (BEFORE EXCAVATION)

Section 5.5 RESULTS

5.5.1 STEP 1: EXCAVATION

The first step of the simulation consists in drilling the space needed for the tube in the bedrock and placing the equipment (described in point 3.4.340) inside the borehole. To do that in dry conditions, water is pumped from the location. Therefore, water pressure at the hole should be lowered to the atmospheric pressure.

The excavation rate is estimated to 1.5m per hour which corresponds to one day to drill the whole borehole. As only the interval subjected to injection is modelled, it will be considered that this interval is to be found in the middle of the borehole (compromise between intervals 2 and 4 in which slow and fast injections tests are respectively performed). This means that twelve hours of drilling are left after excavating the space needed for the interval.

In order to model that, a transition phase from the initial water pressure is applied for two minutes, then it is set to the atmospheric pressure for 12 hours.

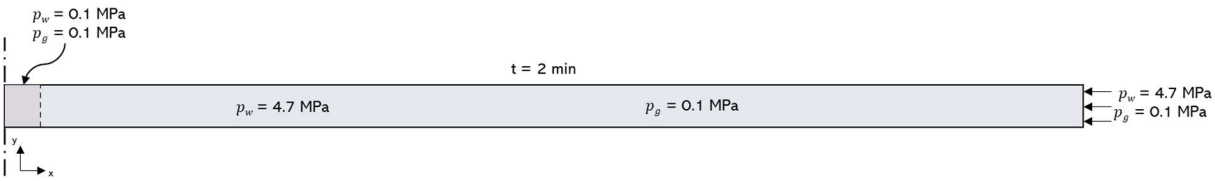

FIGURE 24 – INITIAL AND BOUNDARY CONDITIONS OF 1D MODEL AT STEP 1

In Figure 25, the evolution of pressure with distance to the borehole can be observed at three different times. First, at $t = 0$ min, it can be seen that water pressure is steady on the whole domain at 4.7 MPa. At $t = 2$ min, p_w is lowered to 0.1MPa in the interval and very close to it (without impacting further the domain). Then, after 12 hours, the pressure drawdown at the interval influences water pressure over a greater distance (nearly one meter away from the borehole).

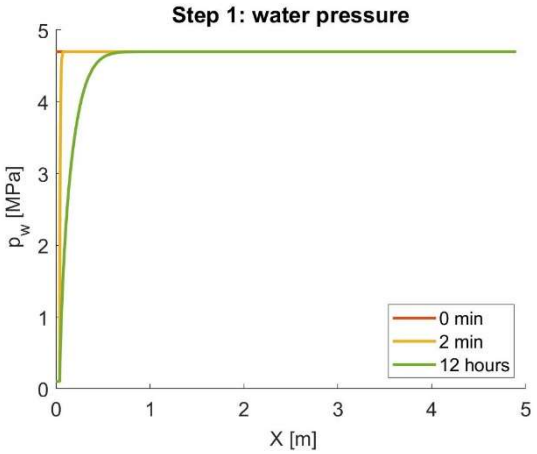

FIGURE 25 – WATER PRESSURE EVOLUTION DURING STEP 1

It should be noted that all graphs computed in one dimension are results of an horizontal cross section at the middle of the model (y = 0.25m).

5.5.2 STEP 2: MAINTENANCE

The second step, called maintenance, happens once the borehole is fully equipped and sealed. It consists in waiting for the water pressure to come back to its initial value. For the simulation this means that results of step 1 were taken as initial values and that water pressure wasn't imposed at any pressure (except at the right boundary) for four months.

The time needed to have a stabilized water pressure could have been determined in an optimized way by trial-and-error simulations. However, it was chosen to wait for four months, as it was done practically for PGZ3.

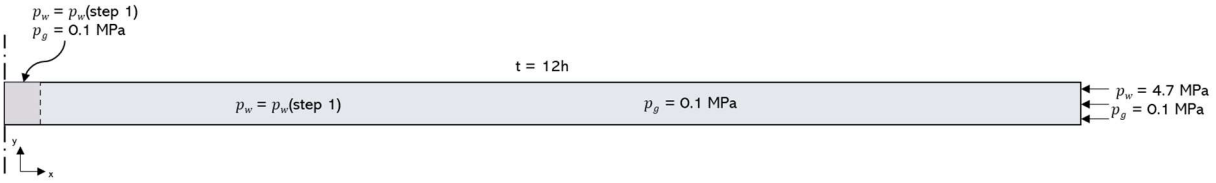

FIGURE 26 – INITIAL AND BOUNDARY CONDITIONS OF 1D MODEL AT STEP 2

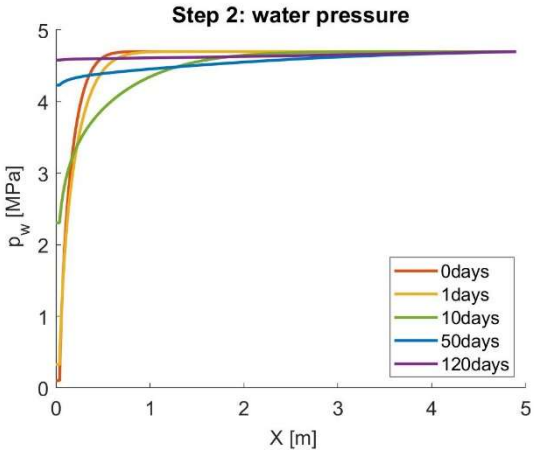

FIGURE 27 – WATER PRESSURE EVOLUTION DURING STEP 2

As it can be seen in the graph above (Figure 27), the pressure in the interval goes up gradually back to nearly 4.7MPa. It should be noted that getting back to 4.7 MPa exactly would have necessitated a lot of additional time which was not pertinent for the slight difference. However, a bit further from the interval, the pressure continues to decrease for some time before going back to its initial value. Indeed, at $x = 1$m, water pressure drops between day 0 and day 1, but also between day 1 and day 10. However, it raises again between day 10 and day 50. This is due to a retardation effect of the drainage in step 1. Indeed, when the draining is stopped, it needs time for the effect to influence the medium at great distances. Therefore, for example at x = 1m, after ten days, the influence of the draining is still felt so the pressure continues to decrease. Then, after 50 days, the influence of the cessation of drainage could percolate and therefore the pression goes up again (but therefore with a retardation compared to points located nearer to the borehole).

5.5.3 STEP 3: DRAINAGE

Once the borehole is equipped and hydrostatic parameters back to their initial value, the injection of gas should be performed. However, as mentioned before, an intermediate step will be needed to empty the interval of water. The reason for that is the compressibility of gas and incompressibility of water. Indeed, if the interval is saturated with water, the gas can't push the water to flow through it. Indeed, as showed in Figure 16, the relative gas permeability tends to zero for an environment saturated with water. This is the reason why a minimal relative gas permeability is imposed. However, in this case, it is not enough. The solution is then to empty the injection cell (through hydraulic lines, not towards the bedrock). This action is called gas/water exchange.

From (de la Vaissière, 2021), it is first known that gas pressure is set up to the hydrostatic pressure to remove water. It is also mentioned that not all water could be removed, the remaining amount being tricky to determine. Once the interval is installed with all equipment in the middle of the borehole, estimating its volume can be tricky. Moreover, it is not possible to determine whether the borehole wall converges (thus making the available volume reduce again), this increases again the complexity of the water volume computation. However, the extracted mass of water was weighted for two intervals, and approximations could be made. As it can be noticed from Table 12, the degree of saturation is highly variable. It was chosen to impose a saturation of 35% in the model

as it corresponds more or less to the average of the four values. However, the impact of this choice will be discussed in point 5.6.4 as a parametric study will be realised on this parameter.

	Interval 4 (PGZ1002)	Interval 4 (PGZ1003)
Water saturation if full convergence of the borehole	9%	63%
Water saturation without convergence of the borehole	40%	28%

TABLE 12 – WATER SATURATION REMAINING IN THE INTERVAL AFTER DRAINING (ADAPTED FROM PGZ EXPERIMENT (N.D.))

The water pressure was then determined thanks to the retention curve computed based on the injection cell properties. The approach was the following. For $S_r = 0.35$, we obtain $p_c = 0.4$ MPa from Equation 4. As gas pressure is imposed to 4.7 MPa, it can be deduced from Equation 2 that water pressure must be set at 4.3 MPa. These conditions are therefore applied in the interval as it is shown in Figure 28.

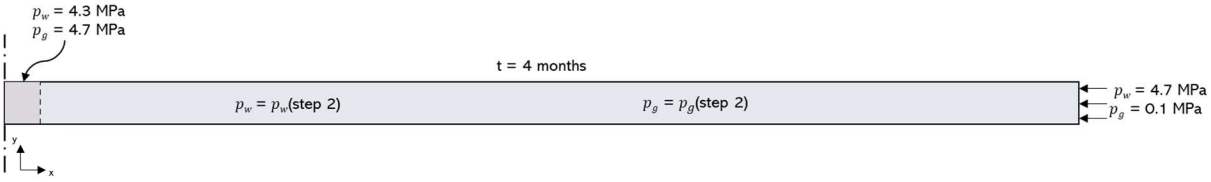

FIGURE 28 – INITIAL AND BOUNDARY CONDITIONS OF 1D MODEL AT STEP 3

The time laps for this step should be long enough to allow numerical calculations but not too much, so that the pressures outside the interval are at first not too much impacted. In these conditions, it was chosen to apply a transition time of three minutes.

The results of the simulation of this third step are displayed in Figure 29 hereunder. The change of imposed pressures in the interval can be observed. It can also be seen that water and gas pressures outside the injection cell seem not to be too much impacted by this gas/water exchange in the interval.

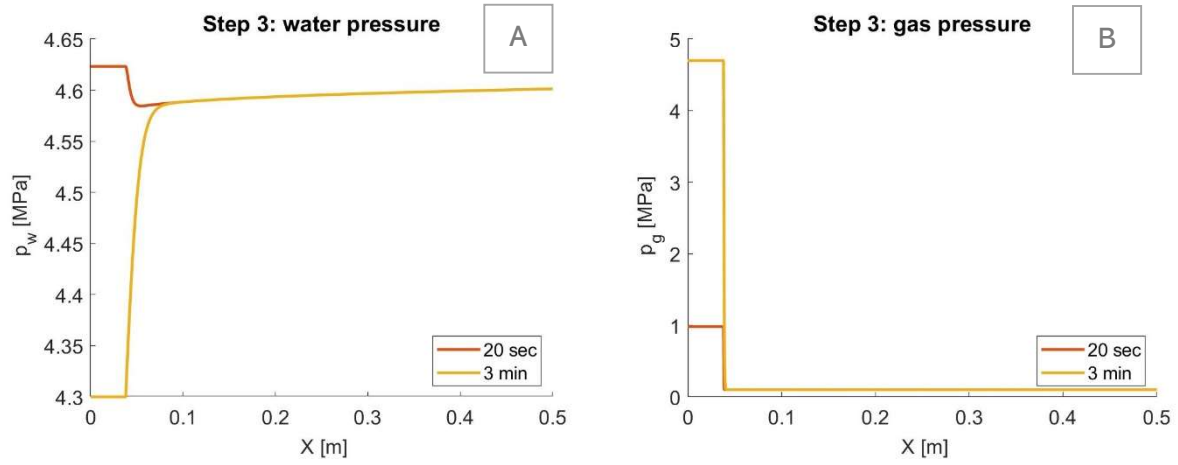

FIGURE 29 – WATER (A) AND GAS (B) PRESSURES EVOLUTION DURING STEP 3

Another parameter that can be observed is water saturation (see Figure 30). The evolution from a full saturation to an imposed degree of saturation of 35% (through pressures) in the interval is highly noticeable. It can also be seen those three minutes of draining already impact the environment outside the injection cell. However, a faster transition is not numerically feasible.

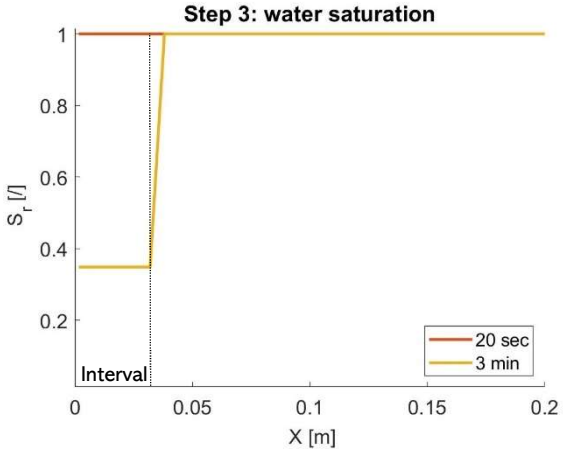

FIGURE 30 – WATER DEGREE OF SATURATION DURING STEP 3

5.5.4 STEP 4: GAS INJECTION

Finally, the model is ready for gas injection. At first, only the first cycle of injection of the slow protocol will be realised. As written in point 3.4.4, slow injection tests consist in the injection of gas at a rate of 1 ml/min during 14 days. Before launching the simulation, the gas rate should be converted to units supported by the software. It was found that the injection rate amounts to $1.63.10^{-7}$ kg/(m².s).

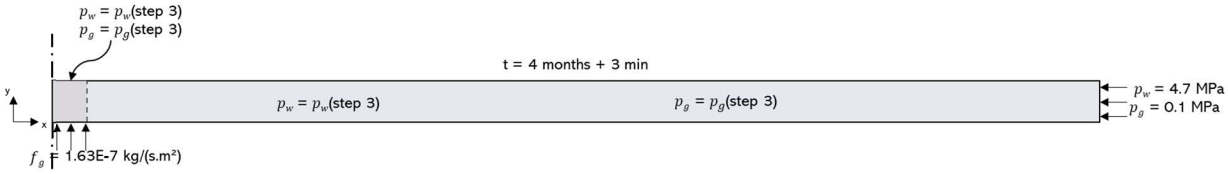

FIGURE 31 – INITIAL AND BOUNDARY CONDITIONS OF 1D MODEL AT STEP 4

From Figure 32A and B, information about the evolution of gas and water pressures when gas is injected can be found. The trend shows a raise in both pressures as gas is injected through time. However, this increase seems to be larger at the beginning of the injection and to slow down with time. Indeed, during the first seven days, gas pressures raise from 0.1 to 7 MPa while it only rose from 7 to around 9 MPa during the second week.

Another information given in Figure 32A and B is the fact that, when the amount of gas becomes important, gas pressure overtakes water pressure.

Finally, the augmentation in pressure is localised near the injection cell while a little further (0.25m), no effects of the gas injection can be seen on gas pressure. This is probably due to the short time during which the injection is performed. In order to highlight the effects on a larger time scale, the simulation of the full cycle of slow injection test will be carried out (see Section 7.4).

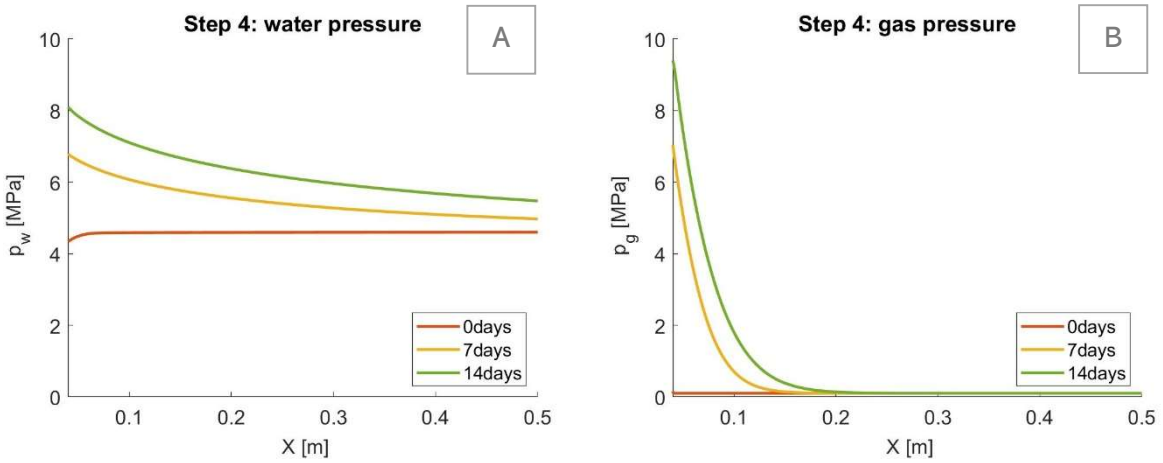

FIGURE 32 – WATER (A) AND GAS (B) PRESSURES EVOLUTION DURING STEP 4

In Figure 34 below, water saturation in the bedrock close to the interval decreases along with the injection of gas. A relation between Figures 33B and 34 can be highlighted. Indeed, the steep increase in gas pressure during the first time step can be associated to the small space available (as the water degree of saturation is reduced of only 0.02% at the border with the interval). During the second time step, water saturation decreases more so the available porous space for gas is enlarged and the rise in gas pressure is slowed down.

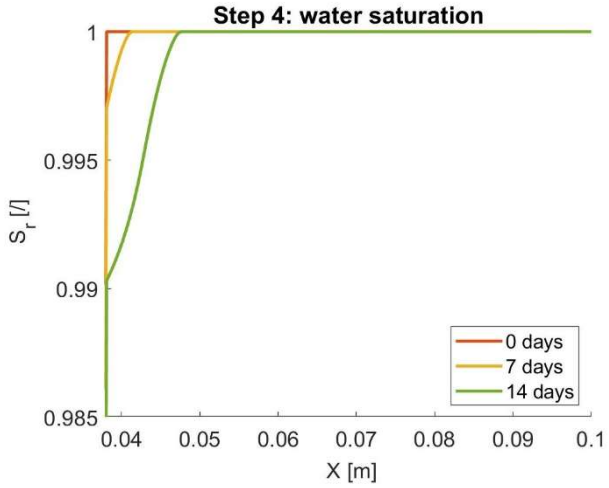

FIGURE 33 – WATER DEGREE OF SATURATION EVOLUTION DURING STEP 4

The next aspect that can be studied is the way gas is transported through the porous media. As a reminder, the different transport mechanisms depending on gas pressure were described in Chapter I.3. It should now be identified which transport mechanisms occur in the framework of the numerical simulation performed here. And, more specifically, how these transports vary upon the gas pressure.

To do that, different properties are considered. It should first be determined if the gas is transported as a single phase or dissolved in water. Then, for the latter, it is characterised by its transport mode (advective or diffusive). The results are displayed in Figure 35.

First, gas is obviously mostly transported as a single phase in the whole interval. However, at a very small distance from the interval, dissolved gas takes over. This overtaking even

so happens a bit further at t = 14 days. The radial distances at which these exchanges of phenomena occur correspond to the ones at which the degree of saturation reaches more or less 99.5% and at which gas pressure is around 7 to 8 MPa. This highlights the direct link between the transport mechanisms and the water saturation and gas pressure. It seems logical as, when gas pressure is too low and the porous medium saturated, gas can't circulate as a single phase and needs to dissolve in water in order to progress in the medium.

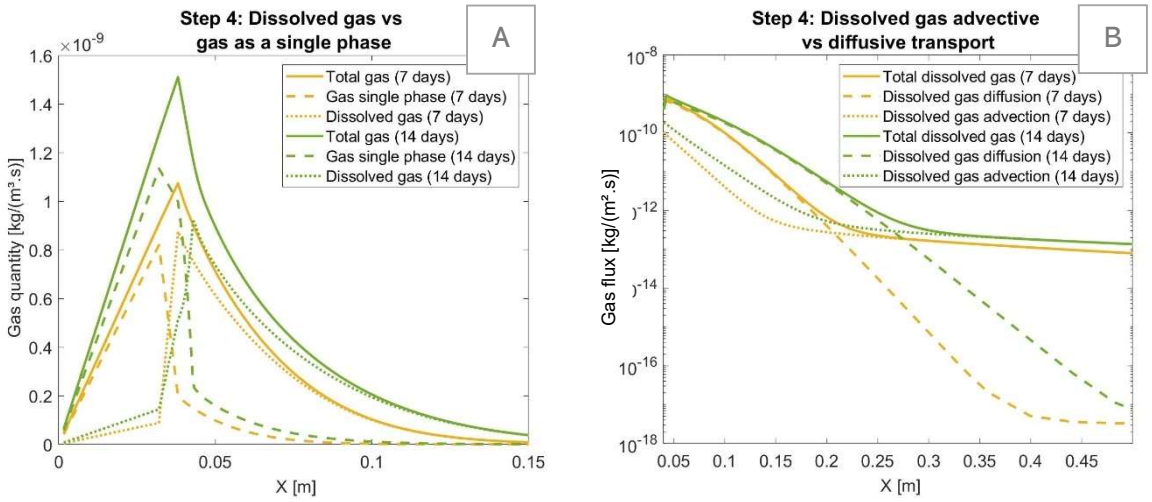

FIGURE 34 – GAS TRANSPORT MECHANISMS DURING STEP 4

Section 5.6 PARAMETRIC STUDY

5.6.1 MINIMAL RELATIVE PERMEABILITY OF GAS

The first parametric study that was performed was to determine the value of the minimal relative permeability of gas. Indeed, as presented in Section 2.6, it was seen that when the medium is saturated with water, the relative permeability of gas is null. It is then complex to inject gas in an environment which is impermeable to gas. To ease the gas injection in the porous medium, a minimal value (superior to zero) of the relative permeability is therefore imposed. However, the chosen value should yet not impact the results. This is why a parametric study is conducted to determine the value of the minimal relative permeability of gas which should be as large as possible to ensure the gas injection in a saturated environment but as small as possible not to influence results.

It should be noted that the final value found from this study is the value that was used to compute the results in the previous sections already.

The methodology used was to choose an initial value of the parameter and make this value decrease until the results are not impacted anymore by the change of value. The initial value that was chosen was 10^{-4} and it was decreased by an order of magnitude at each step. The results for each step are presented in Figure 36. As it can be seen from them, the gas pressure results are steady between 10^{-7} and 10^{-8}, the final value that was chosen to compute all results is then 10^{-7}.

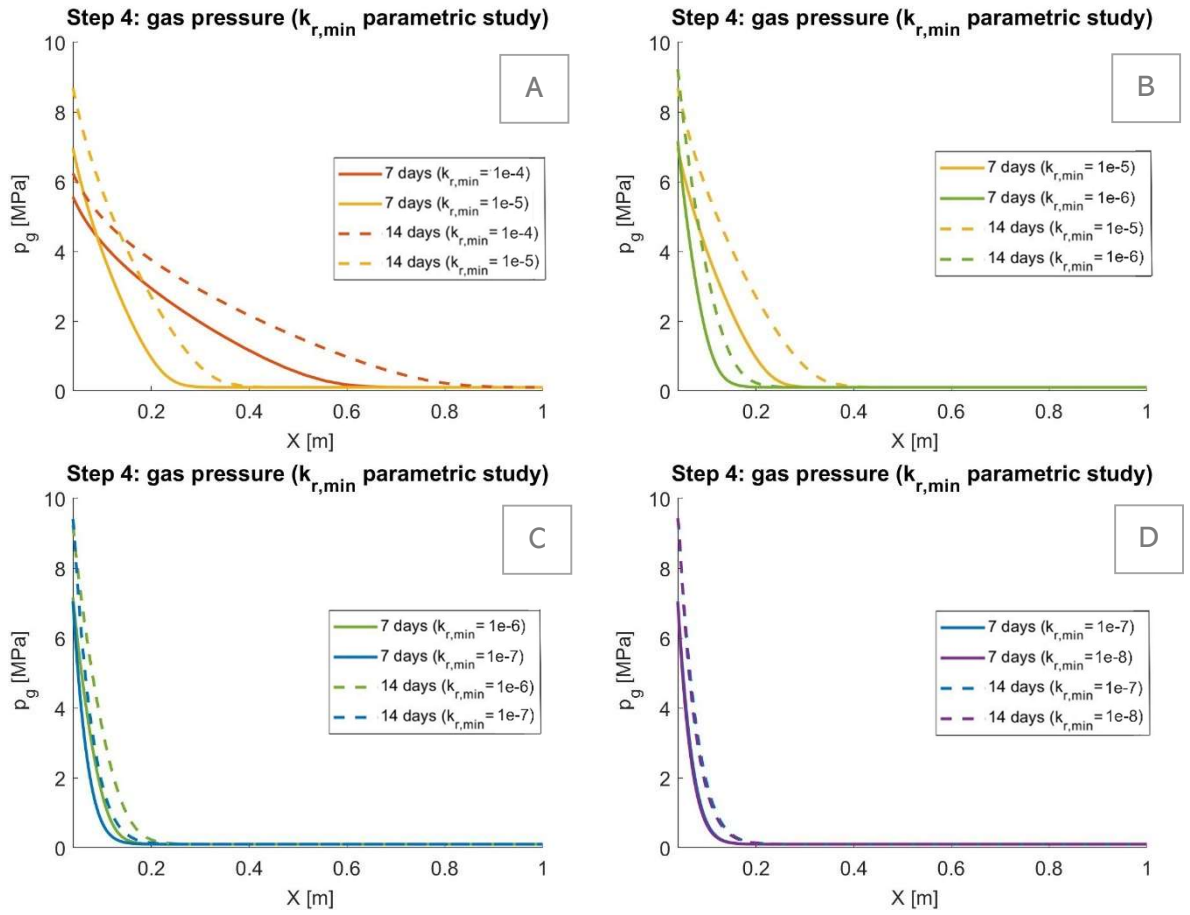

FIGURE 35 – MINIMAL RELATIVE PERMEABILITY OF GAS PARAMETRIC STUDY

5.6.2 POROSITY

The next parameter that is studied is porosity. The initial value (15%), found in the literature, was changed to 25%, which is a non-negligeable change. From the results in Figure 37, it is obtained that, even though the value difference is quite important, the results are not too much impacted. However, the results still show that for a higher porosity, the water and gas pressures are both lowered. This seems natural as more space is available from water and gas, the pressure increases are slightly limited.

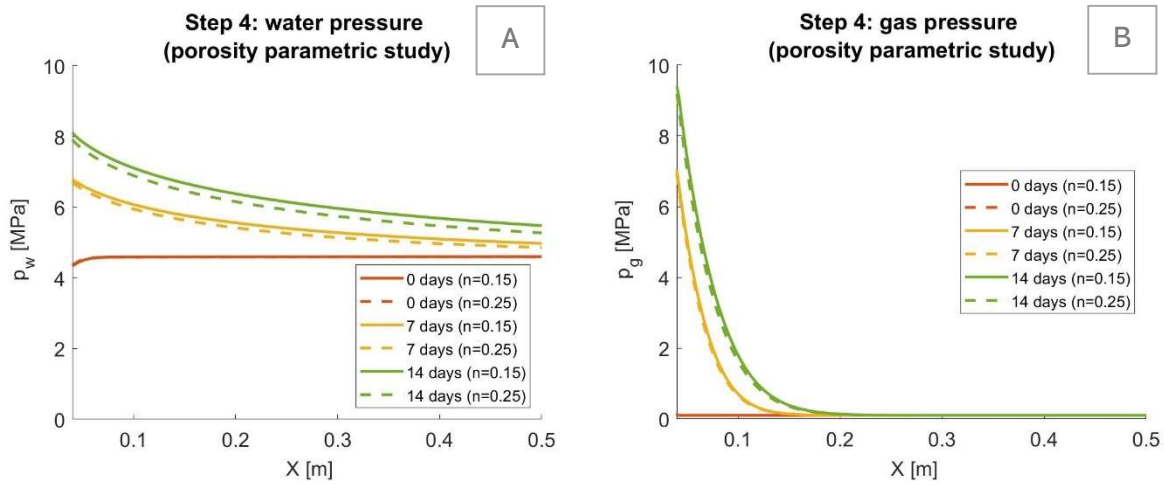

FIGURE 36 – POROSITY PARAMETRIC STUDY (n = 25%)

5.6.3 PERMEABILITY

Then, the influence of intrinsic permeability is studied. As showed in Figure 38, a change of only one order of magnitude (above and under) has already a large impact on the results. Whether the permeability is increased or decreased, the impact on the results is opposite. Indeed, when permeability is increased (A and B), the fluid flows are easier, they can reach distances further from the interval. This is expressed by an increase in gas pressure on longer distances but with a lower rise very near the borehole. When the permeability is decreased, the gas and water pressures raise around the injection cell are more important, but their values stabilise at a smaller radius.

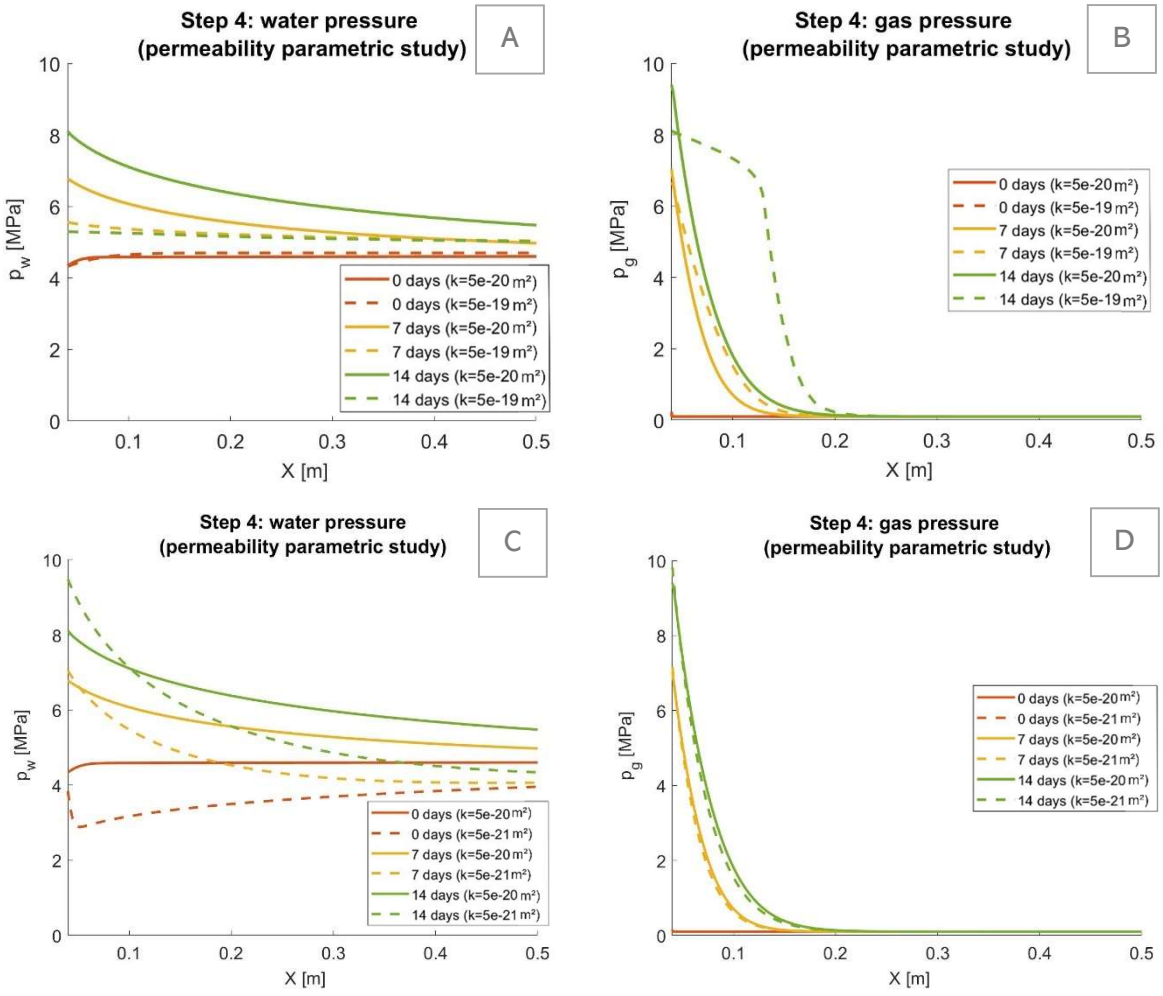

FIGURE 37 – PERMEABILITY PARAMETRIC STUDY

5.6.4 INITIAL SATURATION OF THE INTERVAL

As already mentioned during the description of the 3rd step (point 5.5.3), to allow the gas injection into the interval, it can't be fully filled with water. However, it is never dried up to 100%, there is always a residual amount of water. Given the complexity of the equipment installed in the interval and the possibility of convergence of the borehole wall, the volume of remaining water can be highly variable. The impact of this initial saturation is then studied.

Figures 39A and B show the case where the initial saturation of the interval is decreased from 35 to 10%. From the retention curve presented in Figure 14, it is known that the

water pressure should be decreased a lot in the chamber (this is what is shown in Figure 38A). This induces that the rock around the interval is a lot desaturated which allows gas to flow more easily through the medium (see Figure 38B).

As for the situation where the saturation in the injection chamber is decreased, given the retention curve displayed in Figure 14, it is seen that a modification of the saturation for 35 to 65% in the interval does not impact too much the capillary pressure and consequently the imposed water pressure in the interval. Therefore, the evolution of water and gas pressures is not so much impacted.

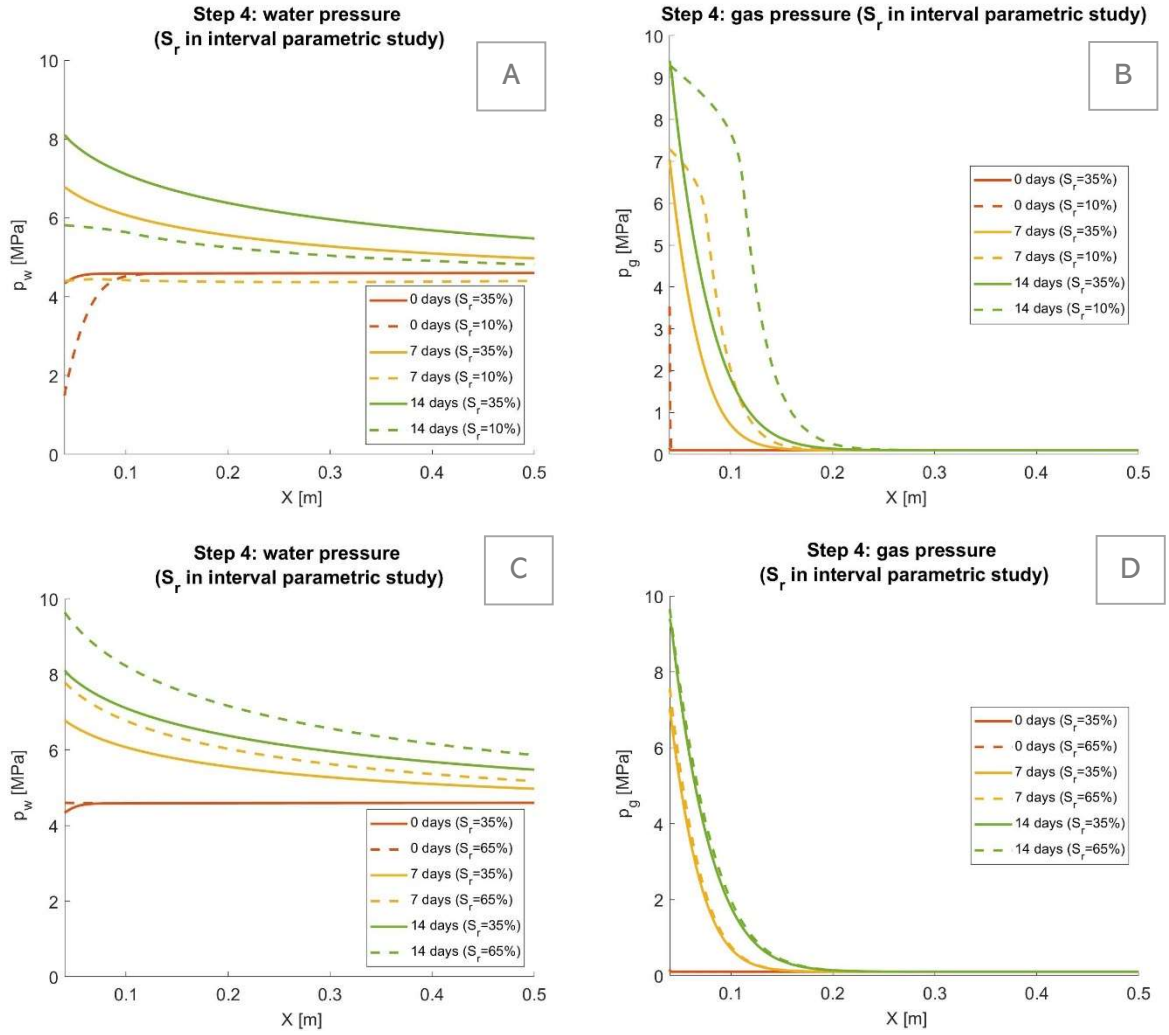

FIGURE 38 – INITIAL WATER SATURATION IN THE INTERVAL PARAMETRIC STUDY

5.6.5 VAN GENUCHTEN PARAMETER P_r

A last parameter for which it is interesting to look at its influence is Van Genuchten parameter P_r appearing in the retention curve formulation (see equation 4). The initial value of the parameter was 15 MPa and it was modified to 5 MPa and 50 MPa. The change of this value has then a direct impact on the saturation of the medium, this can be observed in Figure 40. When P_r is increased, the saturation is smaller, in the opposite it is larger as P_r is decreased. However, the impact is more important when the parameter is reduced.

The varying water saturation impacts directly the gas injection (represented in Figure 41). Indeed, in the case of P_r = 5 MPa, where the water saturation was the most affected, the gas pressure is highly different from the initial case. This comes from the fact that a smaller water saturation implies a bigger gas relative permeability (see point 2.6.2). This means that gas flows more easily through the porous medium, leading to a higher pressure.

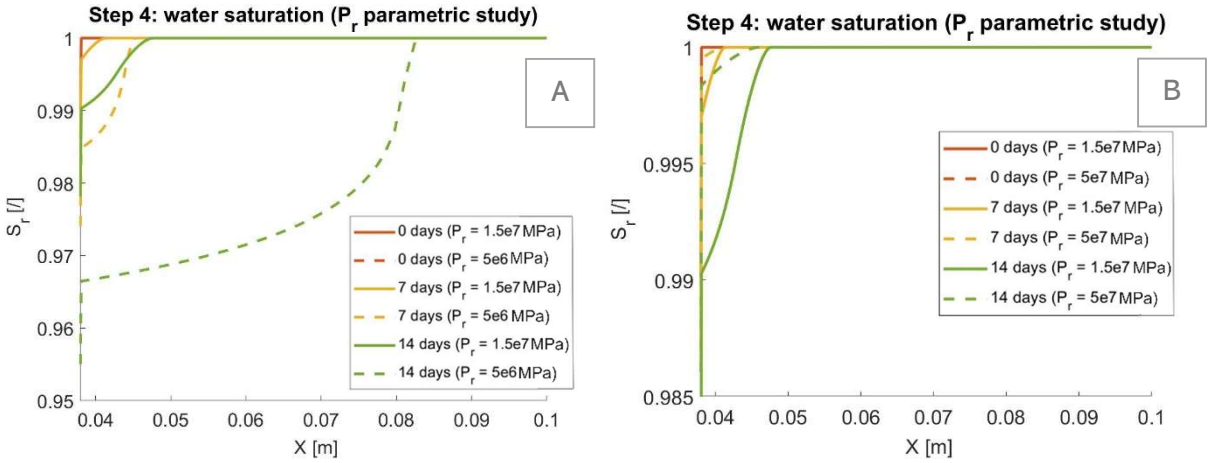

FIGURE 39 – WATER SATURATION DURING VAN GENUCHTEN PARAMETER P_r PARAMETRIC STUDY

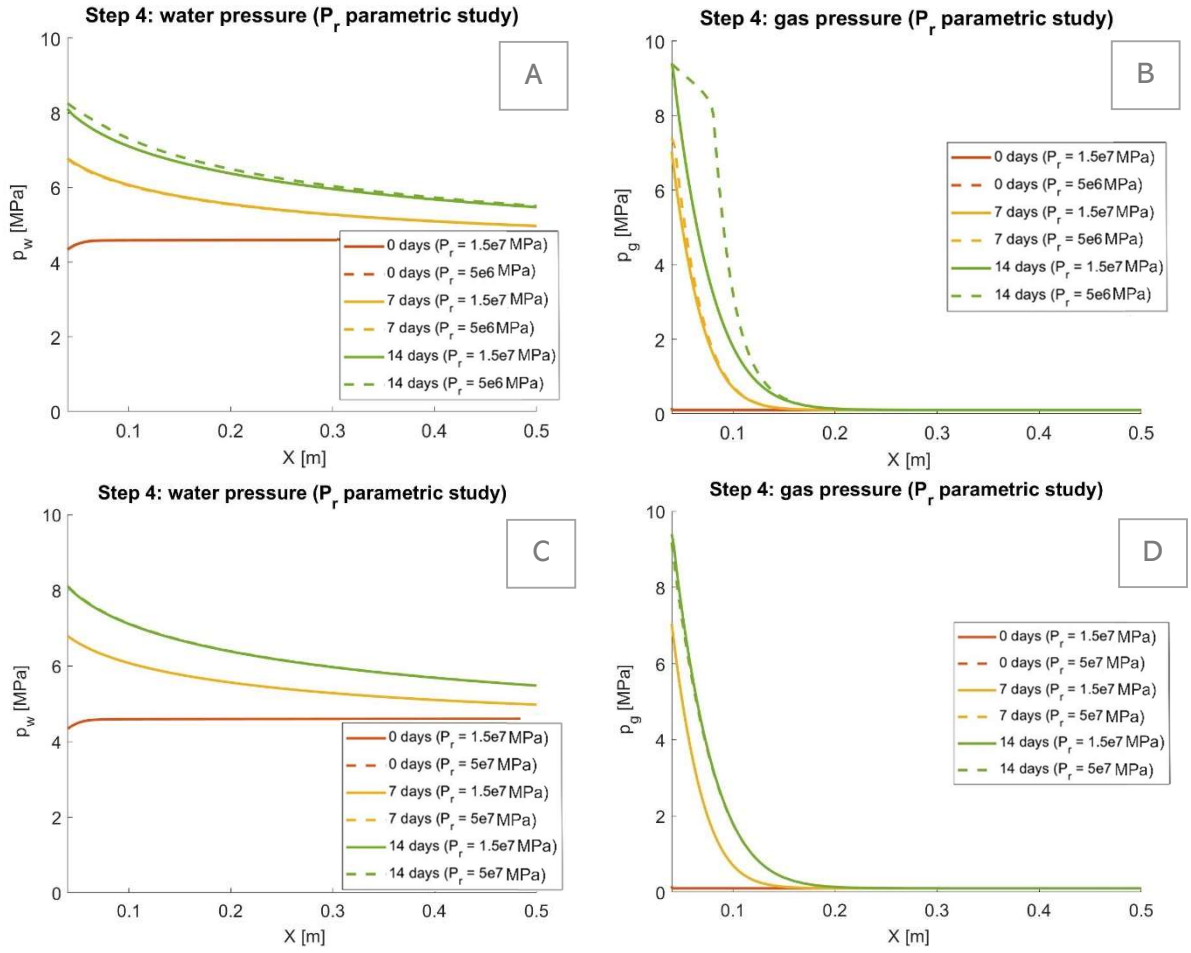

FIGURE 40 – VAN GENUCHTEN PARAMETER P_r PARAMETRIC STUDY

Chapter II.6 MODEL 1D (WITH EDZ)

During the excavation, around the hole created in the rock, a zone where solicitations (compression, traction, shearing) are more important is developed. It is called Excavated Damaged Zone (EDZ). In this zone, it is expected that hydraulic properties of the rock are slightly modified and, therefore, impact the way fluids are transported through the porous medium. The characterisation of the EDZ and its impact on gas pressure and ways of transport is the goal of the section.

To characterise this impact, the four simulation steps were performed again, and the results are compared with previous ones (model without an EDZ) in Figures 42 and 43 hereunder.

Section 6.1 MODEL PARAMETERS

Before taking a look at the results, the changes made to adapt the one-dimensional model should be described.

In the initial geometry, a zone of 40mm length was pre-implmentating. In the first case, without EDZ, this part of the model had the same properties as COX clay. However, in the present case, the properties were changed for the ones in Table 13. All other properties that are not being mentioned in this table are the same as in the argillites. The size of the EDZ was taken from (Charlier, Collin, Gerard, et al., 2012)

Parameters	Value
Horizontal intrinsic permeabilities $k_{xx} = k_{yy}$	2.10^{-19} m²
Vertical intrinsic permeability k_{zz}	$2\text{-}3.10^{-19}$ m²
Van Genuchten's parameter P_r	3 MPa
Relative permeability law multiplicator A	100
Minimal relative permeability $k_{r,min}$	10^{-11}

TABLE 13 – EDZ PROPERTIES (CHARLIER ET AL., 2014)

Section 6.2 RESULTS

Only results for the fourth step are presented in Figures 42A and B. The excavated damage zone can clearly be identified from these figures as the look of the curves in this limited zone is quite different from the remaining part. Indeed, both water and gas pressures tend to remain high in the EDZ and drop in COX while they drop directly when the EDZ is not modelled. This behaviour is quite similar to the one that was observed when the intrinsic permeability was increased in the parametric study (Figures 38A and B) but also when Van Genuchten parameter P_r was decreased (Figures 41A and B). Results are then consistent with the changes that were made to the rock properties in the damaged zone.

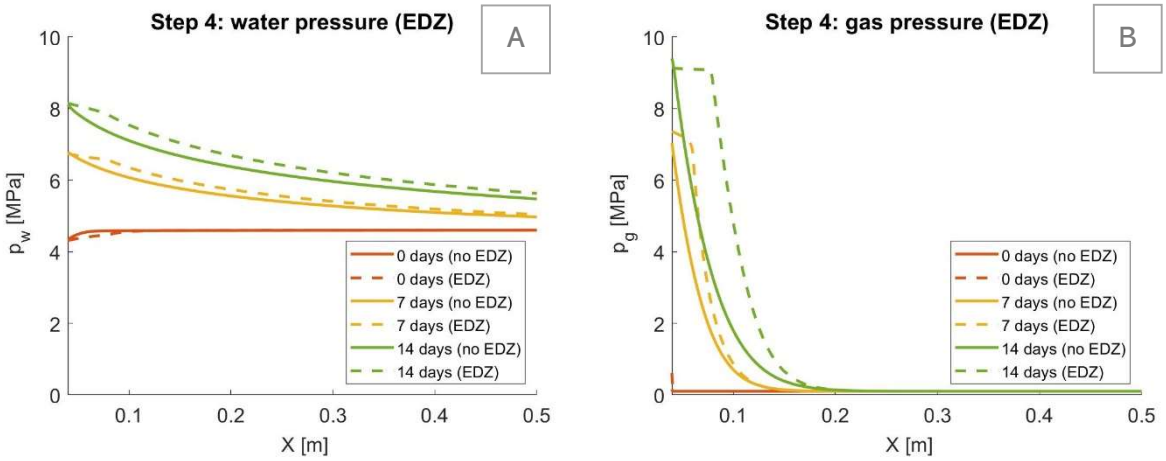

FIGURE 41 – WATER AND GAS PRESSURES WITH PRESENCE OF AN EXCAVATED DAMAGED ZONE (EDZ)

As for water saturation behaviour in the excavated damage zone, Figure 43 shows that it is also largely impacted. The observed trend is a reduction of the saturation. This reduction is due to the properties of the EDZ and more precisely the smaller air entry pressure that implies a larger proportion of gas able to flow through the porous environment.

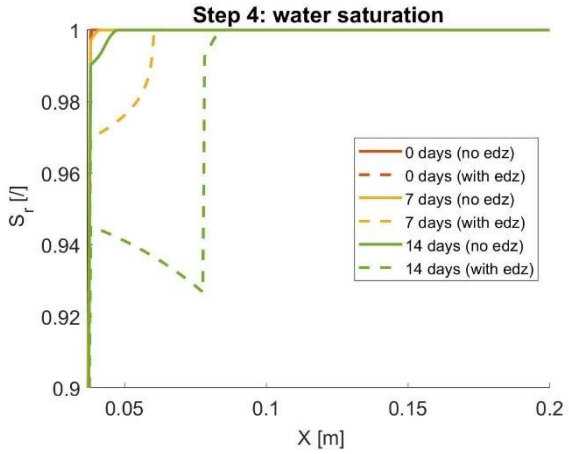

FIGURE 42 – WATER SATURATION DURING STEP 4 WITH AND WITHOUT EDZ

Chapter II.7 1D MODEL WITH MECHANICS

As said in Section 3.2, once gas pressure reaches a given value called "fracturing pressure", fractures are induced in the rock environment. These fractures could put at risk the insulation of the repository. It is then highly important to be able to model this phenomenon and identify the conditions in which it happens to avoid its occurrence.

To be able to model this phenomenon, a mechanical model has to be coupled with the previous one (which was exclusively hydraulic), this is described in this section.

Section 7.1 MODEL PARAMETERS

The mechanical model developed in the framework of this master's thesis is purely elastic for simplification reasons. This means that fractures are not observed as such. Indeed, as the material is considered as elastic, if tensile stresses are applied, the domain should swell with no fracturing/plastic limit. Therefore, the way that is used to identify potential fracturing is to display stresses evolution. If the latter reach the maximum tensile stress of the rock, it will be considered that fracturing happens.

A last comment can be made about the expected fracturing direction. As seen in Figure 18 – Gas transport mechanisms (Marschall et al., 2005), the favoured direction is fracturing along the x direction. The tensile stresses as well as displacements are then expected to be in the y direction.

All mechanical properties are presented in Tables 7 and 9. However, Young's modulus in the interval was determined by a parametric study. Indeed, as already said, the properties of the interval are artificially imposed to fit at most its real behaviour (because the interval equipment with all the pipes as shown in Figure 20 is not fully modelled). Young's modulus value has no influence in the model without mechanics, but it has some here. Its value should be large enough to ensure mechanical stability, but it should not imply too much rigidity and impact the mechanical behaviour of the argillite nearby.

In order to choose the right value for it, the modulus was decreased until the results of mechanical simulation are steady and therefore not impacted by the value anymore. From Figure 44, it can be seen that between $E = 10^7$ MPa and $E = 8.10^6$ MPa, only very slight differences appear in the displacements results. The final value for Young's modulus in the interval was then chosen to 10^7 MPa.

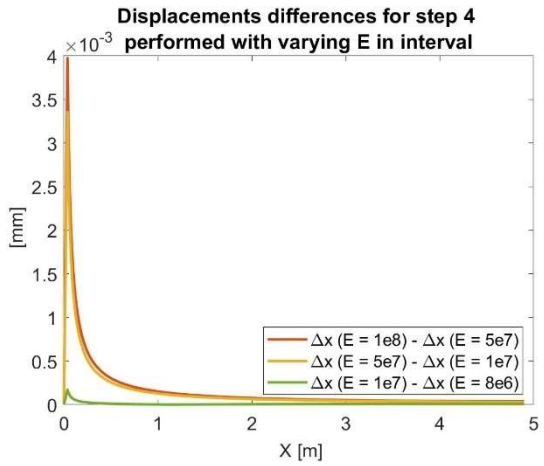

FIGURE 43 – DETERMINATION OF YOUNG'S MODULUS VALUE IN THE INTERVAL

Section 7.2 INITIAL AND BOUNDARY CONDITIONS

The flow initial and boundary conditions applied to this new model are exactly the same as the ones described in Section 5.4. In the present section, the initial and boundary conditions in terms of mechanics are presented.

At first, it was chosen the conditions that seemed the most convenient for a one-dimensional model (see Figure 45). In other words, the displacements according to the y-direction were blocked on the upper and lower boundaries. However, as already said, in case of fracturing, the displacements should happen in the y direction. Given the small height of the domain, blocking displacements at the boundaries also blocks them on the whole domain. Therefore, other boundary conditions were chosen.

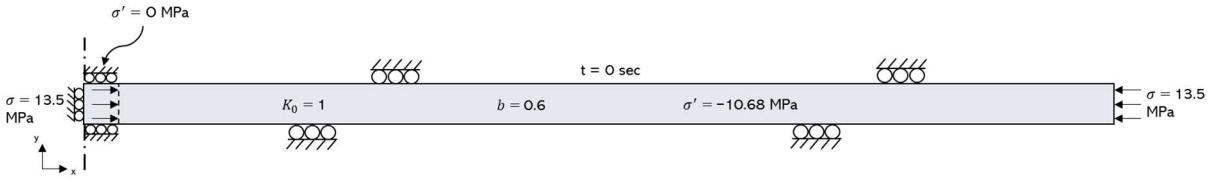

FIGURE 44 – FIRST TRY OF MECHANICAL BOUNDARY AND INITIAL CONDITIONS AT STEP 1

The second conditions that were chosen to tackle this issue (see Figure 46) were to apply a stress (equivalent to total stress state) on the upper boundary of the domain (except on the interval) instead of blocking the displacements. This allows the swelling of the domain if it is required.

As for other boundary conditions, there is a boundary condition on the right boundary that consists in the application of a stress corresponding to the total stress. Additionally, all the interval boundaries in contact with the outside of the domain (so, not the one between the interval and the rock environment) have their displacements blocked in the direction perpendicular to their orientations.

Moreover, there is an application of a linear stress of the total stress value on the boundary between the interval and the argillites at the initial time. This represents the excavation of the borehole. Indeed, before the excavation, the stress state corresponds

to the initial one in the rock. Then, during the excavation, this stress is decreased to reach a value of zero after twelve hours (time of drilling as mentioned for the hydraulic model).

The initial conditions consist in the application of the effective stress in all directions (K_0 = 0) on the whole rock domain. Its value was computed upon Equation 23. It should be noted that because of sign convention for a compressive stress, the initial effective stress applied in Lagamine is negative.

$$\sigma' = \sigma - b.p_w = 13.5 - 0.6 * 4.7 = 10.68 \text{ MPa} \quad \text{(EQUATION 23)}$$

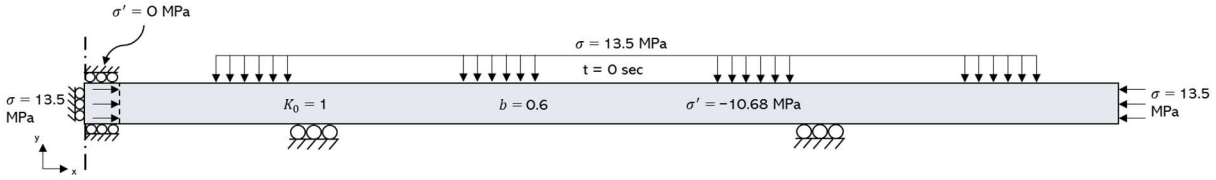

FIGURE 45 – FINAL MECHANICAL BOUNDARY AND INITIAL CONDITIONS AT STEP 1

Once the excavation is realised, the stress state inside the whole domain at the beginning of each step corresponds to the stress state at the end of the previous one (like it was the case for the hydraulic model).

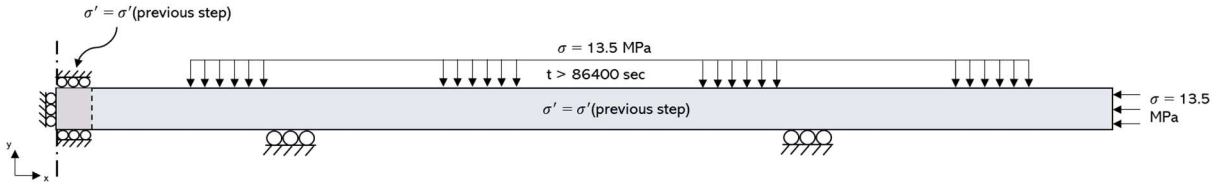

FIGURE 46 - MECHANICAL BOUNDARY AND INITIAL CONDITIONS AT STEPS 2 TO 4

Section 7.3 RESULTS

7.3.1 COMPARISON OF PURELY HYDRAULIC AND HM MODELS

This section aims at highlighting differences between models before and after the introduction of mechanics. It should be noted that the whole sequence of steps was realised with mechanics but only results of the fourth one will be presented here because trends are similar for all of them.

The first results that are displayed (Figures 48A and B) are water and gas pressures. As it can be seen, the addition of mechanics doesn't impact the general trend that was previously observed, even though values are slightly different. Water pressures are a little reduced which can be explained by the slight displacement of rocks (see Figure 51). Indeed, as more volume is available, the fluid pressure decreases.

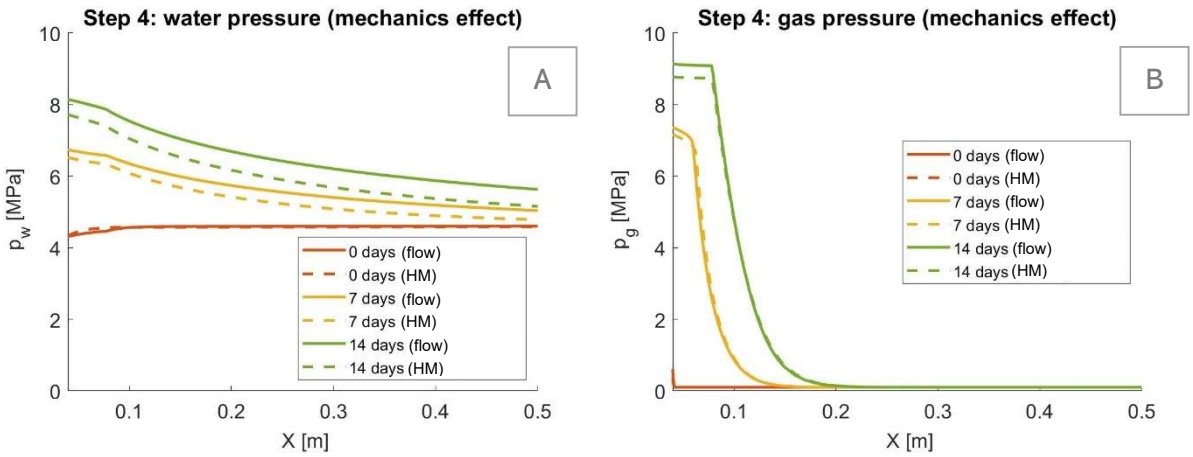

FIGURE 47 – WATER AND GAS PRESSURES DURING STEP 4 FOR FLOW AND HM MODELS

As for water saturation, it also follows the same trend as before the addition of mechanics but with slightly smaller values. This is also due to the displacements and increased volume available for water.

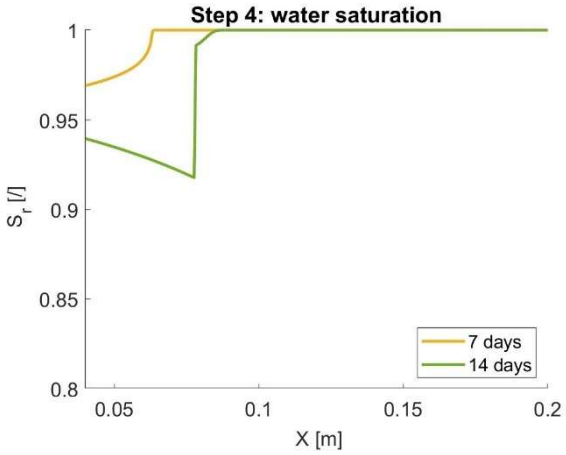

FIGURE 48 – WATER SATURATION DURING STEP 4

As for the way of transport of gas in the porous medium, it still follows the same trend. However, the quantity of gas is ten times larger than it was in the model without mechanics. This is again due to the increasing volume of pores which let more gas enter.

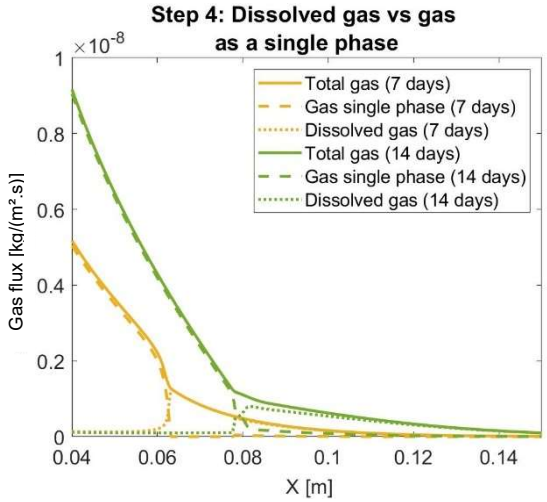

FIGURE 49 – GAS TRANSPORT MECHANISMS DURING STEP 4

Now that hydraulic parameters have been compared with the results obtained without mechanics, the mechanical parameters should be observed. First, in Figures 51A and B, displacements according to the x and y directions show oscillations at the border between the interval and COX.

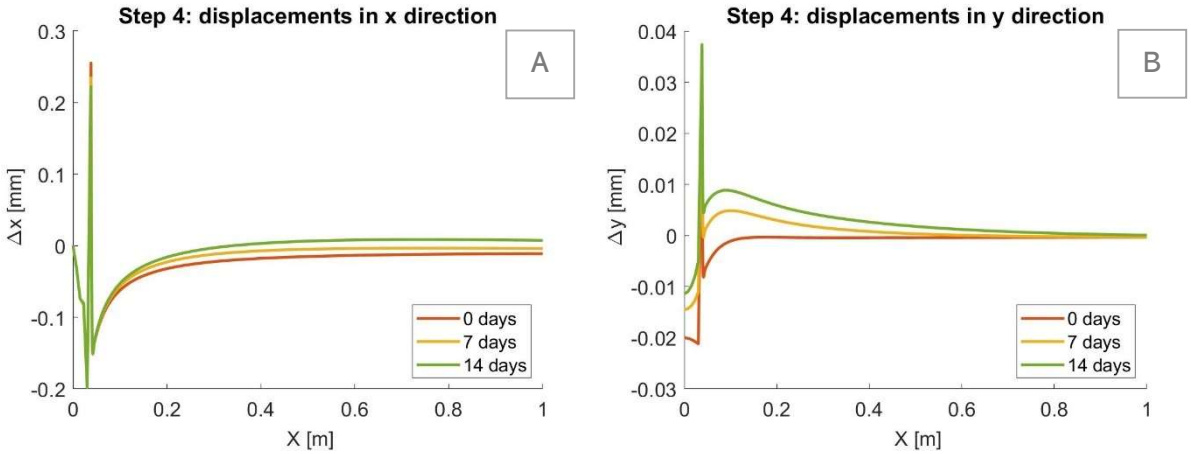

FIGURE 50 – DISPLACEMENTS IN THE X (A) AND Y (B) DIRECTIONS ON THE WHOLE DOMAIN DURING STEP 4

Next, effectives stresses in x and y directions are plotted and displayed in Figures 52A and B. As mentioned before, the stress state is isotropic. This is represented by the value at which stresses stabilise, around -10MPa for all, which corresponds to the imposed initial effective stress state of -10.68 MPa. More specifically, the values it is interesting to look at are the ones at the boundary with the interval. The most interesting direction to look at is the y direction because, as already mentioned, this is the direction in which tension should be observed in the case of fracturing. It can be seen here that it is only increased of maximum 1 MPa near the interval. This means that the current flow rate and period of time applied only induce a slight reduction in the compressive behaviour of the stress but not as much as to induce tension in the medium.

As for the effective stress in the x direction, it is due to the fact that, given the injection of gas, the medium tends to swell towards the direction of gas flow. However, as displacements in the x direction on upper and lower boundaries of the interval are fixed, it creates a tension at the border with the rock.

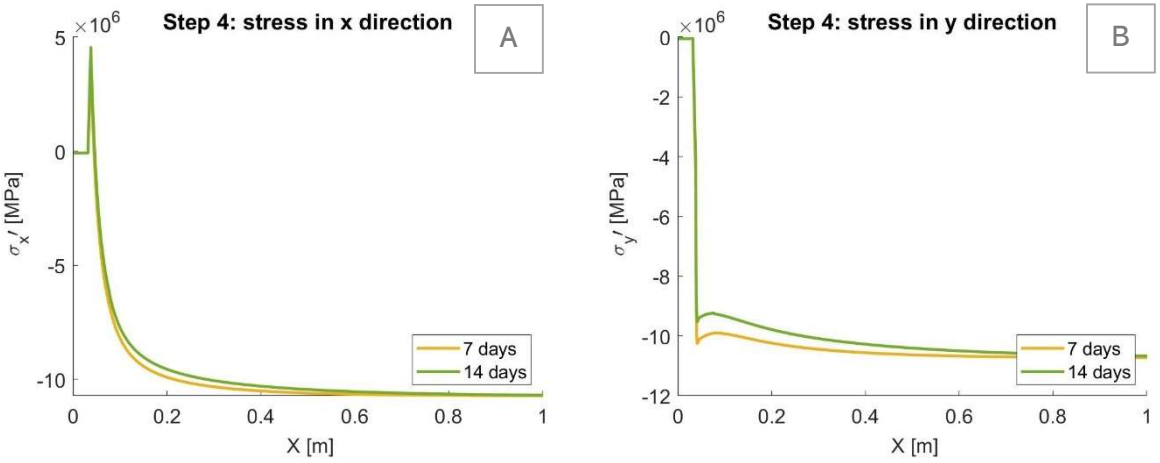

FIGURE 51 – STRESSES IN X AND Y DIRECTIONS DURING STEP 4

Section 7.4 STEP 4: GAS INJECTION – SLOW INJECTION TEST

It is also interesting to see how the different parameters evolve when the slow injection test is performed cyclically as explained in the procedure in point 3.4.4. The injection and rest times can be found in Table 14.

Start time [s]	End time [s]	Cumulated time [days]	Injection rate [kg/(m².s)]
10 435 600	11 645 200	14	$1.63.10^{-7}$
11 645 200	13 459 600	35	0
13 459 600	14 669 200	49	$1.63.10^{-7}$
14 669 200	16 483 600	70	0
16 483 600	17 693 200	84	$1.63.10^{-7}$
17 693 200	19 507 600	105	0
19 507 600	20 717 200	119	$1.63.10^{-7}$
20 717 200	22 531 600	140	0
22 531 600	23 741 200	154	$1.63.10^{-7}$
23 741 200	27 369 600	250	0

TABLE 14 – INJECTION AND REST TIMES FOR SLOW INJECTION TEST (DE LA VAISSIÈRE, 2021)

The simulations for the slow injection test consist in the realisation of the first three steps (excavation, maintenance, draining) as they were performed previously. Then, the fourth step is performed according to the times of injection and rest displayed in Table 14.

In Figures 53A and B, gas and water pressures evolution with time at various distances from the interval are plotted. From these, it can be identified clearly the periods of injection and shut-in when gas and water pressures respectively increase and decrease, peaks corresponding to the moments at which the injection is stopped. Moreover, at the beginning (during the first three cycles), the peak gas pressure increases at each cycle while, after that, it is steady around 11 MPa places at 0.038m (interval boundary) and 0.078m (EDZ boundary). However, water pressure has a different behaviour. Indeed, the peak pressure goes down at each cycle in the area of the borehole and goes up further from it (from 0.35m). Physically, it could be explained by the fact that gas pushed water away from the borehole, implying greater water pressures as the interface between gas and water moves forward.

The behaviour of gas pressure is an important information for the main question of the present work. Indeed, the fact that it stabilises after performing a given number of cycles suggest that, for a given injection rate, the pressure exerted on the rock will not rise without end.

A next observation is the fact that at first pressures are larger in the interval (in red) than a bit further but, with time, they all seem to get closer and closer to finally nearly homogenise. An exception being at x = 2m where water and gas pressures are not yet too much impacted after these five injection phases. This suggests that the effects of the gas injection have a limited spatial impact.

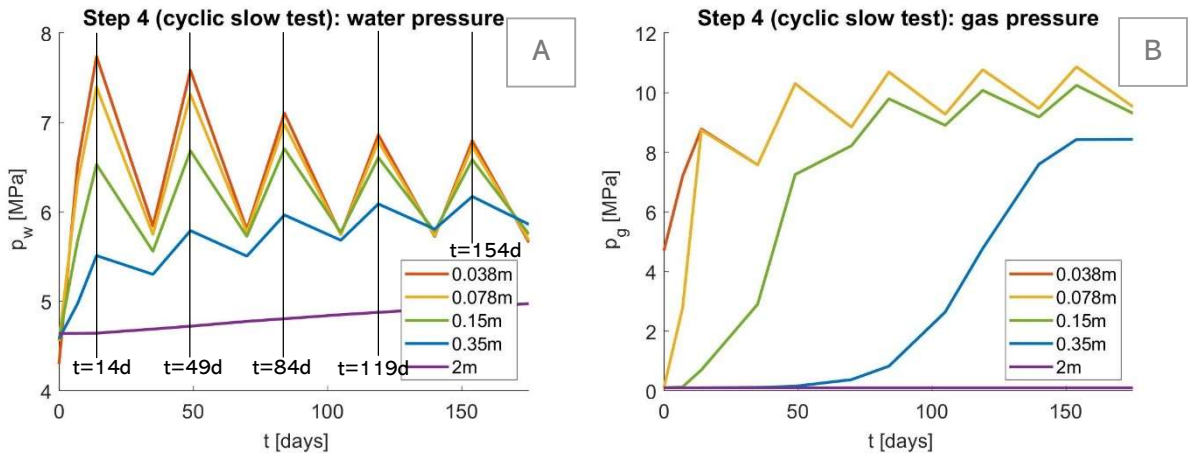

FIGURE 52 – WATER (LEFT) AND GAS (RIGHT) PRESSURES DURING SLOW INJECTION TEST

In Figure 54, it has been plotted how the water saturation evolves according to the x coordinate at each pressure peak. As it could be expected, the more gas is injected, the smaller the value of water saturation at the border with the interval. Additionally, after each injection step, it also decreases each time further from the interval.

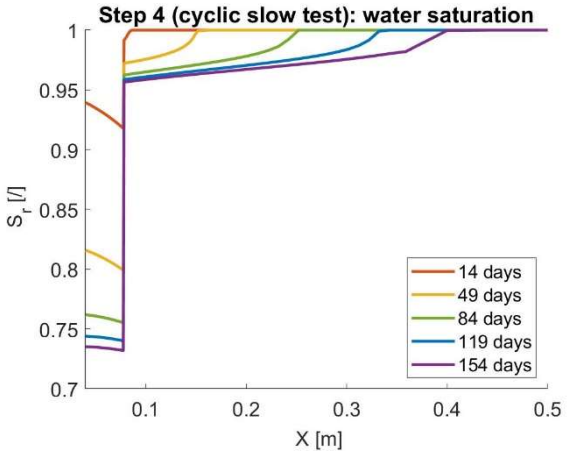

FIGURE 53 – WATER SATURATION EVOLUTION DURING SLOW INJECTION TEST

As for the displacements upon the y direction, it can be seen that the largest effects are observed right next to the interval and are rapidly decreased. Indeed, at x = 0.038m, the displacements are about 0.04mm while they only amount to 0.01mm at x = 0.078mm. However, it can be clearly seen that displacements follow a general trend of swelling and settling with the gas injection phases. However, once gas injection is stopped, even if the displacements go back down, they do not recover their initial value.

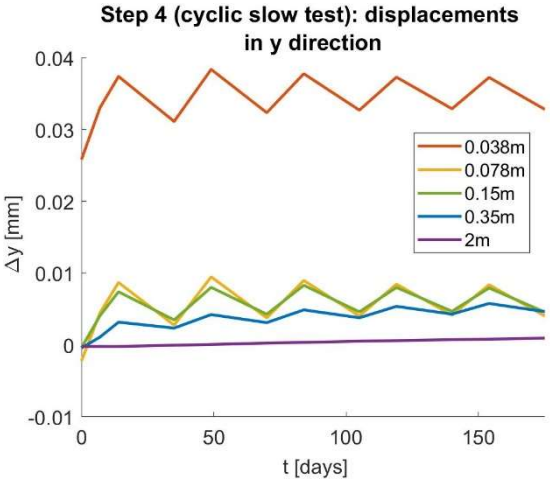

FIGURE 54 – DISPLACEMENTS DURING SLOW INJECTION TEST

Finally, the type of transport for gas can be described. It is displayed in Figure 56. The general trend is the same as it was for the one-phase injection test (red curve). Indeed, the gas is at first transported as a single phase, then when a given pressure is reached, it is transported as a dissolved phase in water. However, as the number of cycles increases, the amount of gas present in the medium at a given distance from the borehole also rises. It is also noticed that the distance over which hydrogen is present as a gaseous phase is much greater. Indeed, it is four times bigger between the first and fifth injections.

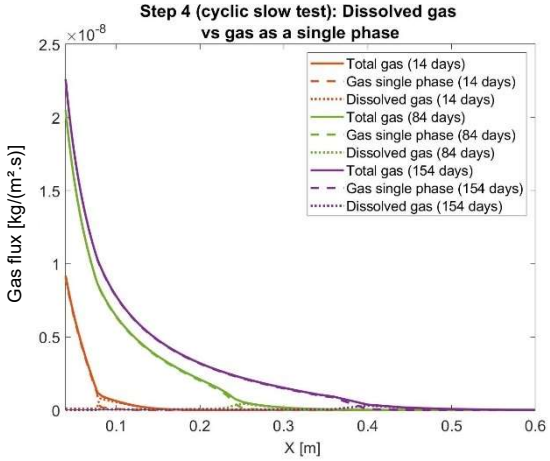

FIGURE 55 – TRANSPORT MECHANISMS DURING SLOW INJECTION TEST

Section 7.5 STEP 4: GAS INJECTION – FAST INJECTION TEST

As mentioned in previous sections, gas injection tests are performed as part of PGZ3 experiment in order to induce fractures and determine their closer pressures and orientations. They consist in the injection of a large flow rate of hydrogen gas ($8.15.10^{-5}$ kg/(m².s)) through the interval until a fracture is induced, then a period of rest and finally an additional injection to determine the closer pressure and the orientation. However, given the single dimension of the present model, only the first step is relevant to be modelled. The initial and boundary flow conditions for this step were adapted according to Figure 57.

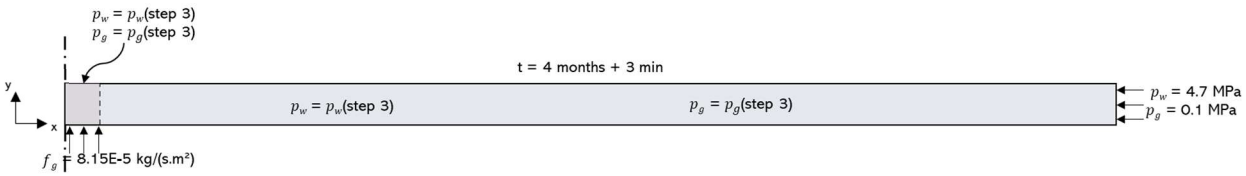

FIGURE 56 – INITIAL AND BOUNDARY CONDITIONS AT STEP 4 DURING FAST INJECTION TEST

From data available in de La Vaissière & Talandier (2022), an injection lasting around three hours was required to induce a first fracturing. Therefore, the simulation was carried out for a period of time of three hours. As for the slow injection test, the first three steps were performed as previously and only the fourth one was adapted.

In Figures 58A and B, water and gas pressures during this procedure are presented. These both reach values a lot more important than during the slow procedure. Indeed, after three hours of injection, water and gas pressures amount respectively to 26 MPa and 28 MPa (against 7.5 MPa and 11 MPa for the slow flow rate). Physically, it is explained by the fact that, given the permeability of the COX, in such a short time interval, the gas flow cannot push water on large distances. Therefore, it accumulates right outside the interval and its pressure raises. Given this accumulation of gas, a pressure is even tough exerted on water whose pressure is thus also increased.

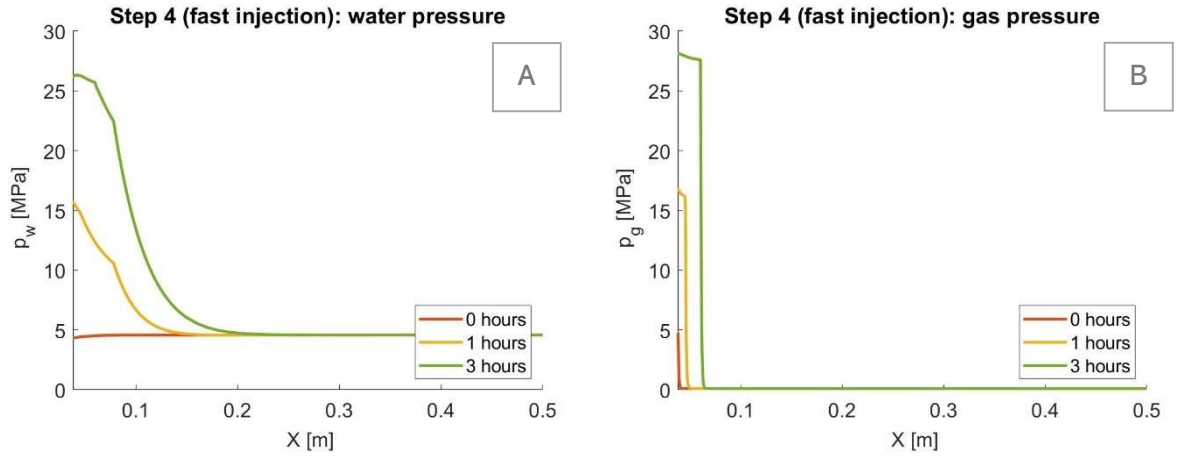

FIGURE 57 – WATER AND GAS PRESSURES DURING FAST INJECTION TEST

As for the water saturation, it decreases significantly in the excavated damage zone (under 90% in only three hours against minimum 92% after fourteen days with the slower injection rate) while it does not at all in the non-damaged zone. This is due to the favoured flow in the EDZ given its greater permeability and smaller gas entry pressure.

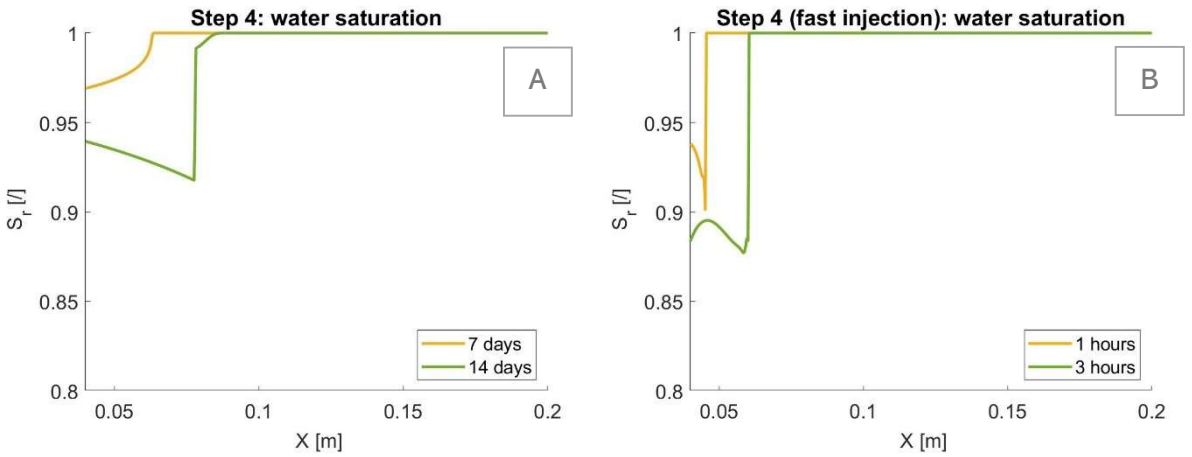

FIGURE 58 – WATER SATURATION DURING 1ST PHASE OF SLOW INJECTION (A) AND FAST INJECTION TESTS (B)

In Figures 60A and B, multiple elements can be highlighted. First, the gas quantity reaches 3.10^{-6} kg/(m².s) while it amounted only to 10^{-8} kg/(m².s) during the slow injection procedure. This seems logical as the injected gas flow is 500 times bigger. All this gas is under a gaseous phase (not dissolved in water), due to its high pressure. However, it can also be noticed that the distances over which gas is found are smaller than they were when gas had more time to percolate through the porous medium during the slow injection procedure.

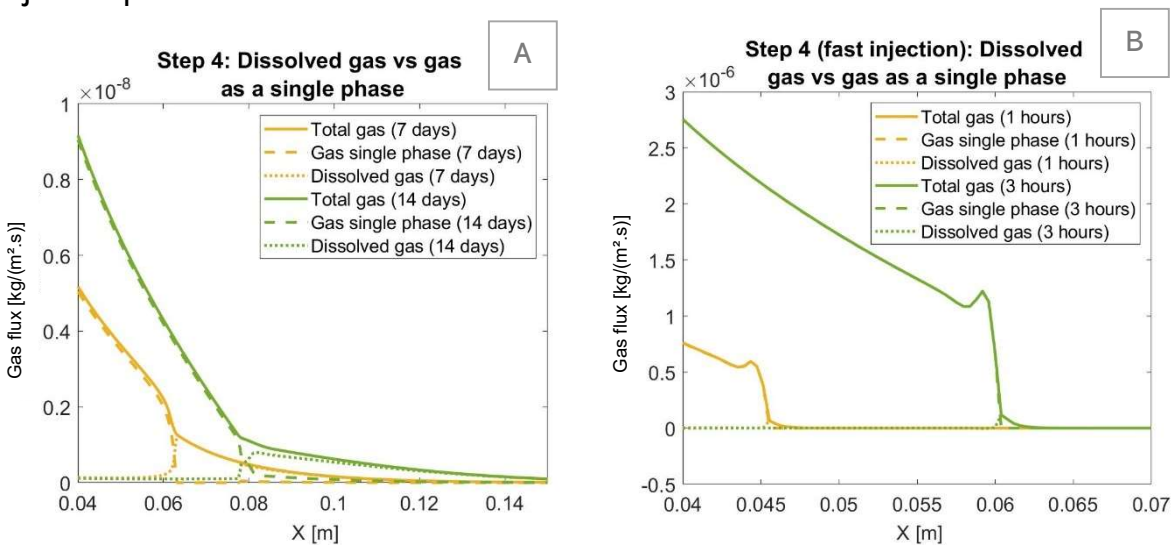

FIGURE 59 – GAS TRANSPORT MECHANISMS DURING 1ST PHASE OF SLOW INJECTION (A) AND FAST INJECTION TESTS (B)

Now that fluids flow behaviours are understood, the mechanical parameters should be described. The displacements as well as the stresses in the y direction are plotted in graphs hereunder (see Figures 61A and B). They show that, after three hours of injection, tensile effective stresses of about 5 MPa are induced around the borehole. This stress induces a quite large displacement of 0.1mm (against 0.04mm during the slow injection procedure). The tensile strength of Callovo-Oxfordian argillites is comprised between 0.9 and 5.4 MPa (Pham, 2006), it should be compared to the total tensile stress computed here which amounts to 5 MPa. These results seem therefore to confirm the hypothesis of the opening of a fracture in the rock substrate.

It should be added that the reason why the important stress and displacements are concentrated right after the interval and do not propagate further in the medium is the elastic behaviour of the model. Indeed, as mentioned previously, as no plastic properties were implemented in the model, the domain can only swell but not break. In reality, once the plastic limit is reached, a fracture is created and gas can easily spread through it (leading to a decrease in gas pressure), accumulate a bit further and once again induce fracturing, and so on. Therefore, the behaviour that would be observed is an increase in both variables with time at x = 0.039mm, a steep decrease right after the fracturing and then a new increase a bit further from the borehole. However, in this case, as no fracturing is generated, the stress and displacement are concentrated in the very near area of the interval.

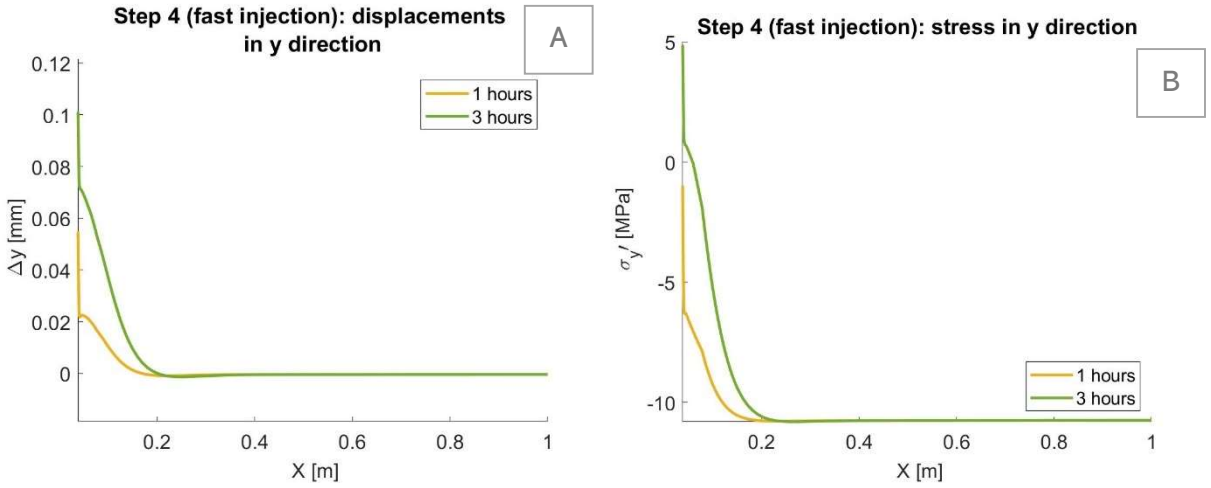

FIGURE 60 – DISPLACEMENTS AND STRESS IN Y DIRECTION DURING FAST INJECTION TEST

Part III NUMERICAL SIMULATIONS (2D)

Once simulations in one dimension and axisymmetric state are well calibrated, the next step is to develop a two-dimensional axisymmetric model. The main purpose of the latter is to characterise the flow in the surroundings of the whole borehole, not only around the injecting interval. It will also be studied the possibility of fluid percolation along the borehole wall (instead of through the rock). Therefore, in this last part of this work, first a 2D model is computed to describe through different aspects the percolation behaviour of gas along the borehole. A second 2D model is then computed with the addition of contact elements between the borehole and the rock, also to characterize the gas percolation. Finally, the last chapter is dedicated to a comparison between results computed with simulations and the ones measured during the in-situ experiment.

Chapter III.8 2D MODEL

Section 8.1 MODEL GEOMETRY

The geometry of PGZ3 experiment was already detailed in point 3.4.3. For this two-dimensional model, not only one interval, and the rock in its prolongation, are modelled, but the whole sequence of packers, resins and interval (and the COX in their extension) is represented. In Figure 61, the 2D axisymmetric model and its specifications (dimensions and number of numerical elements) is shown. Some elements need to be clarified. First, because no flow passes through them, packers and resins are not modelled by numerical elements. Then, the distribution along the x axis is quite similar to what was done in 1D axisymmetric. This means that the mesh size is smaller in the zone corresponding to the EDZ and it increases as the distance with the borehole does. However, even if the trend is similar, the mesh size is larger in the two-dimensional model to limit the number of elements for the model to be not too heavy to run on conventional computers. In the y direction, the mesh is more precise in the area of interval number 2 (see Figure 71) as it is the one from which gas is injected in the domain.

Finally, results for the 2D simulations are presented for different cross-sections along which the different parameters are observed. Both are also represented in Figure 61.

Section 8.2 MODEL LAWS & PARAMETERS

The physical laws and parameters used for the present two-dimensional axisymmetric model are the same as the ones used for the 1D model. These can therefore be found in Section 5.2. It should be mentioned that only a purely hydraulic model is developed, mechanics is not implemented. The reason for that is that implementing mechanics into the two-dimensional model is quite heavy in memory for conventional computers and it would probably not have included major differences with what was observed in 1D because the issue studied here is mostly hydraulic. Moreover, the main goal of this 2D model is to characterize the flow in the direction parallel to the borehole.

The present model is computed directly including an excavated damage zone as defined in Chapter II.6.

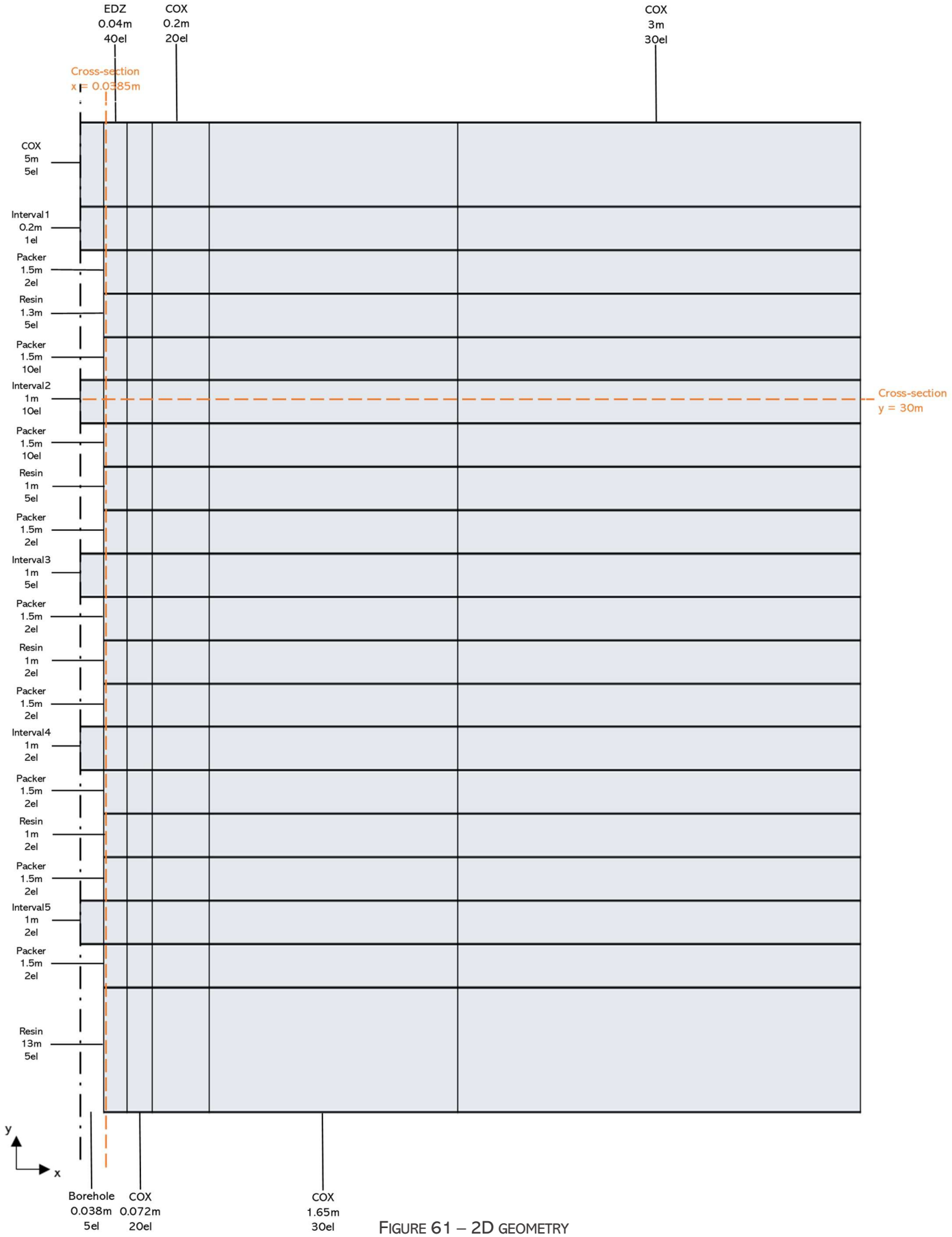

FIGURE 61 – 2D GEOMETRY

Section 8.3 INITIAL AND BOUNDARY CONDITIONS

Initial and boundary conditions are quite similar to the ones used in the one-dimensional model. The simulation is once again performed in the same four steps during which specific conditions are applied. These are described for each corresponding point in Section 8.4 hereunder. However, the initial conditions before the excavation (step 1) are presented in Annex 2. They consist in imposing water and gas pressures of respectively 4.7 and 0.1 MPa on the whole domain.

Section 8.4 RESULTS

8.4.1 FIRST STEP (EXCAVATION)

The excavation step consists in the drilling of the borehole and the placement of all equipment in it. As mentioned for the 1D model, during the excavation, water pressures are fixed to the atmospheric pressure (0.1 MPa). The drawdown is performed in intervals but also all along the left boundary of the domain which is at the interface with the borehole. A representation of these boundary and initial conditions are to be found in Annex 3.

It should be noted here that, unlike the one-dimension model, the whole borehole (and not only half of it) should be drilled. Therefore, the excavation step lasts one day (86400 sec) instead of 12 hours previously.

In Figure 63 and in Annex 8 are represented the evolution of water pressure on the domain in multiple ways. First, in Annex 8, the whole domain is represented. It can be seen that along the left boundary of the model, all pressures are set to 0.1 MPa and that they increase with the distance from the boundary. The exact pressure values in function of the x direction can be more easily observed in Figure 63 (which is a zoom extent on interval 2) and in Figure 64A (which is a cross-section at y = 30m, the middle of interval 2). From these, it is shown that the water pressures distribution has the same profile as it had in 1D.

Lastly, Figure 64B (which is a cross-section at x = 0.0385m) shows that the drawdown is performed steadily along the y axis as pressures are constant from y = 0 to 35m. However, the last five meters represent COX and not the borehole anymore. Therefore, the pressure decrease is lower.

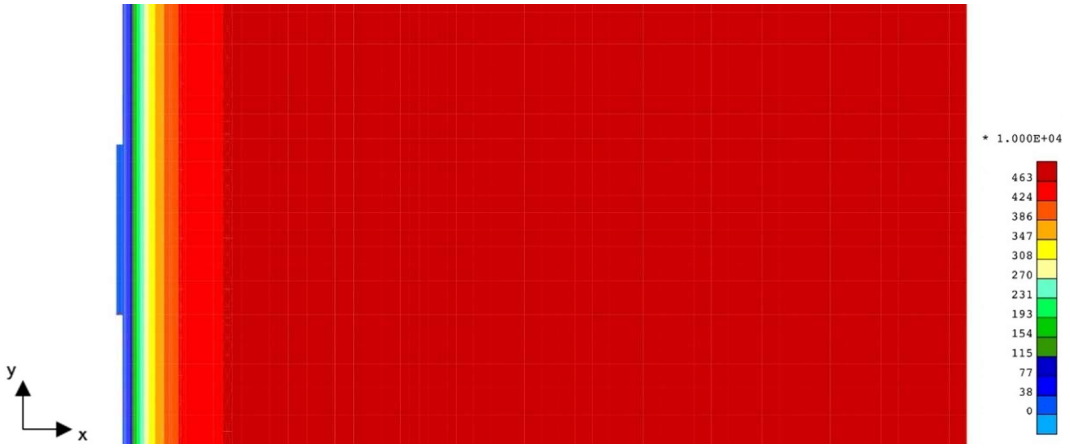

FIGURE 62 – WATER PRESSURES AROUND INTERVAL 2 DURING STEP 1

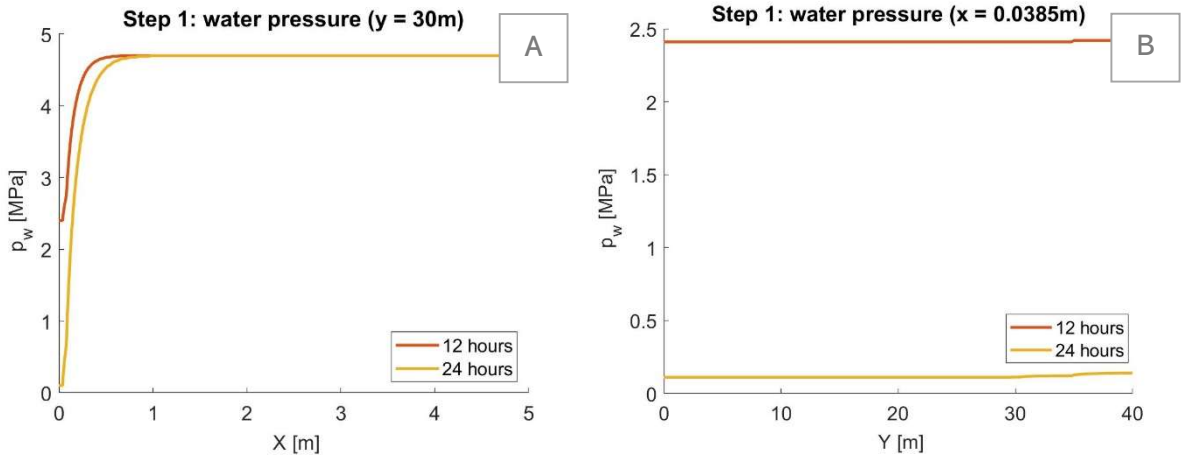

FIGURE 63 – WATER PRESSURE PROFILES ALONG Y = 30M (A) AND X = 0.0385M (B) DURING STEP 1

8.4.2 SECOND STEP (MAINTENANCE)

The second step consists in letting the domain come back to its initial conditions after the introduction of the borehole. As in 1D, the simulation is performed over a period of four months. Once again, the boundary and initial conditions can be found in Annex 4.

In Annex 9, the pressure at the end of the simulation on the whole domain is represented. The pressure is equal to 4.7 MPa nearly everywhere, which means that the domain came back to its initial hydraulic conditions. This is also what can be observed in Figure 65 et Figure 66A.

What can be added from the observation of Figure 67B is that the rise happens faster around the packers and the resins while it takes more time around the intervals. This is because the packers and the resins do not allow water flows across them whereas intervals do. Therefore, the water must also flow through the interval to make the pressure increase inside them as well and it takes more time for the argillites nearby to come back at their initial pressure.

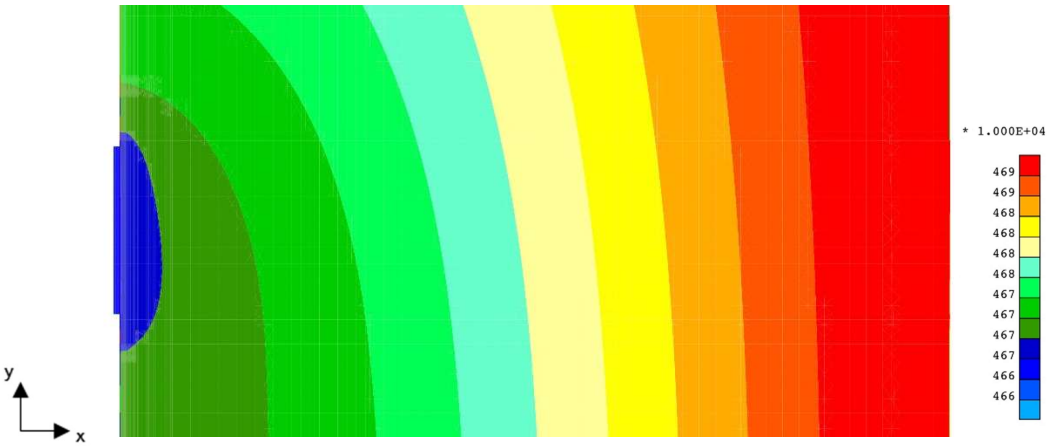

FIGURE 64 – WATER PRESSURES AROUND INTERVAL 2 DURING STEP 2

It should be noted that compared to the results in one dimension, the horizontal profile has a less precise resolution (not well curved line). This is of course due to the fact that there are less numerical elements horizontally and especially in the excavated damage zone.

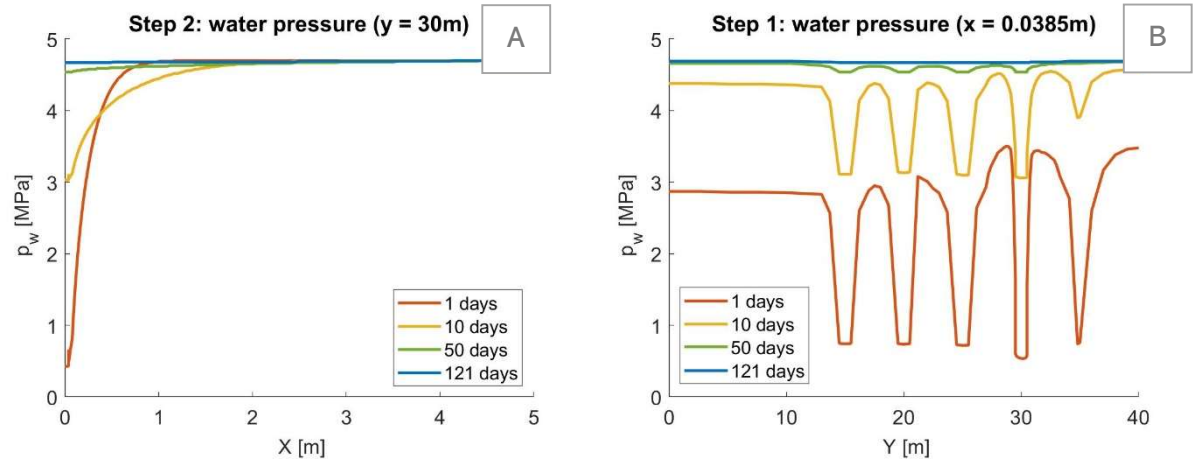

FIGURE 65 – WATER PRESSURE PROFILES ALONG Y = 30M (A) AND X = 0.0385M (B) DURING STEP 2

8.4.3 THIRD STEP (DRAINAGE)

The next step is the drainage. It consists in performing an exchange air/water in the intervals (see point 5.5.3) for more details.

As already said, the injection is performed from the second interval. Therefore, in this first 2D model, the drainage is also only performed in this specific interval and not in the others. This is showed in Annex 5 representing the initial and boundary conditions for the present step.

All results showing water pressure evolution (Annex 10, Figures 67 and 68) clearly show that no other place in the domain than the area around interval 2 is impacted by the drainage. Concerning the evolution nearby the interval of interest, the exact same trend as in 1D is observed. This means that the impact is barely visible outside the interval.

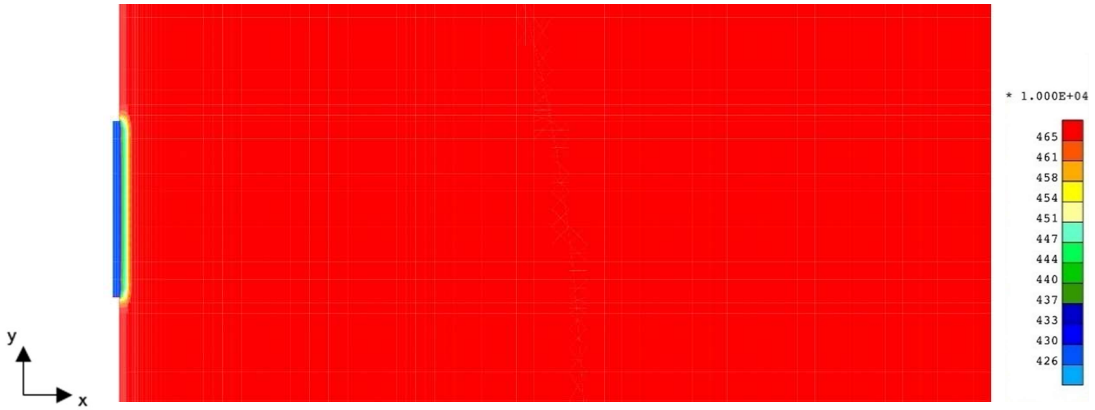

FIGURE 66 – WATER PRESSURES AROUND INTERVAL 2 DURING STEP 3

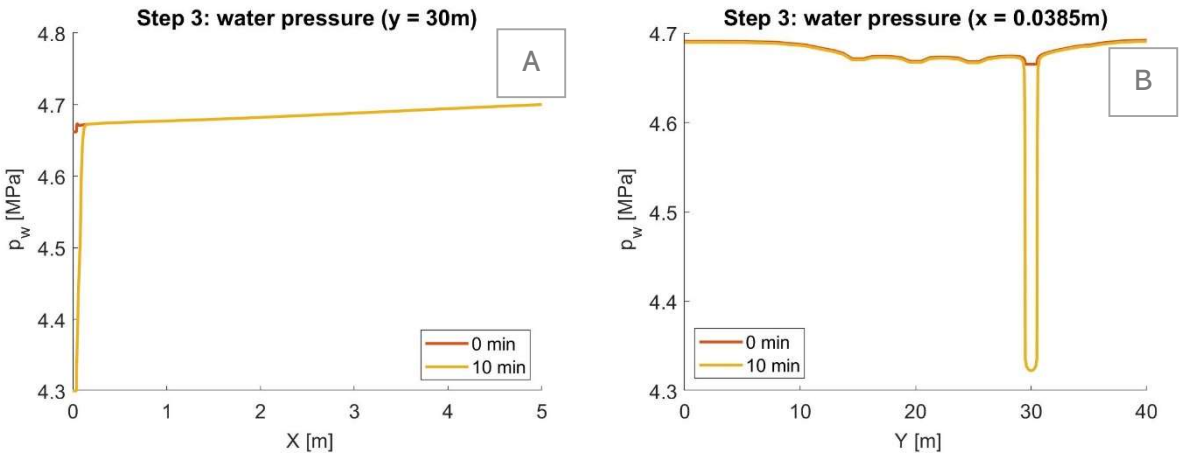

FIGURE 67 – WATER PRESSURE PROFILES ALONG Y = 30M (A) AND X = 0.0385M (B) DURING STEP 3

As for the gas evolution, the trend in the area in the extension of the interval is also the same as in 1D. However, gas also flows slowly along the borehole. But as numerical elements are a few too large and the amount of gas flowing tiny, an equilibrium of pressures cannot be found between element nodes and the results show negative values at these specific locations. Finally, this draining does not impact the gas pressure in other area than around interval 2 (same as water pressures).

It should be noted that it was tried to reduce the size of elements near the injection chamber to avoid this phenomenon. However, the needed size to make the numerical oscillations disappear induced too heavy models and these could not be run in acceptable range of times. This is why it was chosen a compromise between the number of negative occurrences and simulation time.

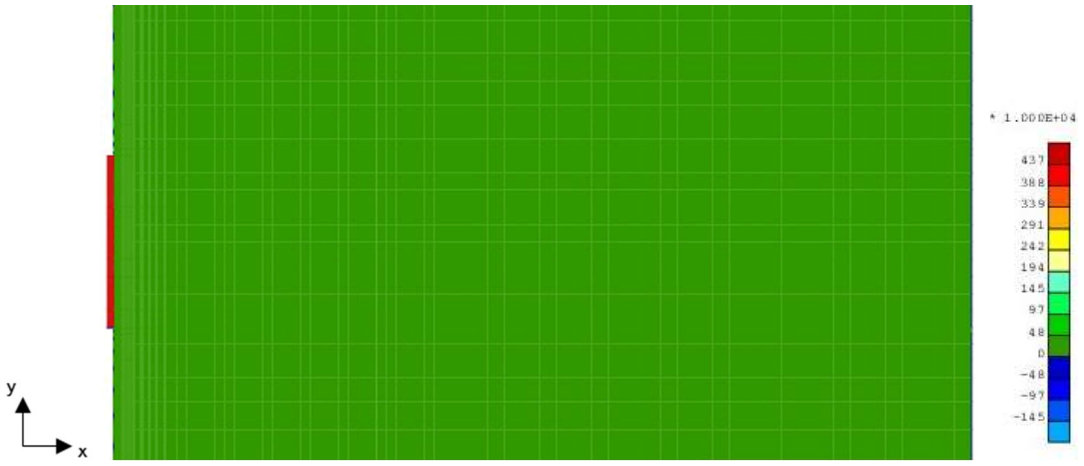

FIGURE 68 – GAS PRESSURES AROUND INTERVAL 2 DURING STEP 3

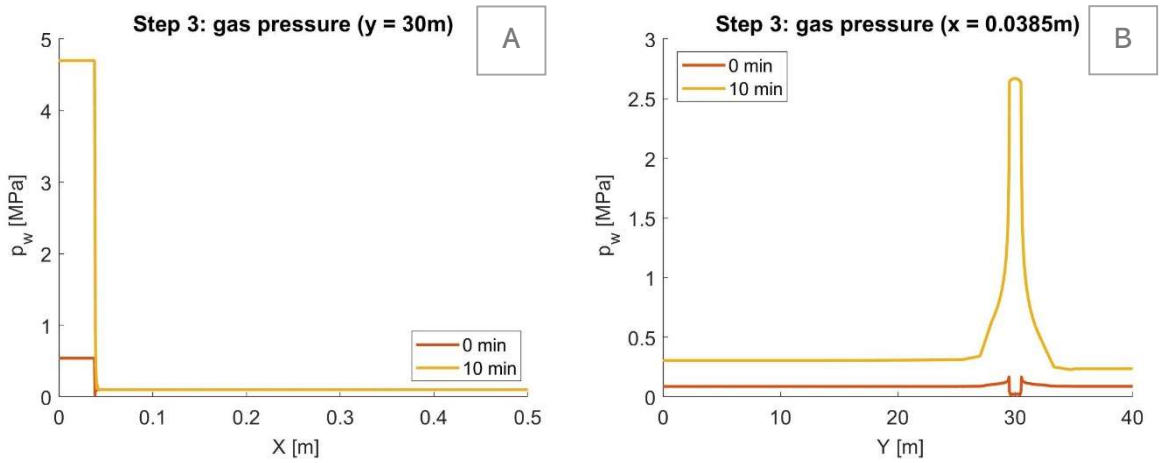

FIGURE 69 - GAS PRESSURE PROFILES ALONG Y = 30M (A) AND X = 0.0385M (B) DURING STEP 3

8.4.4 FOURTH STEP (INJECTION)

Once the borehole has been drilled, the hydraulic initial conditions in the bedrock are back to their initial values and the injection cell has been emptied, the next step is finally to perform the gas injection. The goal in the present section will be to highlight the direction in which the gas flows (potential preferential direction) and if the pressure reaches values with the same order of magnitude than in the one-dimensional model.

The conditions applied to the model during this injection step are the following.

First, let's begin with the behaviour of water. From Figure 72A, it is observed that water pressure does not increase as much as it did in 1D. Indeed, as a reminder, water pressure reached a peak at approximately 8 MPa while it reaches a little more than 5 MPa here. It can be explained by the fact that water can flow not only in the horizontal direction but also in the vertical one (see Figure 71). As no boundaries stuck water in the domain near the injection chamber, its pressure does not increase so much. However, even though water also flows in the vertical direction, it does not impact areas further than one meter away for the interval (see Figure72B and Annex 12).

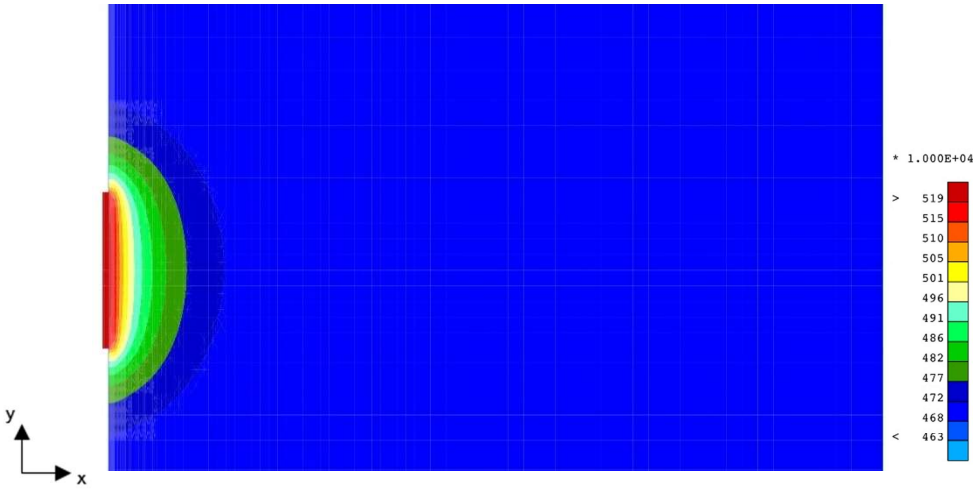

FIGURE 70 – WATER PRESSURES AROUND INTERVAL 2 DURING STEP 4

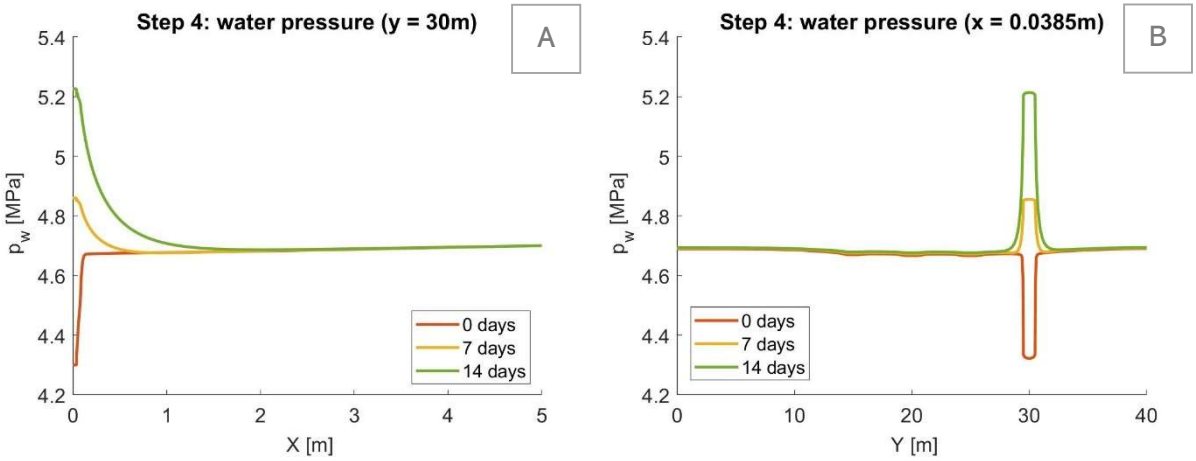

FIGURE 71 – WATER PRESSURE PROFILES ALONG Y = 30M (A) AND X = 0.0385M (B) DURING STEP 4

Concerning gas pressures, they are also significantly reduced compared to the profile computed by the one-dimensional model. Indeed, the maximum value drops by 3 to 4 MPa. However, unlike water, gas does not seem to flow a lot in the vertical direction. Figure 74B shows that, after 14 days of injection, the peak pressure is still narrow and centred on the interval. Therefore, is seems that gas does not flow further than 0.2m horizontally and even less vertically.

FIGURE 72– GAS PRESSURES AROUND INTERVAL 2 DURING STEP 4

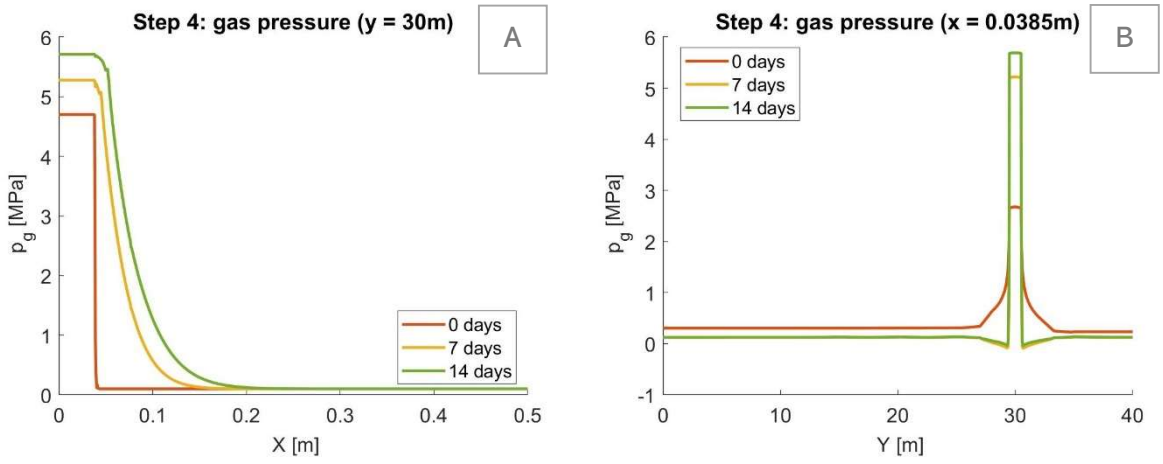

FIGURE 73– GAS PRESSURE PROFILES ALONG Y = 30M (A) AND X = 0.0385M (B) DURING STEP 4

However, the fact that gas does not flow further from the interval is not what was expected. Indeed, from de La Vaissière & Talandier (2022) it is known that, during PGZ3 experiment, the gas percolates to reach the other intervals (interval 3 after two cycles and interval 4 after three cycles). The full procedure of slow injection tests is then performed in the next point even if given the first results available after one injection period, there is no evidence that gas would flow so much further than reaching interval 3 after a second period.

8.4.5 SLOW INJECTION TEST

As it has just been mentioned, the full slow injection test (in five injection cycles) is performed to highlight a potential percolation of gas to other intervals. The procedure according to which the slow injection test is performed is the same as it was for the 1D model, Table 14 with injection times is then still valid.

First, peak water pressure evolution with time at a given point does not follow the same trend as it was for the 1D model. Indeed, in Figure75A, it is seen that the peak pressure increases a few (0.2 MPa) between the first and last periods of injection. However, this increase is very limited as the maximum value which is reached is 5.3 MPa (against 7.5 MPa for the 1D model).

As for the pressure profile along the borehole (see Figure75B), it shows that after the first period of injection the values out of the area of influence of the interval are still a little influenced by the previous step (draining) but not anymore after the third and fifth cycles. It should also be noted that the radius of influence in the vertical direction is also limited despite of the presence of EDZ.

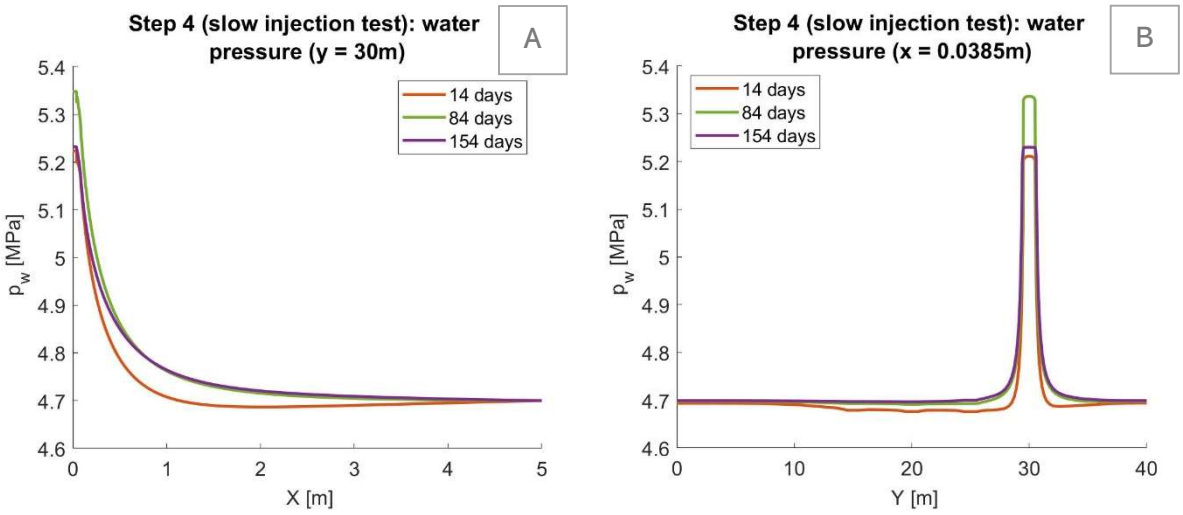

FIGURE 74 - WATER PRESSURE PROFILES ALONG Y = 30M (A) AND X = 0.0385M (B) DURING THE SLOW INJECTION TEST

As for gas pressures, the information that can be taken from Figure 76B is that the gas still does not reach the other intervals even after 5 periods of injection. Additionally, it reaches a peak pressure after 5 cycles that is slightly higher than the one that is reached after only one cycle. However, it amounts a little under 7 MPa which is still much lower than what was reached in 1D (see Figure 52) after five cycles (11 MPa). It is therefore confirmed that the size of the domain has a huge impact on the behaviour of hydraulic properties.

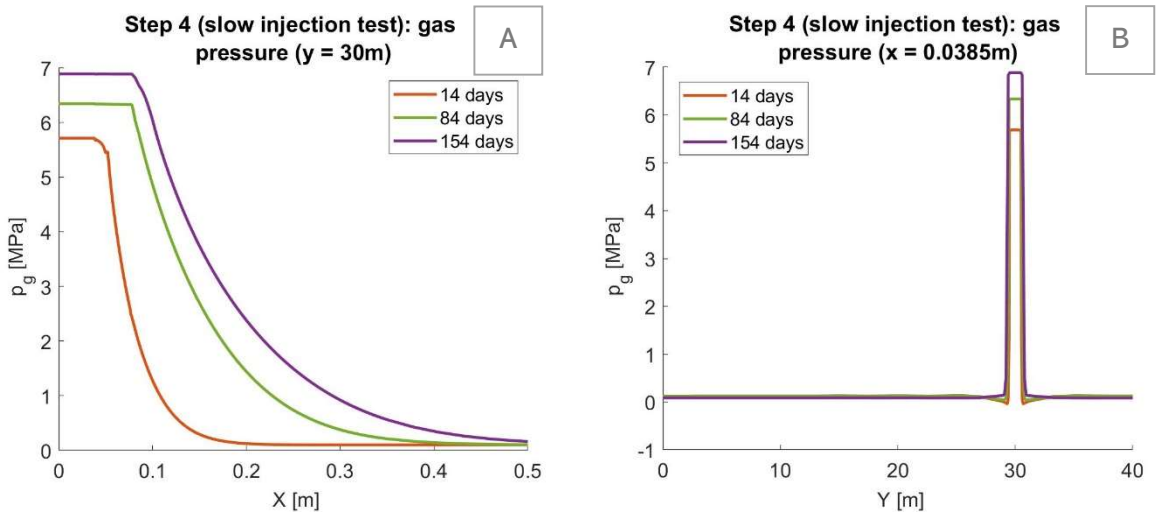

FIGURE 75 - GAS PRESSURE PROFILES ALONG Y = 30M (A) AND X = 0.0385M (B) DURING THE SLOW INJECTION TEST

This slow injection procedure was also performed with larger injection rates. Indeed, during the in-situ experiment, the procedure (which consisted of injection the same amount of gas at each cycle) was not followed and the injection rate was increased at each cycle. The proportions with which they were increased are available in Table 15.

As for the results (displayed in Figures 77A and B), the peak pressure values get closer to what was observed in one dimension. However, even if injection at a bigger rate had a small impact on the quantity of gas transported along the y axis (see Figure77B), it is still not as much as expected.

Injection cycle	Start time	End time [days]	Multiplication coefficient of the injection rate
1	0	14	1
2	35	49	2
3	70	84	4
4	105	119	10
5	140	154	10

TABLE 15 – MULTIPLICATION COEFFICIENTS OF THE INJECTION RATE AT EACH CYCLE OF THE SLOW INJECTION TEST

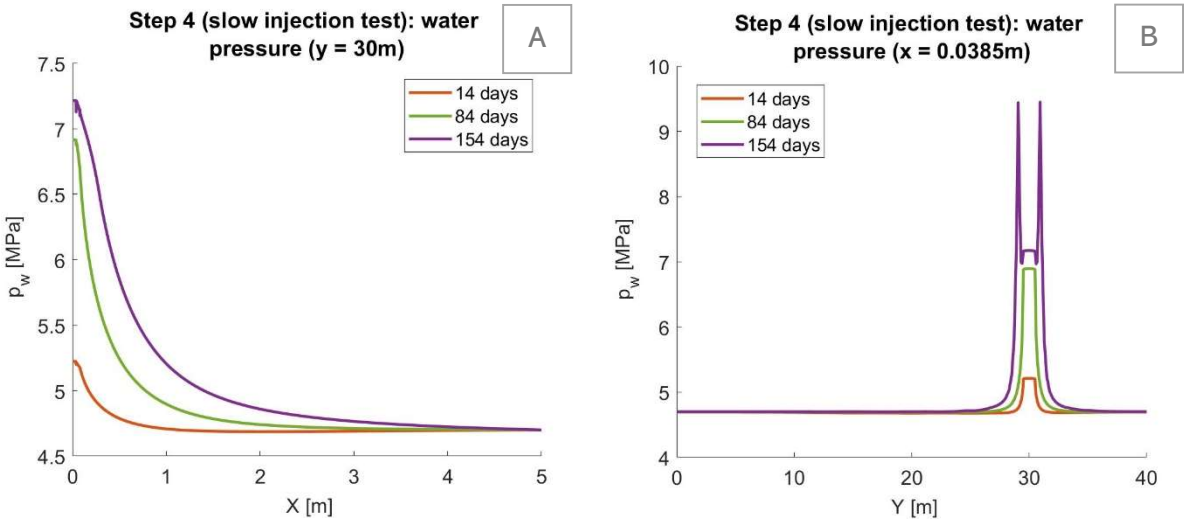

FIGURE 76 – WATER PRESSURE PROFILES ALONG Y = 30M (A) AND X = 0.0385M (B) DURING THE SLOW INJECTION TEST WITH INCREASED INJECTION RATES

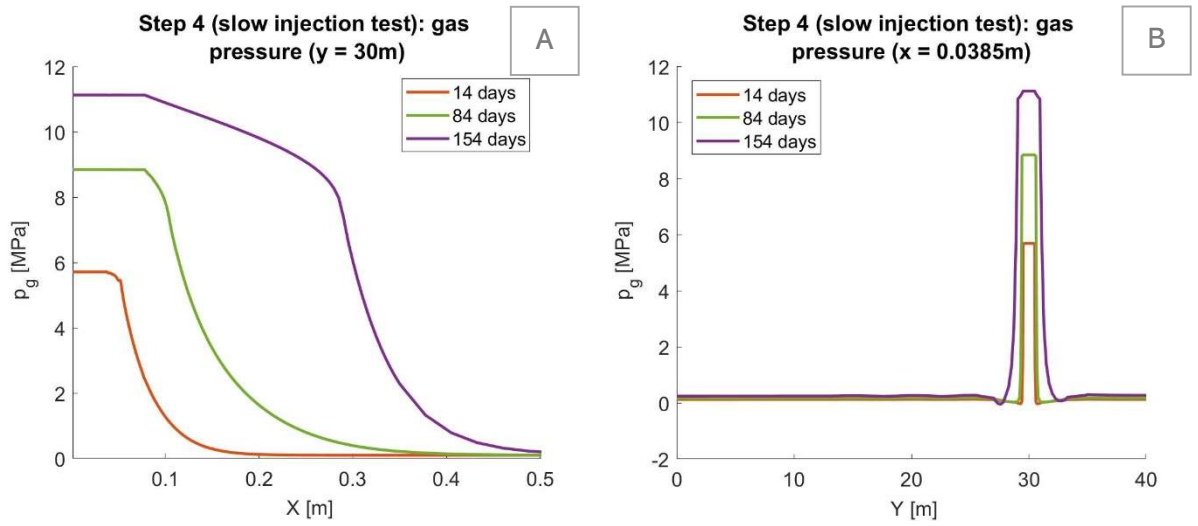

FIGURE 77 – GAS PRESSURE PROFILES ALONG Y = 30M (A) AND X = 0.0385M (B) DURING THE SLOW INJECTION TEST WITH INCREASED INJECTION RATES

From results obtained after this last simulation, it seems that percolation towards other intervals does not happen either if the gas injection is performed during longer times. However, an impact is observed when injection rates are increased. The hypothesis about the percolation of gas is that it flows through the excavated damage zone preferentially (because the permeability is higher and air entry pressure lower). However, these parameters might not be well calibrated, explaining why the impacts of both of them are then studied in the next point. The goal of the following simulations is therefore to identify the origin of the in-situ percolation.

8.4.6 PARAMETRIC STUDIES

As already mentioned, the in-situ results show a percolation of gas from the interval in which the gas injection is performed (interval 2) towards the other intervals. The hypothesis about the reason for the percolation is that the gas flows more easily in the excavated damage zone than in the sound COX because of the hydraulic properties of the porous media. However, in the previous point it was shown that, with current properties, the gas does not flow preferentially towards other intervals. One reason for that is the wrong calibration of the hydraulic parameters in the EDZ. The next simulations consist then in modifying two parameters (intrinsic permeability and air entry pressure) to ease the flow.

The first parameter that was modified is the intrinsic permeability. As mentioned in Table 13, it amounts to 2.10^{-19} m² in the EDZ (one order of magnitude higher than in the argillites). This value was increased of an additional order of magnitude (2.10^{-18} m²). The four simulations steps were then performed with that parameter and results showing the evolutions of water and gas pressures during a slow injection procedure are displayed in Figures 79 and 80. What is observed is that the pressure profiles are not too much impacted by the modification of permeability. Even though water pressure peak values are decreased, the gas ones are not. Moreover, the distance to which the gas flows in the y direction is not at all impacted. Therefore, it appears that the augmentation of permeability in the EDZ does not contribute to stimulate gas percolation along the borehole.

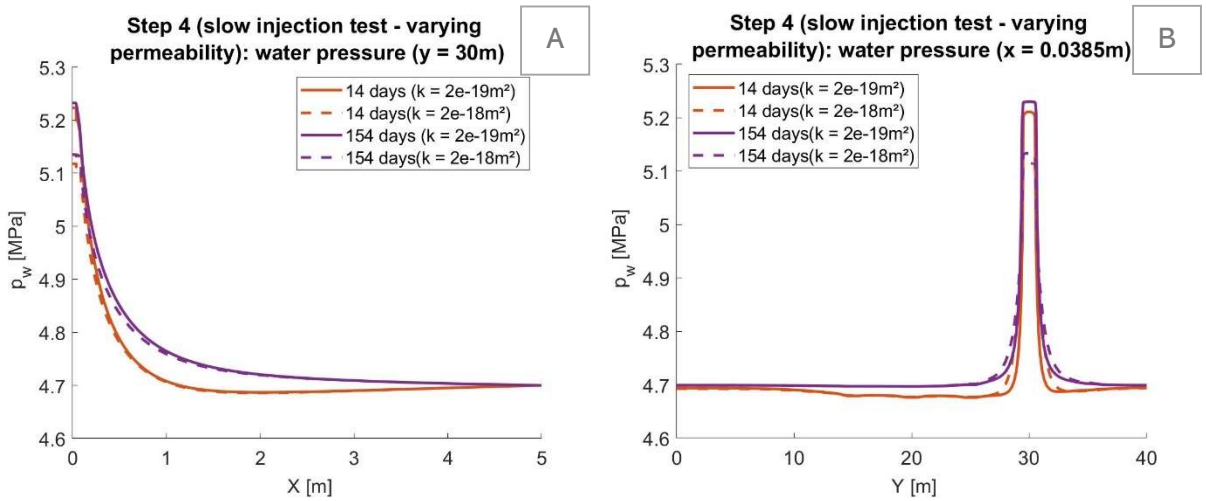

FIGURE 78 – WATER PRESSURE PROFILES ALONG Y = 30M (A) AND X = 0.0385M (B) DURING SLOW INJECTION TEST WITH VARYING PERMEABILITY IN THE EDZ

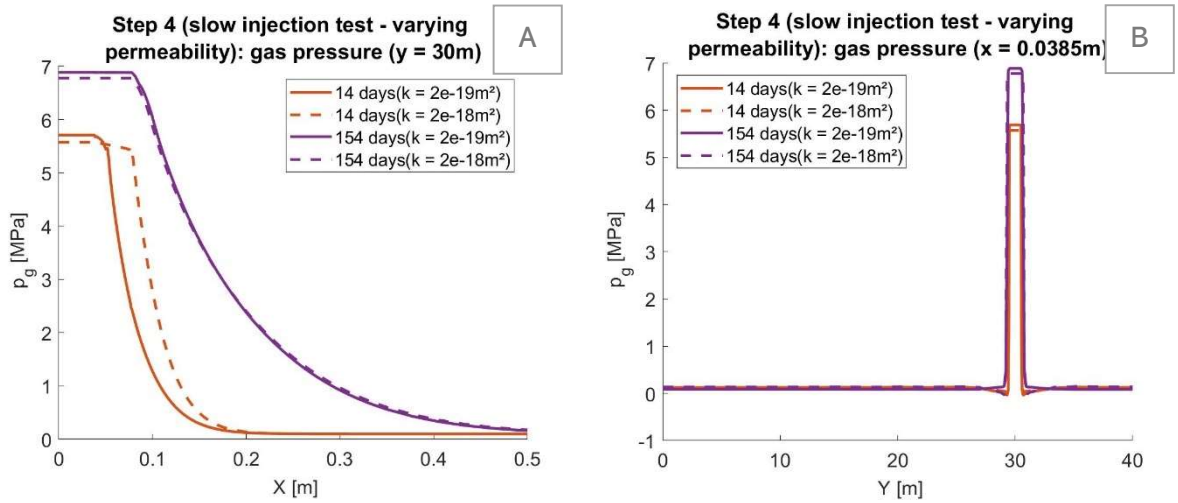

FIGURE 79– GAS PRESSURE PROFILES ALONG Y = 30M (A) AND X = 0.0385M (B) DURING SLOW INJECTION TEST WITH VARYING PERMEABILITY IN THE EDZ

The second parameter is the air entry pressure. As a reminder from Part 1 – Chapter 3, this parameter appears in the saturation expression (see Equation 4). Its initial value was set to 3 MPa (against 15 MPa in COX) and it was replaced for 0.5 MPa to compute results presented in Figures 81 and 82. From these figures, it can be seen that as for permeability, water pressure has a slightly different behaviour as well as the gas pressure profile along the x direction. However, the behaviour of gas along the y direction does not seem to be modified (except a small decrease in peak pressures).

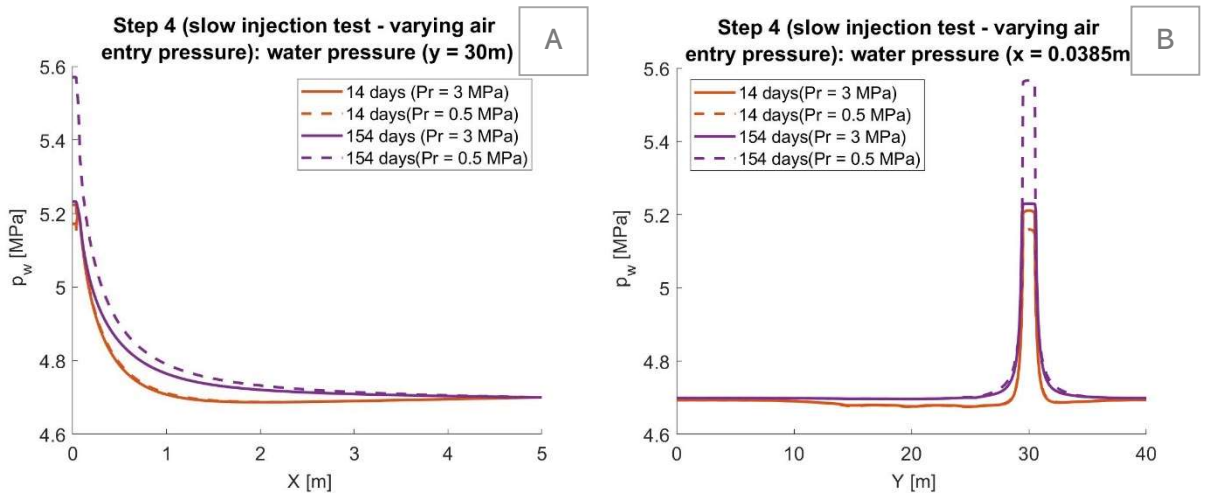

FIGURE 80 – WATER PRESSURE PROFILES ALONG Y = 30M (A) AND X = 0.0385M (B) DURING SLOW INJECTION TEST WITH VARYING AIR ENTRY PRESSURE IN THE EDZ

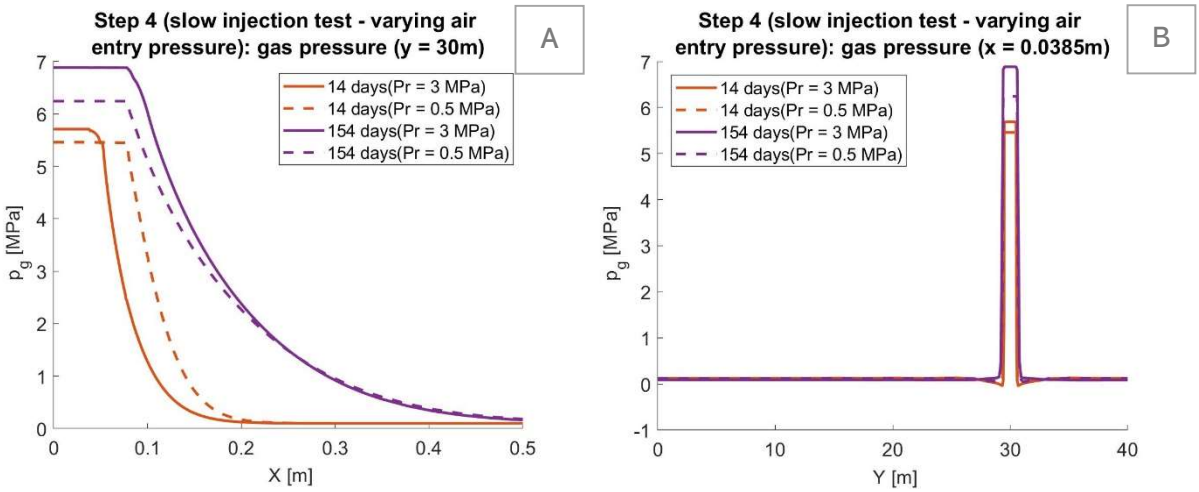

FIGURE 81 – GAS PRESSURE PROFILES ALONG Y = 30M (A) AND X = 0.0385M (B) DURING SLOW INJECTION TEST WITH VARYING AIR ENTRY PRESSURE IN THE EDZ

It seems that the hypothesis of the gas percolating through the excavated damage zone towards the other intervals is not verified. If it had been the case, the modification of properties would have had a greater effect than it did in the previous graphs. The next hypothesis that was thought of is the possibility of the gas to percolate in a very thin contact zone between the borehole and the argillites where the flow would be favoured. This new model is described in the next chapter.

Chapter III.9 2D MODEL (WITH CONTACT ELEMENTS)

Section 9.1 MODEL PARAMETERS

As already mentioned, this model differs from the previous one by adding contact elements on the border between the borehole and the argillites between interval 5 and interval 2. Numerically, these are represented by segments that act like pipes where the gas flow is favoured by the application of a more important permeability than in the EDZ or in the COX formation.

All the properties remain the same as in the 2D model previously developed. However, it should be determined the permeability of the additional contact elements. In order to do that, simulations are performed with different permeabilities ranging from 10^{-14} m² and 10^{-17} m².

Section 9.2 INITIAL AND BOUNDARY CONDITIONS

Initial and boundary conditions differ a little from what was done in the previous 2D model. In particular, during step 3, not only interval 2 is subjected to the draining but also intervals 3 to 5. A representation of these conditions is presented in Annex 6 – Boundary and initial conditions for step 3 (2D with contact elements).

Section 9.3 RESULTS

Finally, a last simulation is performed with a permeability that amounts to 10^{-14} m². This is a quite important increase in the value of intrinsic permeability. In Figures 83 A and B, it can be seen that water pressures are increased in the intervals. However, this increase is even smaller than what could be seen in the previous model without the contact elements.

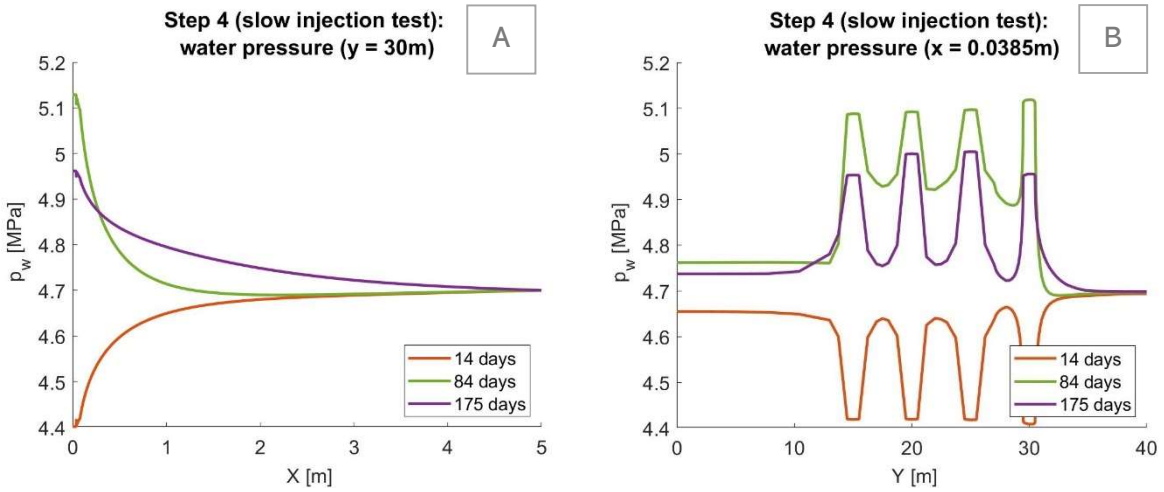

FIGURE 82 – WATER PRESSURE PROFILES ALONG Y = 30M (A) AND X = 0.0385 (B) DURING SLOW INJECTION TEST WITH CONTACT ELEMENTS (k = E-14)

What can be expected is that the gas injection through interval 2 instantly percolates to other intervals and therefore, the peak pressures are reduced. This is exactly what can be seen from Figure 85B. Indeed, the pressure is homogenized all along the borehole between the injection intervals, it can barely be seen that the gas is injected from interval 2 (at y = 30m).

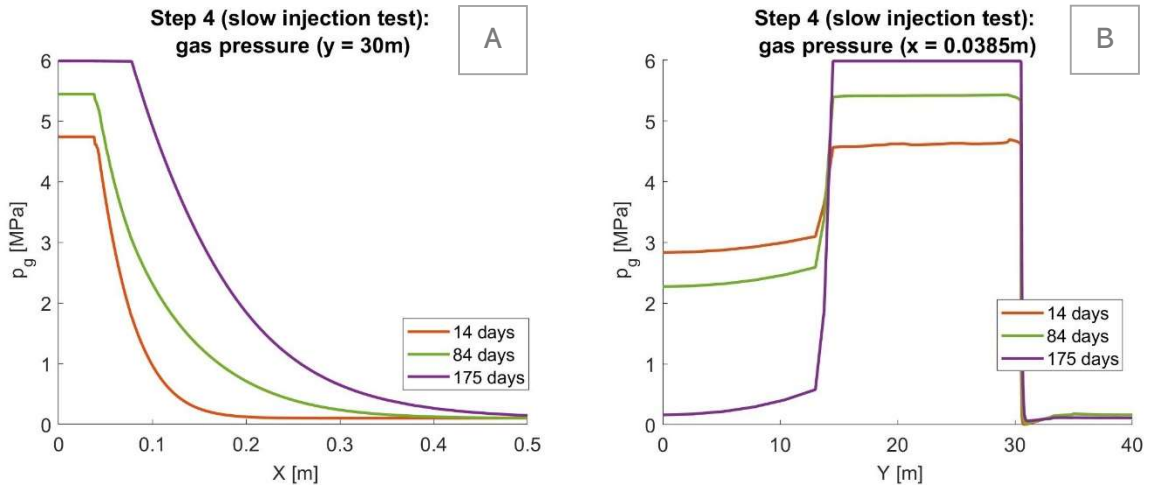

FIGURE 83 – GAS PRESSURE PROFILES ALONG Y = 30M (A) AND X = 0.0385 (B) DURING SLOW INJECTION TEST WITH CONTACT ELEMENTS (k = E-14)

Finally, it is plotted the results of the simulation performed with an increased permeability of 10^{-17} m². It can be seen from Figures 82 and 83 that profiles have exactly the same appearance as with the smaller permeability. The variation of the permeability in the contact elements therefore does not impact the results.

As the profiles that are observed are the same, a different behaviour in interval 2 is still not highlighted.

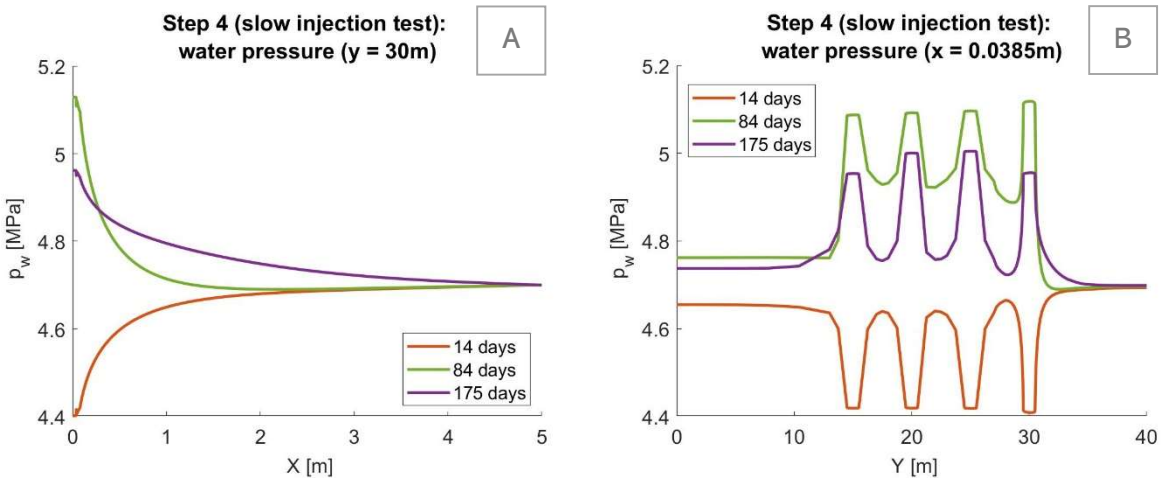

FIGURE 84 - WATER PRESSURE PROFILES ALONG Y = 30M (A) AND X = 0.0385 (B) DURING SLOW INJECTION TEST WITH CONTACT ELEMENTS (k = E-17)

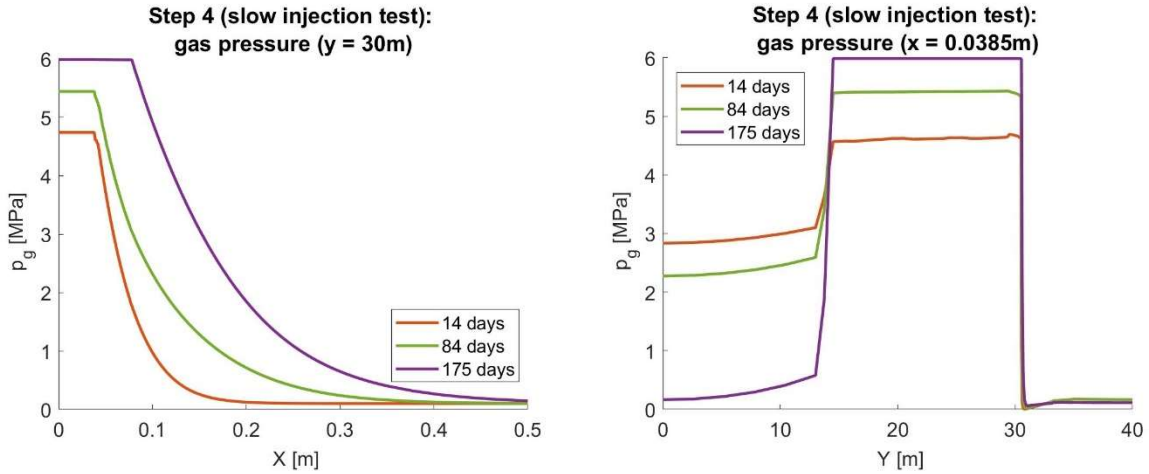

FIGURE 85 – GAS WATER PRESSURE PROFILES ALONG Y = 30M (A) AND X = 0.0385 (B) DURING SLOW INJECTION TEST WITH CONTACT ELEMENTS (k = E-17)

Section 9.4 CONCLUSION

From results here above, it can be seen that the introduction of contact elements definitely has an impact of the gas percolation towards the other intervals. However, even with a limited permeability the percolation is so important that it is immediate. Of course, this is still not what is observed in in-situ experiments.

Chapter III.10 COMPARISON OF SIMULATIONS AND IN-SITU EXPERIMENT RESULTS

Section 10.1 INTRODUCTION

This last chapter aims at comparing the results that were obtained by the various simulations that were performed and the PGZ3 in-situ measurements collected during the different phases of injection. In particular, the simulation results that are used in the present section are the ones from the 1D hydromechanical model and the 2D model. For both of them, only gas pressure profiles during slow and fast injection tests are considered.

Section 10.2 1D HYDROMECHANICAL MODEL

10.2.1 SLOW INJECTION TEST

As mentioned before, the in-situ test was realised with larger injection value than was it was planned, therefore only the two first steps are compared below in Figure 86. Both profiles correspond to the time evolution of the pressure in interval 2. What can be seen from this graph is that the trends in gas pressure profiles are similar but peak values tend to be larger in the simulation results. This is due to the dimensionality of the model which does not allow transfer along the y direction but only the x one. Therefore, gas accumulates, and its pressure increases more. A limit of the 1D model is therefore identified here.

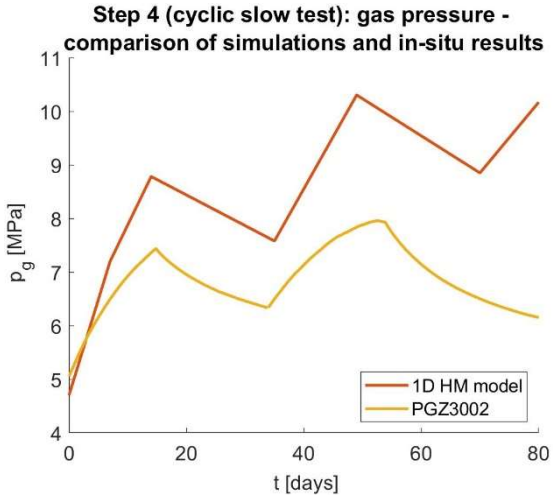

FIGURE 86 – COMPARISON OF SLOW INJECTION TEST PERFORMED IN-SITU (IN PGZ3002 BOREHOLE) AND NUMERICALLY (1D HM MODEL)

10.2.2 FAST INJECTION TEST

Then, gas pressure profiles in the injection interval during the fast injection test are compared. As already mentioned, the in-situ results show a breaking in the curve (which was interpreted as fracturing by de La Vaissière & Talandier (2022)) that is not present in the model results because of the elastic properties of the material. Moreover, the slope

of the rise in pressure is steeper for the simulations than what was observed in-situ. The reason for that is the same that for the slow injection results. As no flow can cross the borders of the one-dimensional model (which are quite close to each other), the fluids flow is limited to the x direction and accumulates more in the area of the injection interval which induces higher pressures.

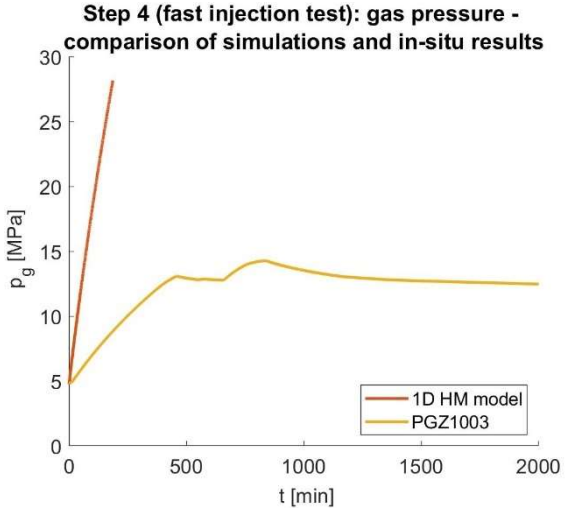

FIGURE 87 – COMPARISON OF FAST INJECTION TEST PERFORMED IN-SITU (IN PGZ1003 BOREHOLE) AND NUMERICALLY (1D HM MODEL)

10.2.3 CONCLUSION

Even if trends in both cases are similar, the one-dimensional model shows some limits in the sense that as the model height is quite small, the gas rises more in pressure. In this framework, the two-dimensional model, which allows flow in both directions, should be more aligned with the reality. This is what is described in the next section.

Section 10.3 2D MODEL

10.3.1 SLOW GAS INJECTION

Once again, the in-situ slow injection procedure does not correspond exactly to the procedure that is used for the numerical model. Therefore, comparing values of the peak pressures with precision is not completely pertinent. However, the trend observed here is not constant. Indeed, at the beginning, in-situ values are more important that the simulation ones while after the third peak the ones computed with the model are larger. This can be due by the fact that during simulations five injection cycles are performed while only four are carried out.

It should however be noted that the general trend (increasing pressure peaks at each cycle) and the orders of magnitude are following the same tendency.

One other comparison that can be made is looking at the evolution of the gas pressure in other intervals than the one in which gas is injected. However, from the previous chapters it is known that gas pressure in other intervals does not rise at all or steadily with the injection interval, while in reality they are impacted progressively.

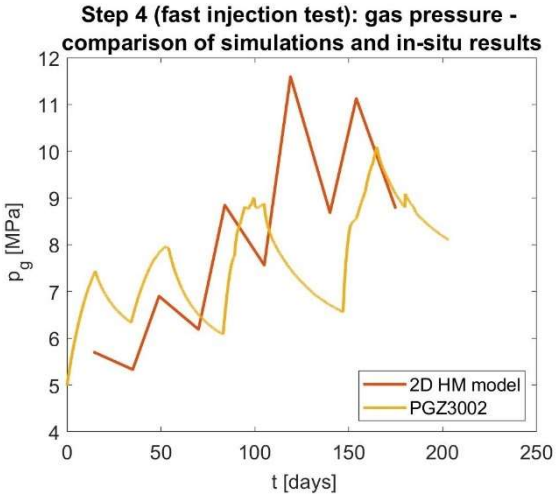

FIGURE 88 – COMPARISON OF SLOW INJECTION TEST PERFORMED IN-SITU (IN PGZ3002 BOREHOLE) AND NUMERICALLY (2D MODEL)

Section 10.4 CONCLUSION

From this section, it can be highlighted that, even if the models that were developed follow logical physical trends, they do not reproduce with precision what is observed during in-situ campaigns. This means that numerical models developed in the framework of this master's thesis can still be improved in various ways.

CONCLUSION AND PERSPECTIVES

In conclusion, this master's thesis aimed at reproducing of the PGZ3 experiment by numerical models. As a reminder, PGZ3 is a campaign of gas injection tests performed by ANDRA in their underground lab to study the perturbations induced by gas migrations in order to assess the feasibility of deep geological repositories for radioactive wastes. After a first part dedicated to a theoretical background, different model simulations with an increasing complexity were carried out.

Results from the one-dimensional model allowed to get a first idea of the flow characteristics such as the fact that gas is transported initially as a single phase and then, when the gas pressure is too low, it is transported dissolved in water. After the introduction of mechanical characteristics, it could be seen that when the gas injection rate is more important, tensile stress is induced along the direction perpendicular to the injection. The value of the stress suggests that fracturing might be happening. However, as the developed model is purely elastic, this could not be confirmed by the gas pressure profile. Therefore, introducing a plastic behaviour of the rock would be an interesting upgrading of the HM model. A last observation arising from the one-dimensional model is that when gas is steadily injected through the rock (slow injection procedure), the gas pressure does not increase without limits. Indeed, it seems that after three to four cycles the pressures tend to stabilise.

As for the results of the two-dimensional model, it was shown that the percolation along the borehole as observed in-situ is not so much due to the EDZ properties that ease the flow but more to the injection rate and the contact zone between the borehole and the rock. It was also noticed that peak pressures are reduced compared to what was observed in one dimensional model. Concerning the additions of contact elements to favour the percolation, it indeed implies some. However, it is too important. Therefore, a combination of the model

The comparisons between simulation and in-situ experiments show that in interval 2 (the one in which the gas injection is performed) the trends are similar to each other but the peak pressure values are not exactly the same. Therefore, this suggests that further calibration of the model could be again made. Additionally, in-situ, pressure measurements can only be performed in the borehole, the fact that pressure profiles across the COX argillites are available with numerical simulations is a real benefit for the understanding of the flow phenomena.

As this work is part of a master's thesis, the time dedicated to it was limited. Therefore, choices needed to be made on the aspects that are broached. However, there are still a wide range of possible improvements that could be the subject of future works. Some of these possible enhancements are presented below.

First, an important aspect to be considered is temperature. As already mentioned, the radioactive wastes produce heat during hundred years after their disposal. However, an increase in temperature will have as effect an increase in volume of gas and water which would result in higher pressures. Therefore, the introduction of temperature would have a direct effect on all conclusions that were made in this work.

Another aspect that could be discussed is the isotropy that was considered in axisymmetric models. Indeed, argillites are rocks with anisotropic characteristics (such as permeability or stresses) that could affect gas transport in the medium. Therefore, the impact of this simplification could be studied. Additionally, a perfectly isotropic circular excavated damage zone was then considered. It is known that it is more likely to be elliptic than circular at this kind of depth. This could not be considered in an axisymmetric model but should definitely be for 2D models.

Once simulations are well calibrated, the purpose is to observe the physical phenomena at larger time scale. The goal of this thesis being more focussed on the reproduction part of experimental results, this kind of simulations was not performed. However, these would be really interesting in order to assess the long-term stability of the disposal, which is the main goal of the research conducted by ANDRA.

A last characteristic that is studied in the PGZ3 experiment is the impact of the size of the borehole. This is highly important as the larger the borehole, the larger the EDZ (which impacts a lot the results). Moreover, cannisters containing radioactive wastes are way larger than the experimental borehole of 76mm of diameter. It should then be known whether the relation between the effects of gas pressure and the size of the borehole is proportional or not. This would not be a lot more complex to introduce in the models, however, as already said, other aspects such as the addition of a second dimensionality was favoured.

As a conclusion, it can be said that models developed during this master's thesis each had an importance in the identification of several phenomena (such as fracturing, way of transport of gas, percolation along the borehole, etc.). However, none of them perfectly fits to the results that are observed during PGZ3 experiment. In order to do that, the different foods for though presented hereabove are likely to help to again more accurate models.

BIBLIOGRAPHY

AFCN. (2017, November 27). *Unités de mesure de la radioactivité*. https://afcn.fgov.be/fr/dossiers-dinformation/la-radioactivite/les-unites-de-mesure-de-la-radioactivite

ANDRA. (2005a). *Dossier 2005 - Granite*.

ANDRA. (2005b). *Dossier 2005 argile*. https://www.andra.fr/sites/default/files/2017-12/266.pdf

ANDRA. (2005c). *Projet HAVL – Dossier 2005. Référentiel site Meuse/Haute-Marne. Rapport Andra C.RP.ADS.04.0022.*

ANDRA. (2020). *Inventaire Andra*. https://inventaire.andra.fr/les-donnees/les-dechets-radioactifs/dechets-radioactifs-bilan-fin-2020

ANDRA. (2022). *ANDRA*. https://www.andra.fr/

Armand, G., Conil, N., Talandier, J., & Seyedi, D. M. (2017). Fundamental aspects of the hydromechanical behaviour of Callovo-Oxfordian claystone: From experimental studies to model calibration and validation. *Computers and Geotechnics*, *85*, 277–286. https://doi.org/10.1016/j.compgeo.2016.06.003

Charlier, R., Collin, F., Gérard, P., & Radu, J. P. (2012). *Numerical modelling of the PGZ1 insitu test - 3D and 1D modelling*.

Charlier, R., Collin, F., Gerard, P., & Radu, J.-P. (2012). *Numerical modelling of the PGZ1 insitu test - 3D and 1D modelling - Simulation of gas injection GAS1 and hydraulic tests – Prediction of gas injection GAS2*.

Charlier, R., Collin, F., & Radu, J.-P. (2014). *Numerical modelling of the PGZ1 in-situ test – Simulation of GAS1, two hydraulic tests, GAS2 and future gas injections*.

Cochard, T. (2017). *Contribution à la génération de séquences pour la conduite de systèmes complexescritiques. Automatique / Robotique. U* [niversité de Lorraine,]. https://tel.archives-ouvertes.fr/tel-01754706

Collin, F. (2003). *Couplages thermo-hydro-mécaniques dans les sols et les roches tendres partiellement saturés* [Université de Liège]. https://orbi.uliege.be/handle/2268/87866

Collin, F. (2021). *Environmental geotechnics 2021 course*.

de la Vaissière, R. (2021). *PGZ experiment*.

de La Vaissière, R., & Talandier, J. (2022). *Overview of in-situ gas injection test into COx - Meeting « Gas migration into COx »*.

Forum Nucléaire. (2022). *Belgoprocess : diviser le volume des déchets nucléaires par 80*. Belgoprocess : diviser le volume des déchets nucléaires par 80

Gerard, P. (2011). *Impact des transferts de gaz sur le comportement poro-mécanique des matériaux argileux*. Université de Liège.

Gonzalez-Blanco, L. (2017). *Gas migration in deep argillaceous formations : Boom clay and indurated clays*.

IAEA. (2003). *Scientific and Technical Basis for the Geological Disposal of Radioactive Wastes*. https://www-pub.iaea.org/MTCD/Publications/PDF/TRS413_web.pdf

IAEA. (2009). *Geological disposal of radioactive waste: technological implications for retrievability*. https://www-pub.iaea.org/MTCD/Publications/PDF/Pub1378_web.pdf

IAEA. (2020). *Design Principles and Approaches for Radioactive Waste Repositories*. https://www-pub.iaea.org/MTCD/Publications/PDF/PUB1908_web.pdf

IAEA. (2022). Status and trends in spent fuel and radioactive waste management. *IAEA Nuclear Energy Series*, *NW-T-1.14*(1), 1–102.

IEA. (2021). *International energy agency - Data and Statistics*. https://www.iea.org/data-and-statistics/

IRSN. (n.d.). *La séparation/transmutation des déchets à vie longue*. Retrieved February 14, 2022, from https://www.irsn.fr/dechets/cigeo/Documents/Fiches-thematiques/IRSN_Debat-Public-Cigeo_Fiche-Transmutation.pdf

Jean-Baptiste, P., Lavielle, B., Fourre, E., Smith, T., & Pagel, M. (2017). Vertical distribution of helium and 40Ar/36Ar in porewaters of the Eastern Paris Basin (Bure/Haute-Marne): constraints on transport processes through the sedimentary sequence. *Geological Society, London, Special Publications*, *443*(1), 179–192. https://doi.org/10.1144/SP443.25

Jenni, A., Wersin, P., Thoenen, T., Baeyens, B., Ferrari, A., Gimmi, T., Mäder, U., Marschall, P., Hummel, W., & Leupin, O. (2019). *Technical report 19-03 - Bentonite backfill performance in a high-level waste repository: a geochemical perspective*.

Jungjohann, A., & et al. (2019). *World nuclear waste report 2019 - Focus Europe*. https://worldnuclearwastereport.org/wp-content/themes/wnwr_theme/content/World_Nuclear_Waste_Report_2019_Focus_Europe.pdf

Lagamine. (2020). *Lagamine manuals*. http://www.lagamine.uliege.be/dokuwiki/doku.php/start

L'élémentarium. (2022). *L'élémentarium - Fiche uranium*. https://lelementarium.fr/element-fiche/uranium/

Marschall, P., Horseman, S., & Gimmi, T. (2005). Characterisation of Gas Transport Properties of the Opalinus Clay, a Potential Host Rock Formation for Radioactive Waste Disposal. *Oil & Gas Science and Technology*, *60*(1), 121–139. https://doi.org/10.2516/ogst:2005008

NEA, & IAEA. (2020). *Uranium 2020: Resources, Production and Demand*. https://www.oecd-nea.org/jcms/pl_52718/uranium-2020-resources-production-and-demand

Norris, S. (2017). Radioactive waste confinement: clays in natural and engineered barriers – introduction. *Geological Society, London, Special Publications*, *443*(1), 1–8. https://doi.org/10.1144/SP443.26

NWMO. (2022). *What is used nuclear fuel?* https://www.nwmo.ca/~/media/Site/Files/PDFs/2022/03/28/20/56/Backgrounder-2022--What-is-used-nuclear-fuel.ashx?la=en

ONDRAF. (2022a). *ONDRAF - Recherches sur le stockage géologique*. https://www.ondraf.be/recherches-sur-le-stockage-g%C3%A9ologique

ONDRAF. (2022b). *ONDRAF - Traitement des déchets*. https://www.ondraf.be/traitement

ONDRAF. (2022c, February). *ONDRAF - Sortes de déchets nucléaires*. https://www.ondraf.be/sortes-de-dechets-radioactifs

Oxford Languages. (2022). *Oxford Dictionary*. https://languages.oup.com/google-dictionary-en/

Pham, Q. T. (2006). *Effets de la désaturation et de la resaturation sur l'argilite dans les ouvrages souterrains* [Ecole Polytechnique X]. https://pastel.archives-ouvertes.fr/pastel-00001810/document

Plúa, C., Vu, M. N., Armand, G., Rutqvist, J., Birkholzer, J., Xu, H., Guo, R., Thatcher, K. E., Bond, A. E., Wang, W., Nagel, T., Shao, H., & Kolditz, O. (2021). A reliable numerical analysis for large-scale modelling of a high-level radioactive waste repository in the Callovo-Oxfordian claystone. *International Journal of Rock Mechanics and Mining Sciences*, *140*, 104574. https://doi.org/10.1016/j.ijrmms.2020.104574

Popov, V., Adey, R., Pusch, R., & Kasbohm, J. (2019). Disposal of radioactive waste in abandoned mines. *Journal of Earth Sciences and Geotechnical Engineering*, *9*(3), 1–38.

Radioactivity.eu. (2022). *Properties of spent reactor fuel*. https://www.radioactivity.eu.com/site/pages/Reactor_Spent_Fuel.htm#:~:text=In%20normal%20operating%20conditions%2C%20a,0.2%25%20intermediate%2Dlived%20elements

Rebeix, R., le Gal La Salle, C., Michelot, J.-L., Verdoux, P., Noret, A., Monvoisin, G., Gianesinni, S., Lancelot, J., & Simler, R. (2011). Tracing the origin of water and solute transfers in deep groundwater from Oxfordian, Dogger and Trias formations in the east of the Paris Basin – France. *Physics and Chemistry of the Earth, Parts A/B/C*, *36*(17–18), 1496–1510. https://doi.org/10.1016/j.pce.2011.07.015

Sillen, X. (2012). Keynote on repository-induced perturbations of the host rock, in the context of the safety case for the geological disposal of VHLW and SF in clay formations. *European Commission TIMODAZ-THERESA*, 159–171.

SOS Great Lakes. (2022). *What is a DGR?* http://www.sosgreatlakes.org/new-page-26

Synatom. (2022). *Synatom*. https://synatom.be/fr/

Talandier, J. (2005). *La production et le transfert de gaz dans le stockage et dans la couche du Callovo-Oxfordien – Lien entre le transitoire hydraulique – Site de Meuse/Haute-Marne. Rapport Andra C.NT.ASCM.03.0042.*

World nuclear association. (2022). *Reactor database*. https://world-nuclear.org/information-library/facts-and-figures/reactor-database.aspx

ANNEXES

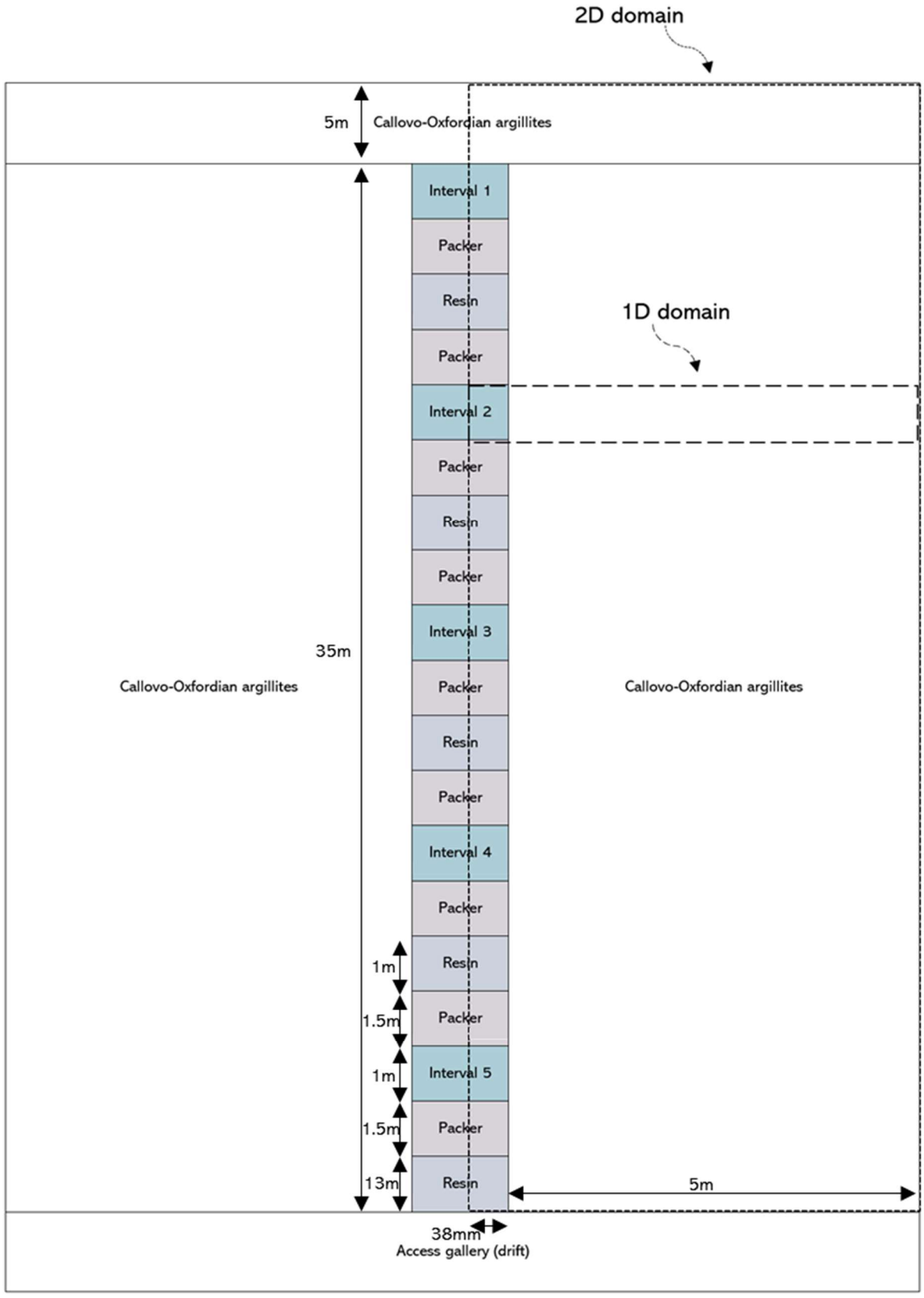

ANNEX 1 – IDENTIFICATION OF MODELLED DOMAINS IN 1D AND 2D WITH RESPECT TO THE EXPERIMENTAL SETTING

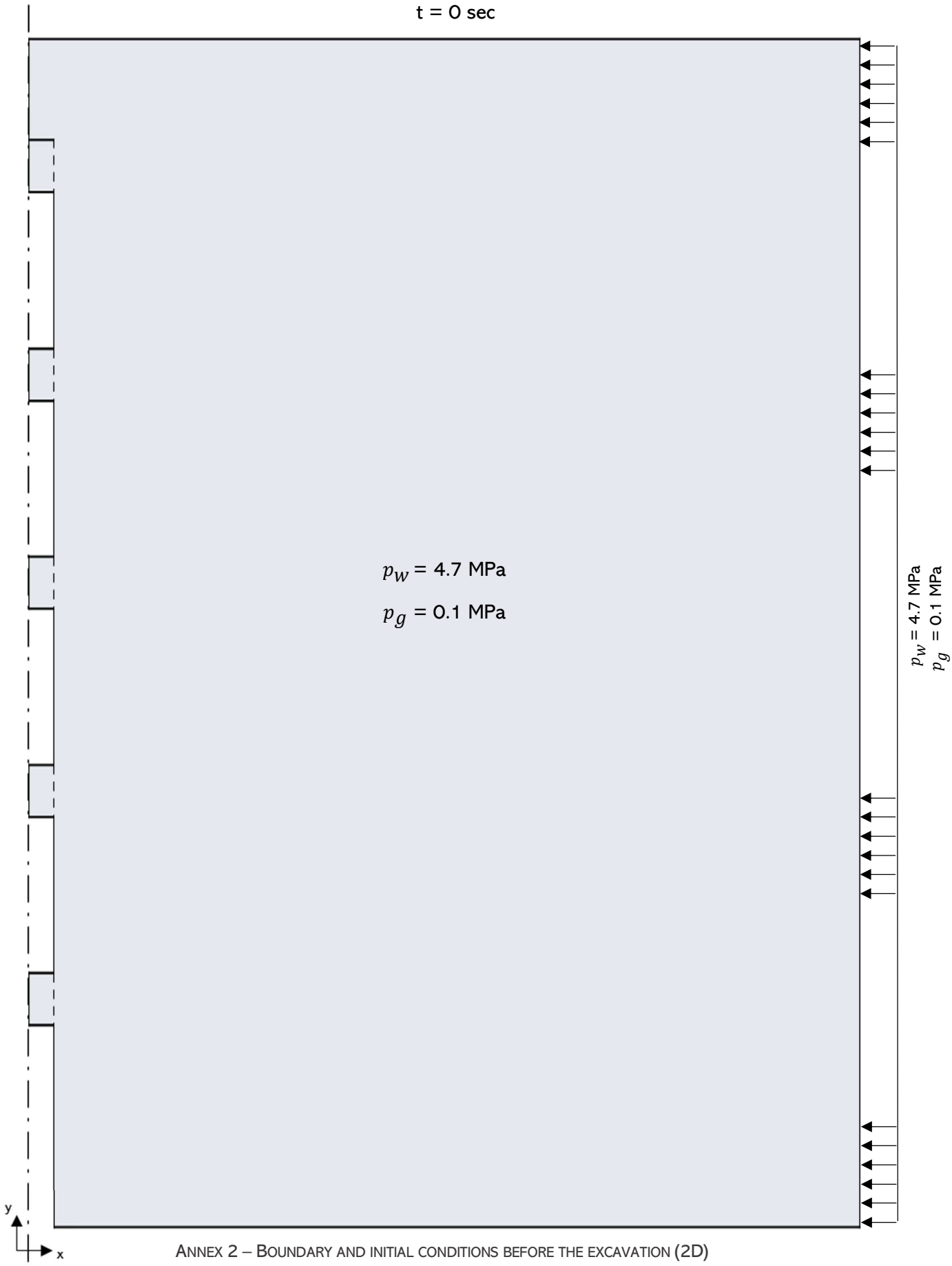

ANNEX 2 – BOUNDARY AND INITIAL CONDITIONS BEFORE THE EXCAVATION (2D)

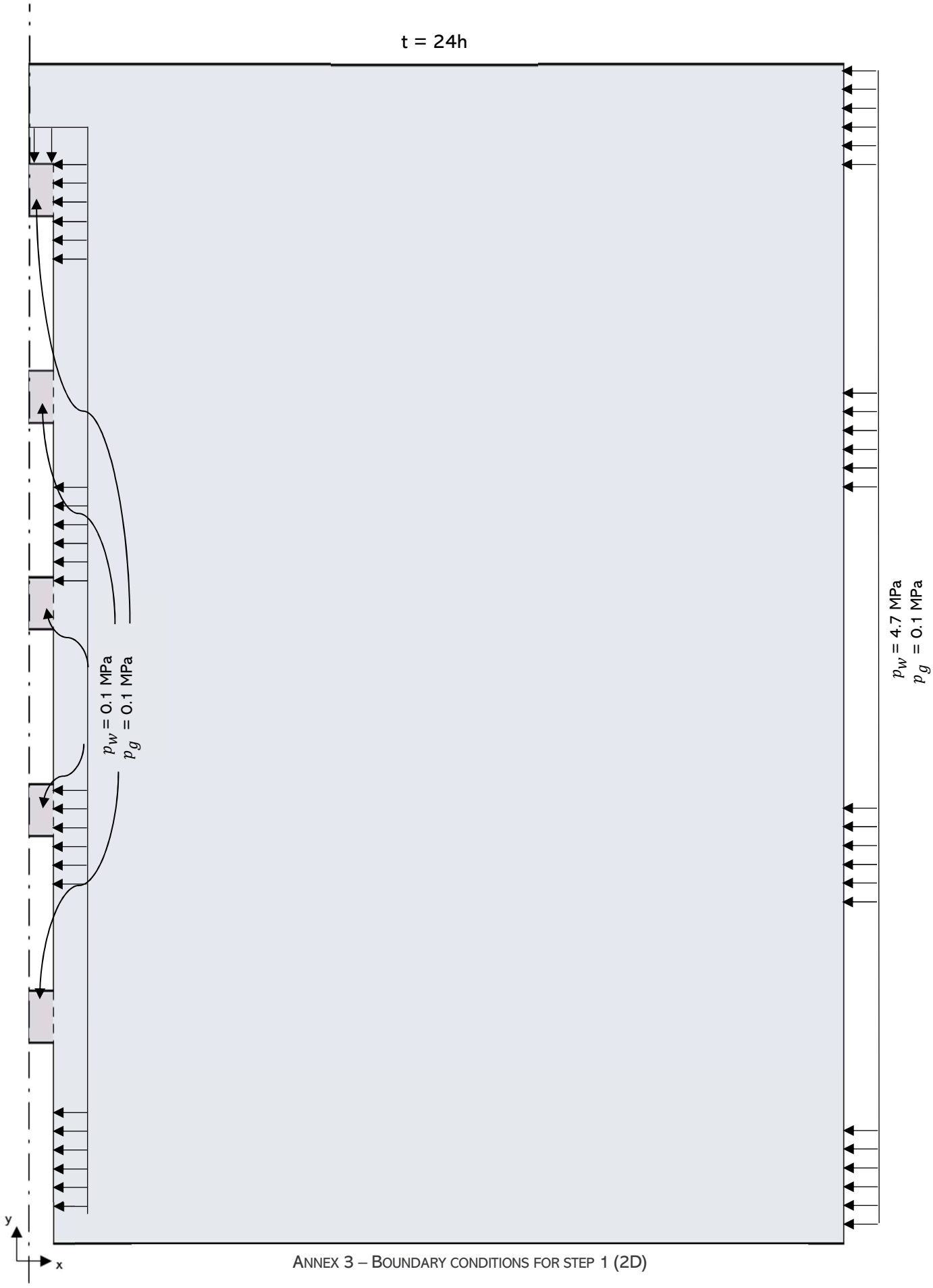

ANNEX 3 – BOUNDARY CONDITIONS FOR STEP 1 (2D)

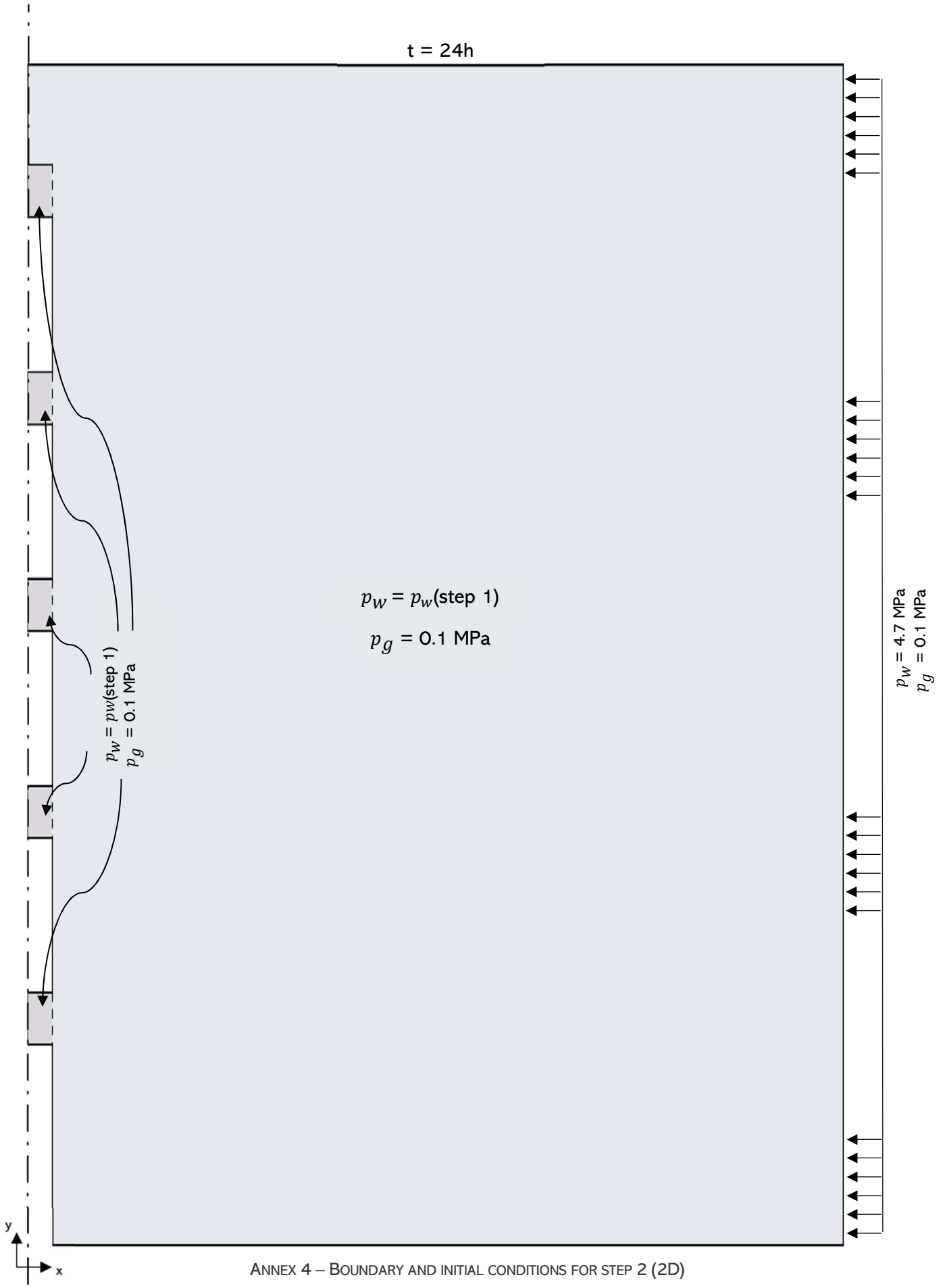

ANNEX 4 – BOUNDARY AND INITIAL CONDITIONS FOR STEP 2 (2D)

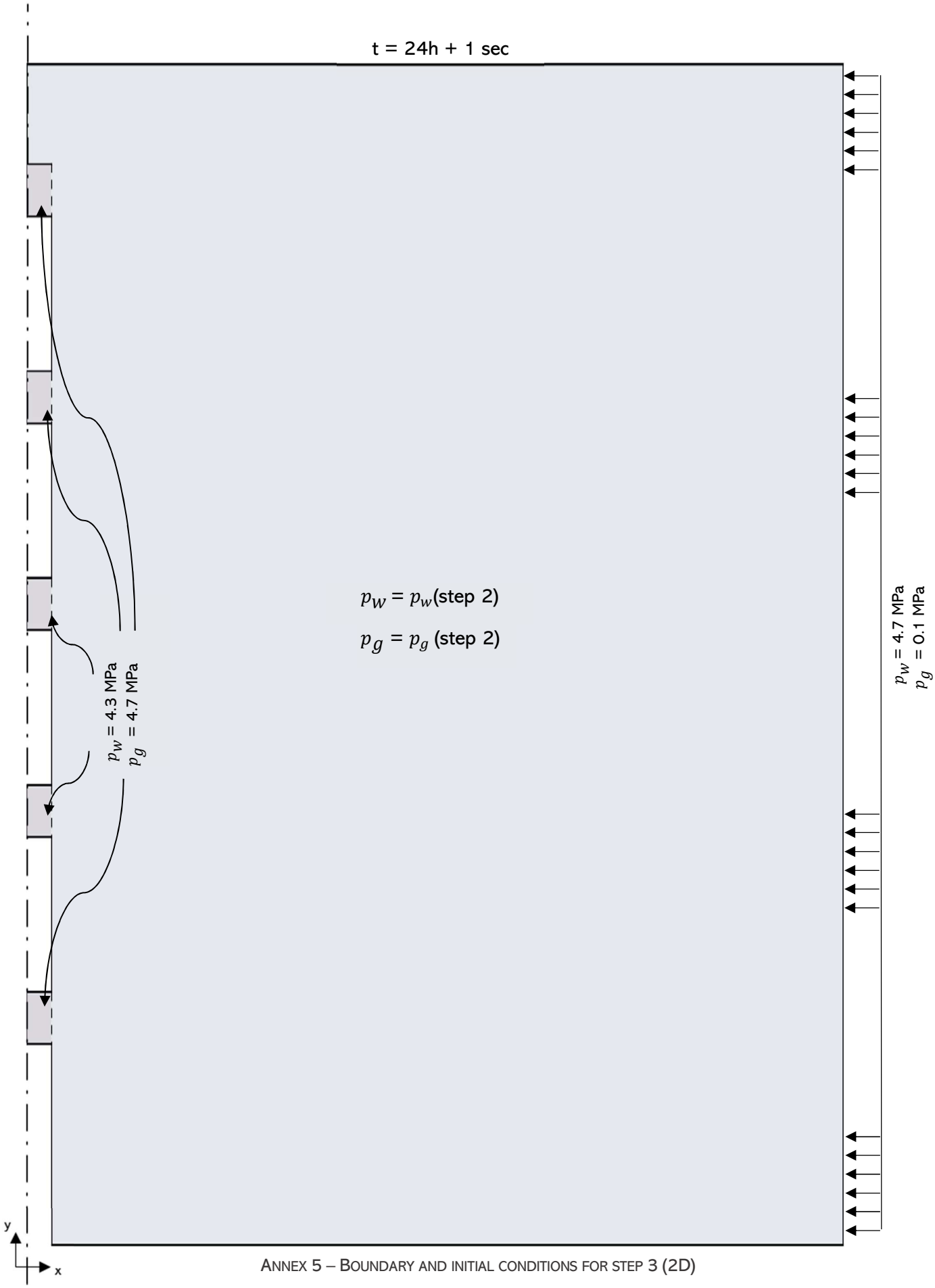

ANNEX 5 – BOUNDARY AND INITIAL CONDITIONS FOR STEP 3 (2D)

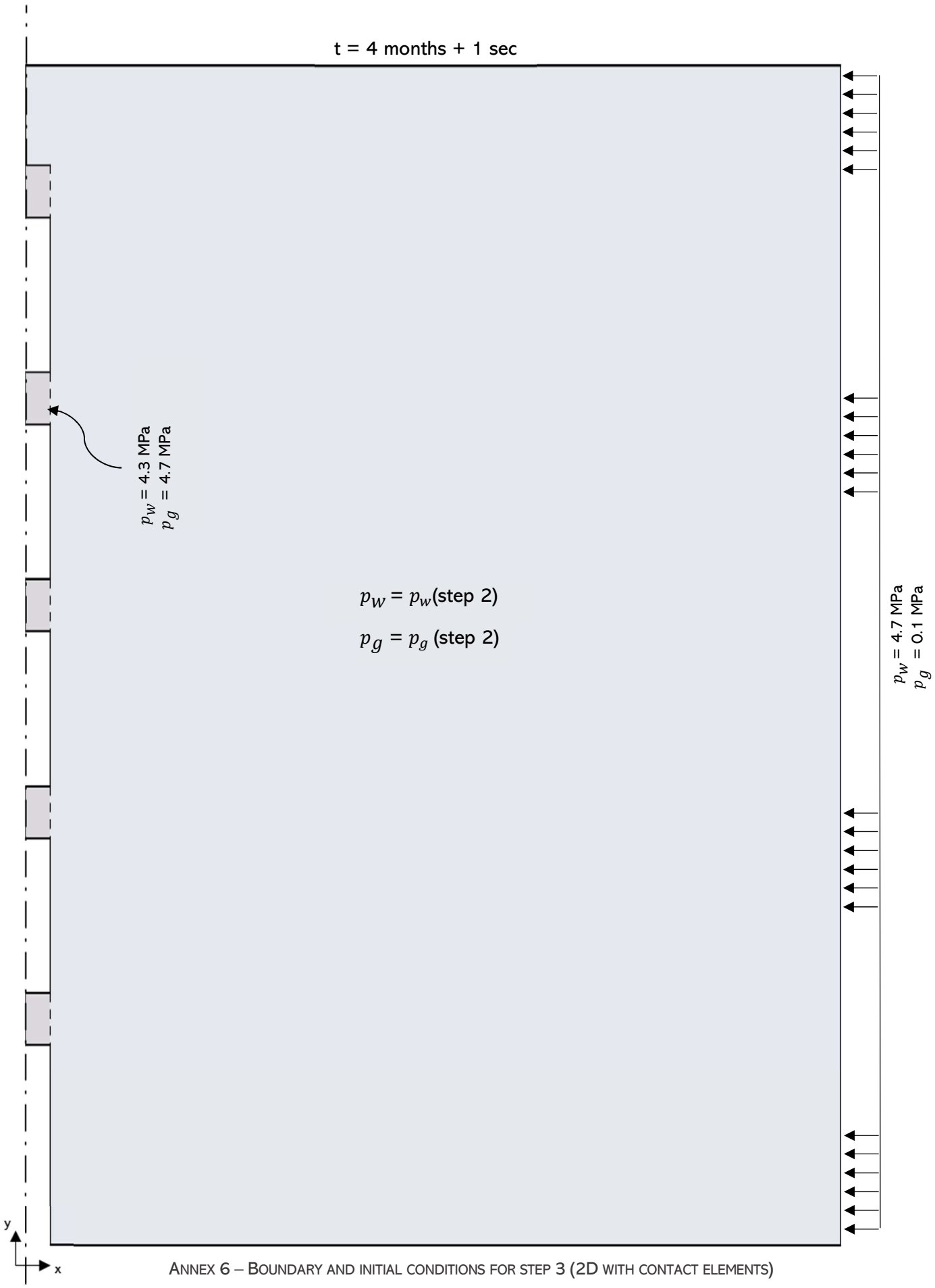

ANNEX 6 – BOUNDARY AND INITIAL CONDITIONS FOR STEP 3 (2D WITH CONTACT ELEMENTS)

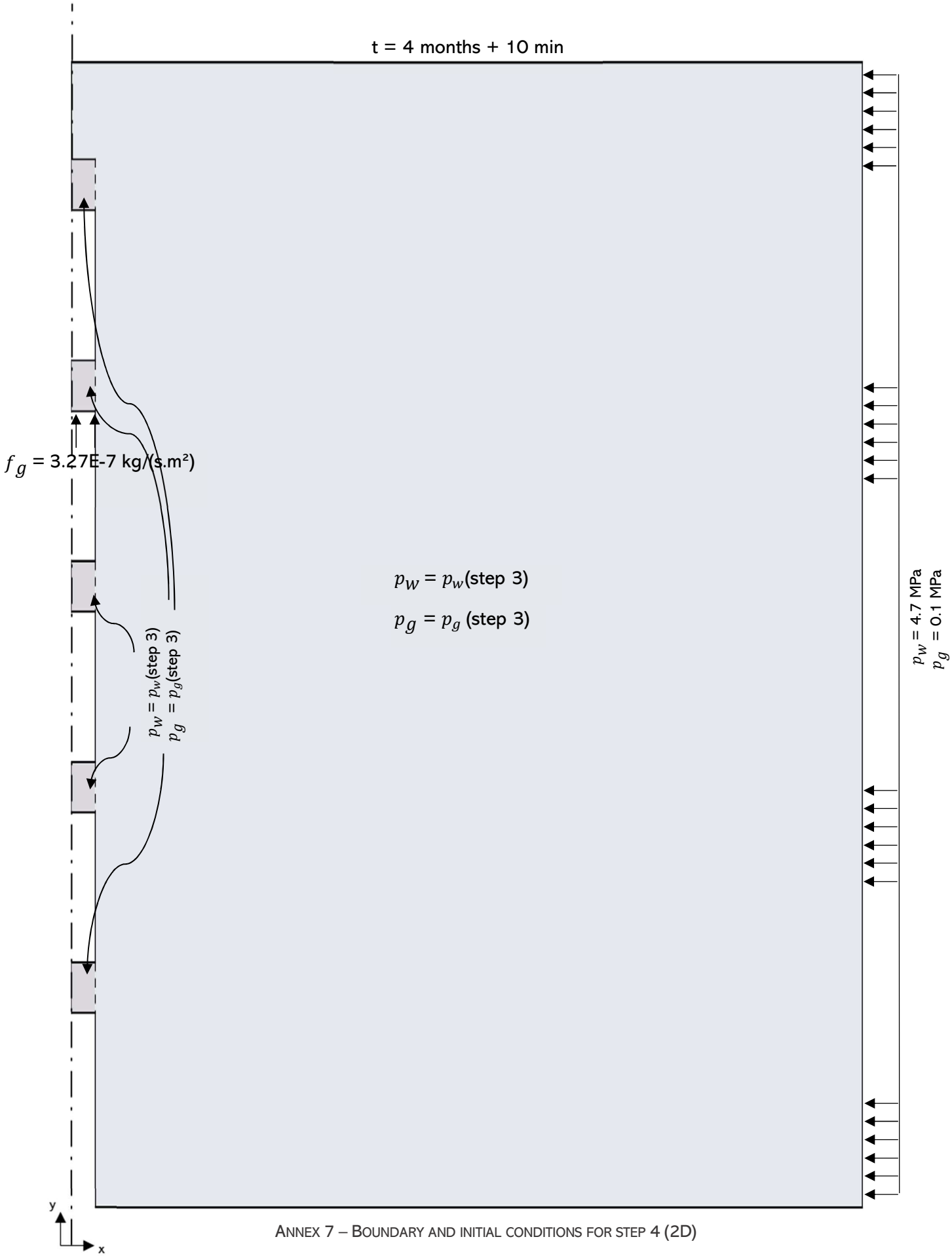

ANNEX 7 – BOUNDARY AND INITIAL CONDITIONS FOR STEP 4 (2D)

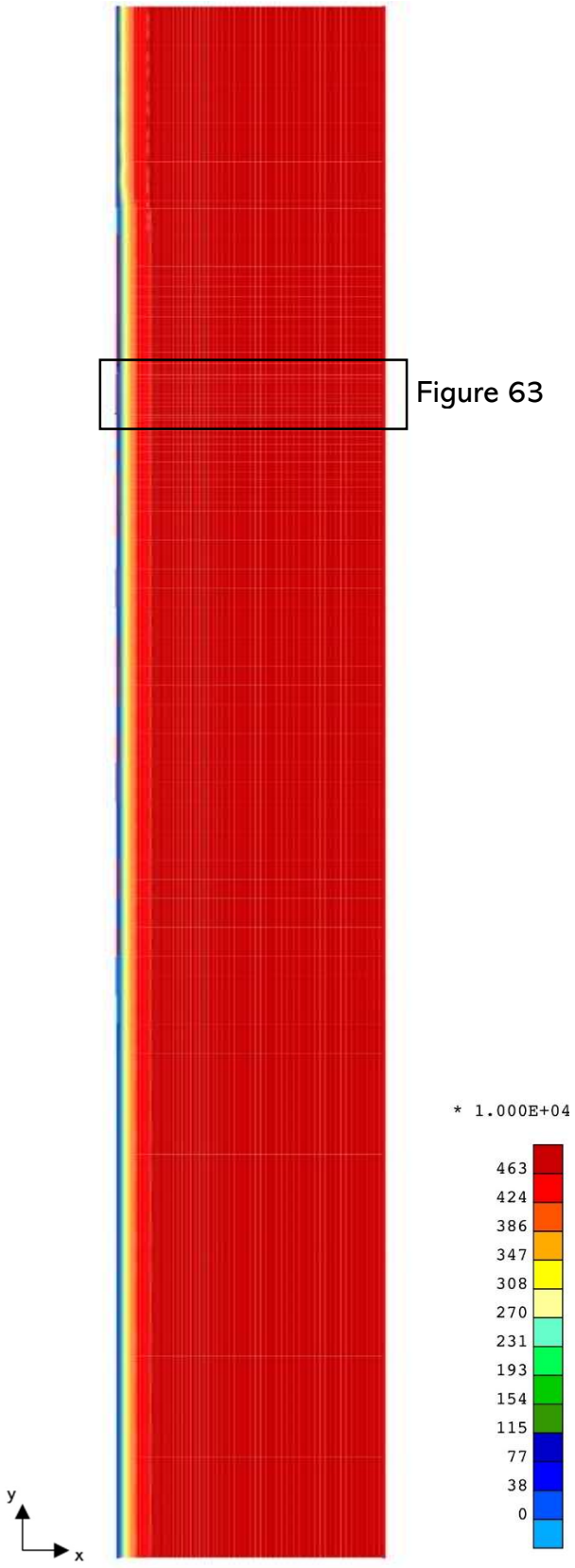

ANNEX 8 – WATER PRESSURES ON THE WHOLE DOMAIN DURING STEP 1

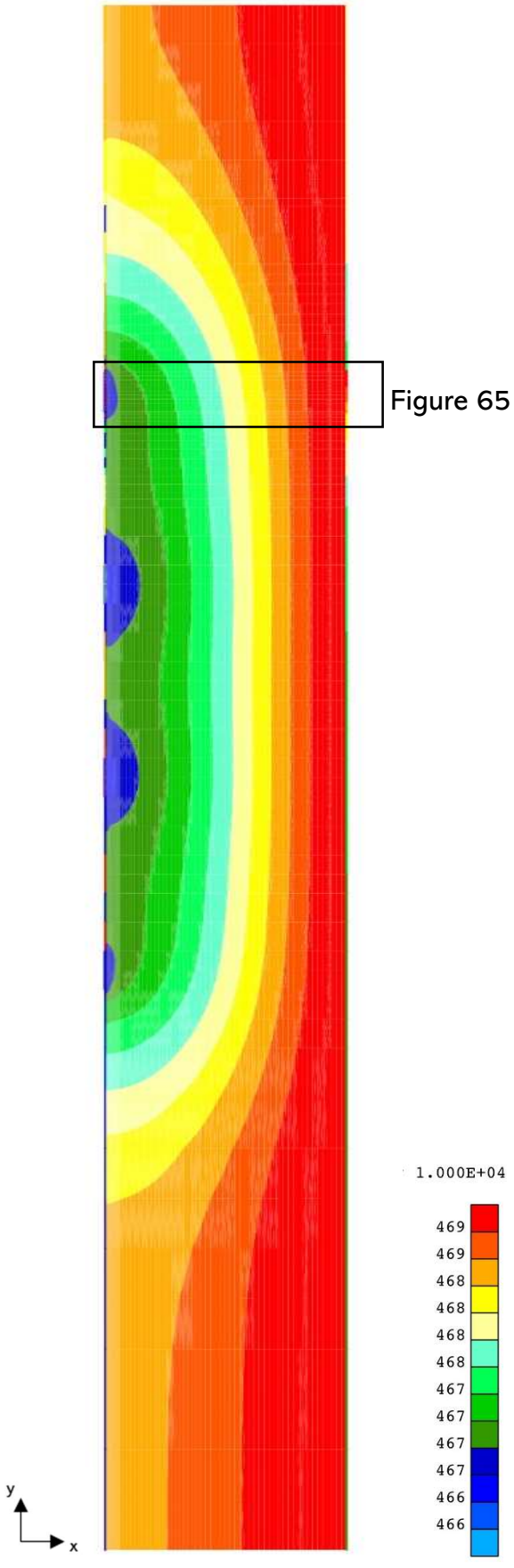

ANNEX 9 – WATER PRESSURES ON THE WHOLE DOMAIN DURING STEP 2

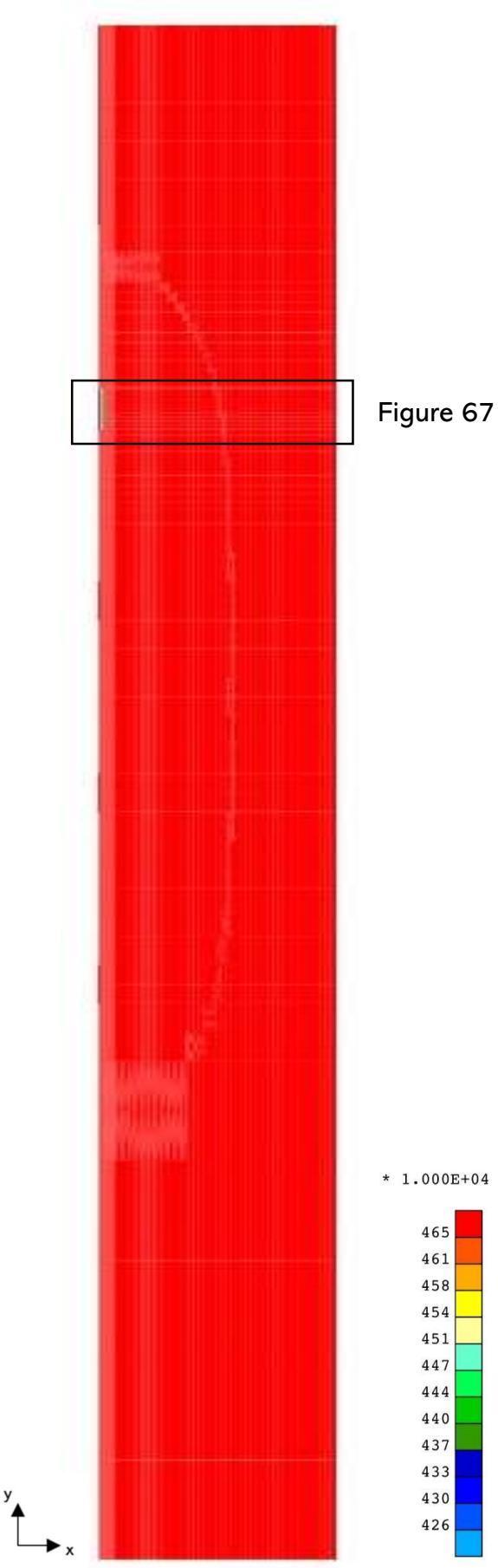

ANNEX 10 – WATER PRESSURES ON THE WHOLE DOMAIN DURING STEP 3

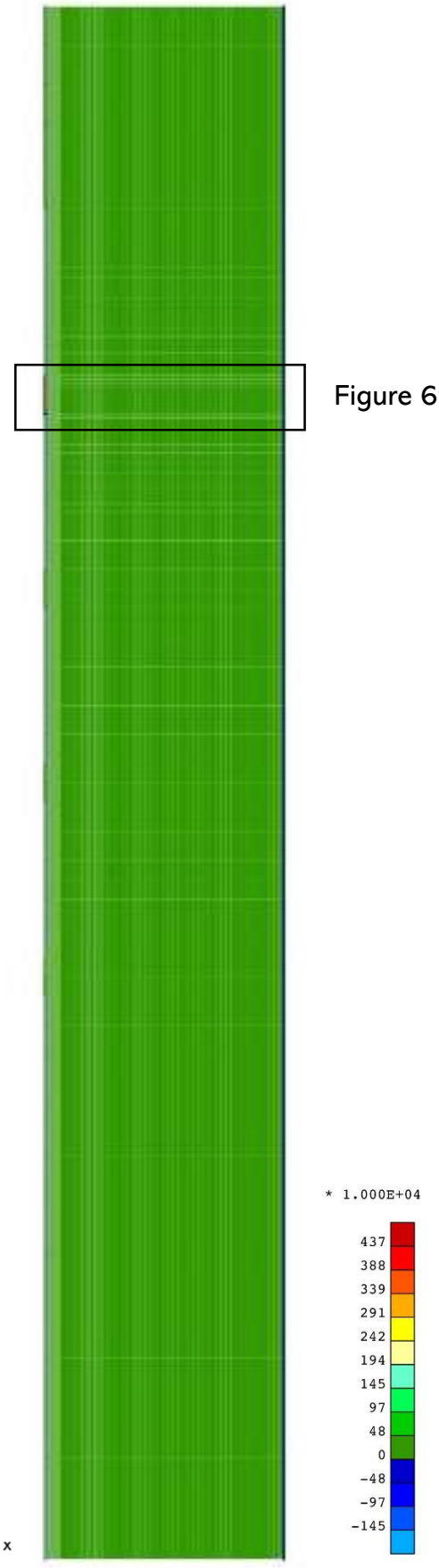

ANNEX 11 – GAS PRESSURES ON THE WHOLE DOMAIN DURING STEP 3

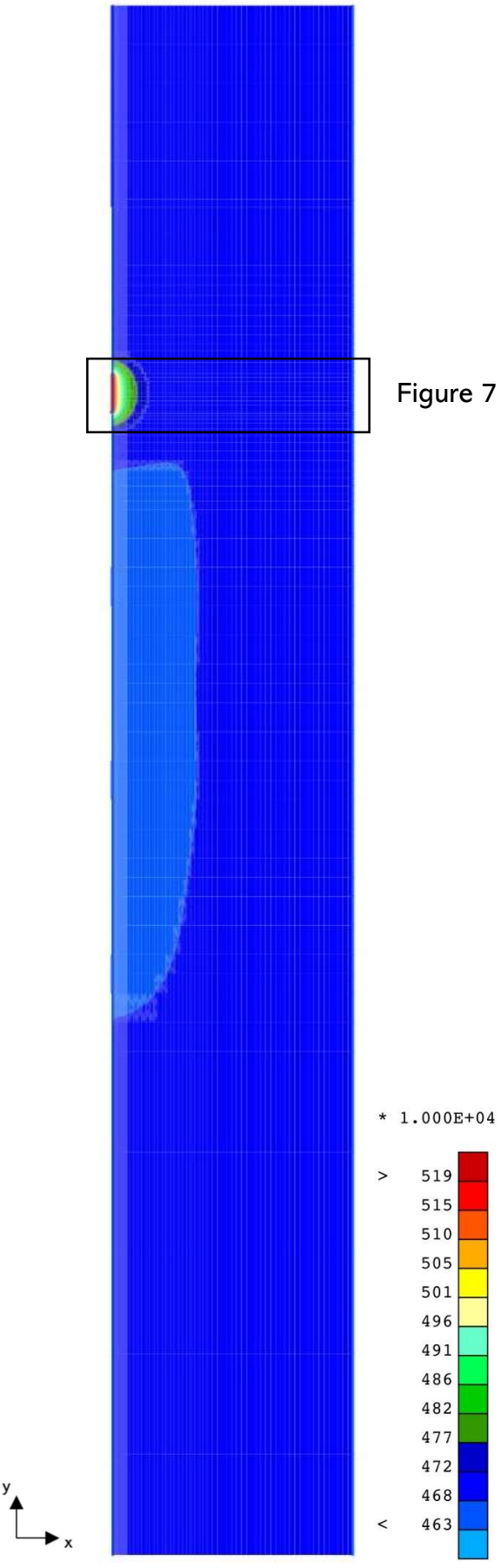

ANNEX 12 – WATER PRESSURES ON THE WHOLE DOMAIN DURING STEP 4

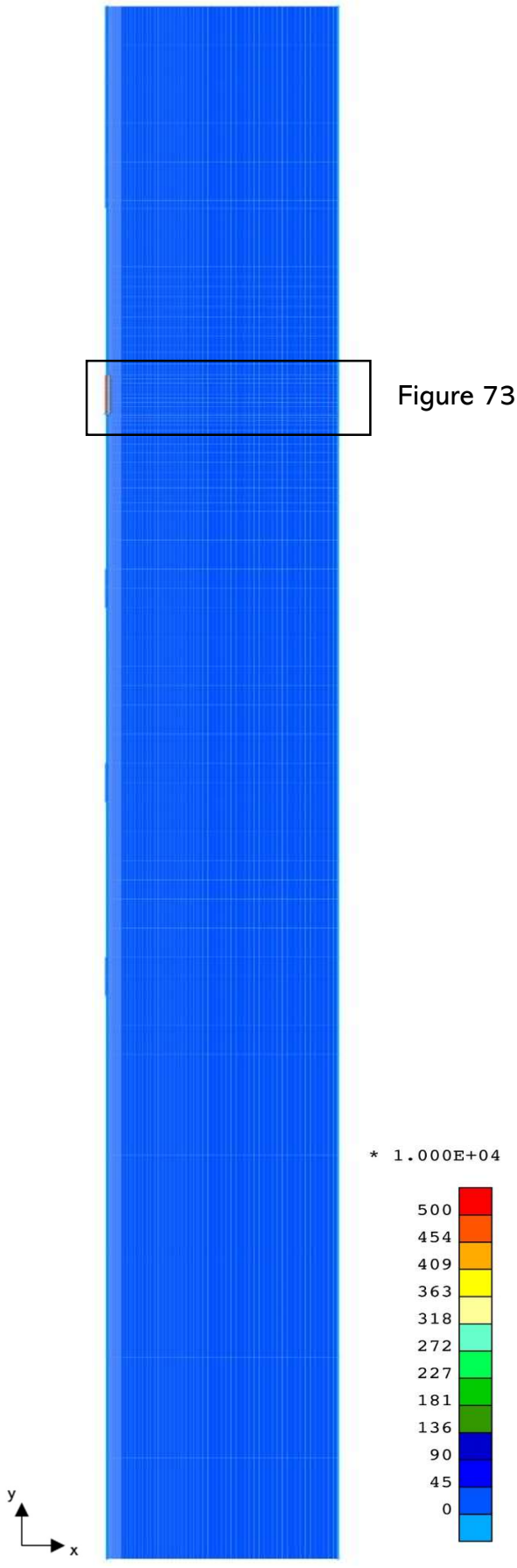

ANNEX 13 – GAS PRESSURES ON THE WHOLE DOMAIN DURING STEP 4